AD-A118 212 NAVAL POSTGRADUATE SCHOOL MONTEREY CA F/G 20/4
OSCILLATING FLOW ABOUT YAWED CYLINDERS.(U)
MAR 82 D O TRYTTEN
UNCLASSIFIED NL

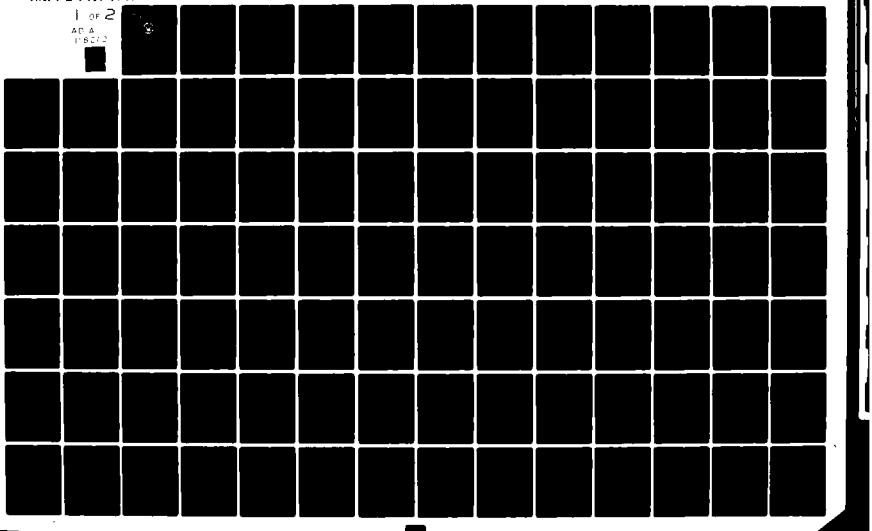

NAVAL POSTGRADUATE SCHOOL
Monterey, California

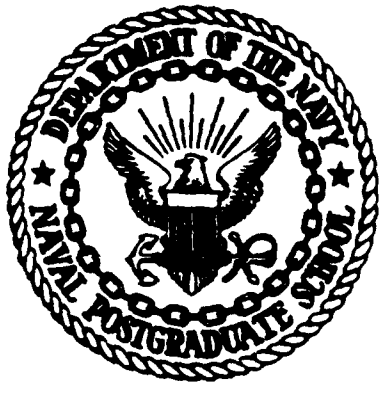

THESIS

OSCILLATING FLOW ABOUT YAWED CYLINDERS

by

Dean O. Trytten

March 1982

Thesis Advisor: T. Sarpkaya

Approved for public release, distribution unlimited.

SECURITY CLASSIFICATION OF THIS PAGE (When Data Entered)

REPORT DOCUMENTATION PAGE	READ INSTRUCTIONS BEFORE COMPLETING FORM
1. REPORT NUMBER	2. GOVT ACCESSION NO. AD-A118212	3. RECIPIENT'S CATALOG NUMBER
4. TITLE (and Subtitle) Oscillating Flow About Yawed Cylinders	5. TYPE OF REPORT & PERIOD COVERED Master's Thesis March 1982
	6. PERFORMING ORG. REPORT NUMBER
7. AUTHOR(s) Dean O. Trytten	8. CONTRACT OR GRANT NUMBER(s)
9. PERFORMING ORGANIZATION NAME AND ADDRESS Naval Postgraduate School Monterey, California 93940	10. PROGRAM ELEMENT, PROJECT, TASK AREA & WORK UNIT NUMBERS
11. CONTROLLING OFFICE NAME AND ADDRESS Naval Postgraduate School Monterey, California 93940	12. REPORT DATE March 1982
	13. NUMBER OF PAGES 129
14. MONITORING AGENCY NAME & ADDRESS(if different from Controlling Office)	15. SECURITY CLASS. (of this report)
	15a. DECLASSIFICATION/DOWNGRADING SCHEDULE

16. DISTRIBUTION STATEMENT (of this Report)

Approved for public release, distribution unlimited.

17. DISTRIBUTION STATEMENT (of the abstract entered in Block 20, if different from Report)

18. SUPPLEMENTARY NOTES

19. KEY WORDS (Continue on reverse side if necessary and identify by block number)

Oscillating Flow
Yawed Cylinders

20. ABSTRACT (Continue on reverse side if necessary and identify by block number)

The forces acting on yawed smooth and rough circular cylinders in oscillating flow have been investigated for the purpose of determining the appropriate force-transfer coefficients and the applicability of the "independence principle." The results have shown that the flow about each cylinder is unique and the independence principle does not hold true. In addition, a comprehensive sensitivity analysis has been

DD FORM 1 JAN 73 1473 EDITION OF 1 NOV 65 IS OBSOLETE
S/N 0102-014-6601

SECURITY CLASSIFICATION OF THIS PAGE (When Data Entered)

Block 20 Continued:

carried out to investigate the effects of undetected environmental disturbances on the force-transfer coefficients and the limits of probable errors have been delineated.

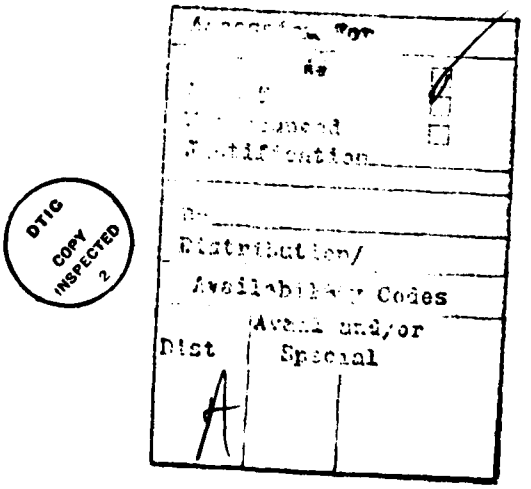

Approved for public release, distribution unlimited.

OSCILLATING FLOW ABOUT YAWED CYLINDERS

by

Dean O. Trytten
Lieutenant Commander, United States Navy
B.S., North Carolina State University, 1970

Submitted in partial fulfillment of the
requirements for the degree of

MASTER OF SCIENCE IN MECHANICAL ENGINEERING

from the

NAVAL POSTGRADUATE SCHOOL

March 1982

Author: Dean Orville Trytten

Approved by: Thesis Advisor

Chairman, Department of Mechanical Engineering

Dean of Science and Engineering

ABSTRACT

The forces acting on yawed smooth and rough circular cylinders in oscillating flow have been investigated for the purpose of determining the appropriate force-transfer coefficients and the applicability of the "independence principle." The results have shown that the flow about each cylinder is unique and the independence principle does not hold true. In addition, a comprehensive sensitivity analysis has been carried out to investigate the effects of undetected environmental disturbances on the force-transfer coefficients and the limits of probable errors have been delineated.

TABLE OF CONTENTS

I. INTRODUCTION ---------- 15

II. EXPERIMENTAL APPARATUS AND CYLINDERS ---------- 20

III. DATA ACQUISITION AND PROCESSING ---------- 24

IV. GOVERNING PARAMETERS ---------- 26

V. EXPERIMENTAL RESULTS ---------- 28

A. PRESENTATION OF RESULTS ---------- 28

B. DISCUSSION OF RESULTS ---------- 28

1. Inertia and Drag Coefficients ---------- 28

2. RMS Values of the Inertia and Drag Coefficients ---------- 31

3. Transverse (Lift) Force ---------- 32

VI. SENSITIVITY ANALYSIS ---------- 34

A. PHASE SHIFT EFFECTS ---------- 34

B. RANDOM SQUARE WAVE EFFECTS ---------- 37

VII. CONCLUSIONS ---------- 43

FIGURES ---------- 45

LIST OF REFERENCES ----------128

INITIAL DISTRIBUTION LIST ----------129

LIST OF FIGURES

1. Schematic of Cylinder Installation and Calibration ---------- 45

2a. C_m Versus K for β = 4057, α = 60 Deg., k/D = 0.00 -- 46

b. C_m Versus K for β = 2271, α = 60 Deg., k/D = 0.00 -- 47

c. C_m Versus K for β = 1021, α = 60 Deg., k/D = 0.00 -- 48

d. C_m Versus K for β = 2322, α = 60 Deg., k/D = 0.01 -- 49

e. C_m Versus K for β = 1042, α = 60 Deg., k/D = 0.01 -- 50

3a. C_d Versus K for β = 4057, α = 60 Deg., k/D = 0.00 -- 51

b. C_d Versus K for β = 2271, α = 60 Deg., k/D = 0.00 -- 52

c. C_d Versus K for β = 1021, α = 60 Deg., k/D = 0.00 -- 53

d. C_d Versus K for β = 2322, α = 60 Deg., k/D = 0.01 -- 54

e. C_d Versus K for β = 1042, α = 60 Deg., k/D = 0.01 -- 55

4a. C_{arms} Versus K for β = 4057, α = 60 Deg., k/D = 0.00 ---------- 56

b. C_{arms} Versus K for β = 2271, α = 60 Deg., k/D = 0.00 ---------- 57

c. C_{arms} Versus K for β = 1021, α = 60 Deg., k/D = 0.00 ---------- 58

d. C_{arms} Versus K for β = 2322, α = 60 Deg., k/D = 0.01 ---------- 59

e. C_{arms} Versus K for β = 1042, α = 60 Deg., k/D = 0.01 ---------- 60

5a. C_{mr} Versus K for β = 4057, α = 60 Deg., k/D = 0.00 ---------- 61

b. C_{mr} Versus K for β = 2271, α = 60 Deg., k/D = 0.00 ---------- 62

c. C_{mr} Versus K for β = 1021, α = 60 Deg., k/D = 0.00 ---------- 63

d. C_{mr} Versus K for β = 2322, α = 60 Deg., k/D = 0.01 ---------- 64

e. C_{mr} Versus K for β = 1042, α = 60 Deg., k/D = 0.01 ---------- 65

6a. C_{dr} Versus K for β = 4057, α = 60 Deg., k/D = 0.00 ---------- 66

b. C_{dr} Versus K for β = 2271, α = 60 Deg., k/D = 0.00 ---------- 67

c. C_{dr} Versus K for β = 1021, α = 60 Deg., k/D = 0.00 ---------- 68

d. C_{dr} Versus K for β = 2322, α = 60 Deg., k/D = 0.01 ---------- 69

e. C_{dr} Versus K for β = 1042, α = 60 Deg., k/D = 0.01 ---------- 70

7a. C_{lrms} Versus K for β = 4077, α = 60 Deg., k/D = 0.00 ---------- 71

b. C_{lrms} Versus K for β = 2272, α = 60 Deg., k/D = 0.00 ---------- 72

c. C_{lrms} Versus K for β = 1022, α = 60 Deg., k/D = 0.00 ---------- 73

d. C_{lrms} Versus K for β = 2322, α = 60 Deg., k/D = 0.01 ---------- 74

e. C_{lrms} Versus K for β = 1043, α = 60 Deg., k/D = 0.01 ---------- 75

8a. Comparison of C_m Versus K for β = 4040, k/D = 0.00, α = 90, 60, and 45 Deg. ---------- 76

b. Comparison of C_m Versus K for β = 2345, k/D = 0.00, α = 90, 60, and 45 Deg. ----------77

c. Comparison of C_m Versus K for β = 1045, k/D = 0.00, α = 90, 60, and 45 Deg. ----------78

d. Comparison of C_m Versus K for β = 4100, k/D = 0.01, α = 90, 60, and 45 Deg. ----------79

e. Comparison of C_m Versus K for β = 2325, k/D = 0.01, α = 90, 60, and 45 Deg. ----------80

f. Comparison of C_m Versus K for β = 1040, k/D = 0.01, α = 90, 60, and 45 Deg. ----------81

9a. Comparison of C_d Versus K for β = 4040, k/D = 0.00, α = 90, 60, and 45 Deg. ----------82

b. Comparison of C_d Versus K for β = 2345, k/D = 0.00, α = 90, 60, and 45 Deg. ----------83

c. Comparison of C_d Versus K for β = 1045, k/D = 0.00, α = 90, 60, and 45 Deg. ----------84

d. Comparison of C_d Versus K for β = 4100, k/D = 0.01, α = 90, 60, and 45 Deg. ----------85

e. Comparison of C_d Versus K for β = 2325, k/D = 0.01, α = 90, 60, and 45 Deg. ----------86

f. Comparison of C_d Versus K for β = 1040, k/D = 0.01, α = 90, 60, and 45 Deg. ----------87

10a. Comparison of C_{arms} Versus K for β = 4040, k/D = 0.00, α = 90, 60, and 45 Deg. ----------88

b. Comparison of C_{arms} Versus K for β = 2345, k/D = 0.00, α = 90, 60, and 45 Deg. ----------89

c. Comparison of C_{arms} Versus K for β = 1045, k/D = 0.00, α = 90, 60, and 45 Deg. ----------90

d. Comparison of C_{arms} Versus K for β = 4100, k/D = 0.01, α = 90, 60, and 45 Deg. ----------91

e. Comparison of C_{arms} Versus K for β = 2325, k/D = 0.01, α = 90, 60, and 45 Deg. ----------92

f. Comparison of C_{arms} Versus K for β = 1040, k/D = 0.01, α = 90, 60, and 45 Deg. ----------93

11a. Comparison of C_{mr} Versus K for β = 4040, k/D = 0.00, α = 90, 60, and 45 Deg. ----------94

b. Comparison of C_{mr} Versus K for β = 2345, k/D = 0.00, α = 90, 60, and 45 Deg. ----------95

c. Comparison of C_{mr} Versus K for β = 1045, k/D = 0.00, α = 90, 60, and 45 Deg. ----------96

d. Comparison of C_{mr} Versus K for β = 4100, k/D = 0.01, α = 90, 60, and 45 Deg. ----------97

e. Comparison of C_{mr} Versus K for β = 2345, k/D = 0.01, α = 90, 60, and 45 Deg. ----------98

f. Comparison of C_{mr} Versus K for β = 1040, k/D = 0.01, α = 90, 60, and 45 Deg. ----------99

12a. Comparison of C_{dr} Versus K for β = 4040, k/D = 0.00, α = 90, 60, and 45 Deg. ----------100

b. Comparison of C_{dr} Versus K for β = 2345, k/D = 0.00, α = 90, 60, and 45 Deg. ----------101

c. Comparison of C_{dr} Versus K for β = 1045, k/D = 0.00, α = 90, 60, and 45 Deg. ----------102

d. Comparison of C_{dr} Versus K for β = 4100, k/D = 0.01, α = 90, 60, and 45 Deg. ----------103

e. Comparison of C_{dr} Versus K for β = 2345, k/D = 0.01, α = 90, 60, and 45 Deg. ----------104

f. Comparison of C_{dr} Versus K for β = 1040, k/D = 0.01, α = 90, 60, and 45 Deg. ---------- 105

13a. Comparison of C_{lrms} Versus K for β = 4040, k/D = 0.00, α = 90, 60, and 45 Deg. ---------- 106

b. Comparison of C_{lrms} Versus K for β = 2365, k/D = 0.00, α = 90, 60, and 45 Deg. ---------- 107

c. Comparison of C_{lrms} Versus K for β = 1060, k/D = 0.00, α = 90, 60, and 45 Deg. ---------- 108

d. Comparison of C_{lrms} Versus K for β = 4100, k/D = 0.01, α = 90, 60, and 45 Deg. ---------- 109

e. Comparison of C_{lrms} Versus K for β = 2390, k/D = 0.01, α = 90, 60, and 45 Deg. ---------- 110

f. Comparison of C_{lrms} Versus K for β = 1060, k/D = 0.01, α = 90, 60, and 45 Deg. ---------- 111

14a. Force-Transfer Coefficients Versus Phase Angle for K = 6.66 ---------- 112

b. Force-Transfer Coefficients Versus Phase Angle for K = 10.41 ---------- 113

c. Force-Transfer Coefficients Versus Phase Angle for K = 14.08 ---------- 114

d. Force-Transfer Coefficients Versus Phase Angle for K = 14.51 ---------- 115

e. Force-Transfer Coefficients Versus Phase Angle for K = 25.44 ---------- 116

15a. Normalized Force Plus a Random Disturbance of Frequency Ratio 1 ---------- 117

b. Normalized Force Plus a Random Disturbance of Frequency Ratio 2 ---------- 118

c. Normalized Force Plus a Random Disturbance of Frequency Ratio 6 ---------- 119

d. Normalized Force Plus a Random Disturbance of Frequency Ratio 36 ---------- 120

e. Normalized Force Plus a Random Disturbance of Frequency Ratio 180 ---------- 121

16a. Response of C_m and the Corresponding C_d to Random Disturbances of Various Frequency Ratios, K = 14.08 ---------- 122

b. Response of C_d and the corresponding C_m to Random Disturbances of Various Frequency Ratios, K = 14.08 ---------- 123

17a. Response of C_m and the Corresponding C_d to Random Disturbances of Various Frequency Ratios, K = 6.66 ---------- 124

b. Response of C_d and the Corresponding C_m to Random Disturbances of Various Frequency Ratios, K = 6.66 ---------- 125

18a. Response of C_m and the Corresponding C_d to Random Disturbances of Various Freqency Ratios, K = 25.44 ---------- 126

b. Response of C_d and the Corresponding C_m to Random Disturbances of Various Frequency Ratios, K = 25.44 ---------- 127

TABLE OF SYMBOLS AND ABBREVIATIONS

A_n	Coefficients of sin $n\theta$ in Fourier Series
B_n	Coefficient of cos $n\theta$ in Fourier Series
C	Normalized force coefficient, $C = 2F/(\rho DU_m^2)$
C_{arms}	Actual RMS value of C
C_F(spp)	Semi-Peak-to-Peak force coefficient
C_d	Drag coefficient
C_{dr}	Drag coefficient normalized by the RMS value of C_d
C_{lrms}	RMS value of the normalized lift force
C_m	Inertia coefficient
C_{mr}	Inertia coefficient normalized by RMS value of C
D	Diameter of the test cylinder
F	In-line force
F_m	Measured in-line force
f_{sw}	Frequency of square wave disturbance
f_t	Frequency of the tunnel, $f_t = 1/T$
K	Keulegan-Carpenter number, $K = U_mT/D = 2\pi A/D$
k	Mean sand-roughness height
k/D	Relative roughness
L	Cylinder length
Re	Reynolds number, $Re = U_mD/\nu$
t	Time
T	Period of flow oscillations
U	Instantaneous velocity, $U = -U_m \cos\theta$

U_m	Maximum velocity in a cycle
α	Yaw angle, measured between ambient flow direction and cylinder axis
β	Frequency parameter, $\beta = Re/K = D^2/\nu T$
θ	Angle, $\theta = 2\pi t/T$
ν	Kinematic viscosity of water
ρ	Density of water

ACKNOWLEDGEMENT

The author wishes to thank Professor T. Sarpkaya for his continual guidance and patience throughout this investigation. It has been both a privilege and a most worthwhile experience to work with a man of such professional stature.

Great appreciation is also expressed to Mr. J. McKay of the Machine Shop in the Department of Mechanical Engineering who is truly an artisan in every sense of the word.

Also, the author wishes to thank the United States Navy for providing him the opportunity to further his professional development.

Finally, the author wishes to thank his wife for the continual understanding that she provides regardless of the circumstances.

I. INTRODUCTION

The study of time dependent flow about yawed cylinders is a topic which presently has great interest, both theoretically and practically. Of the great variety of time-dependent flows about yawed cylinders, the wave motion and sinusoidally oscillating flow are of such importance as to warrant immediate investigation. For lack of adequate information concerning time-dependent flows, industry is often forced to adopt steady flow relations to time-dependent flow situations. This research proposes to investigate the forces acting upon yawed circular cylinders immersed in sinusoidally oscillating uniform flow and to examine the validity or limitations of the present methods of analysis.

In 1950, Morison, et al. [1] introduced an equation for calculating the in-line force due to unbroken surface waves acting on a vertical pile. For a cylinder of diameter D, the force per unit length is expressed as:

$$F = \frac{1}{2} \rho D C_d U|U| + 0.25 \rho \pi D^2 C_m \frac{DU}{dt} \qquad (1)$$

where U represents the incident flow velocity; C_d, the drag coefficient; and C_m, the inertia coefficient. The coefficients C_m and C_d were considered to be time-invariant and constant along the length of the cylinder. Morison's paper

was intended as a preliminary report with follow-on studies to be done on other structures in various wave actions. Morison, et al. did not consider the contributions of transverse forces and vortex shedding in the calculation of the in-line forces.

Attempts have been made to extend this rather simple relation to far more complex situations such as combined wave and current flow, hydro-elastic oscillations, and yawed cylinders. Heideman, et al. [2] studied Morison's equation using ocean data and concluded that Morison's equation was satisfactory for normal cylinders. The utilization of an equation unproven even under ideal flow situations to correlate ocean data so as to prove the validity of the equation is not a very meaningful exercise. Sarpkaya and Isaacson [3] reviewed in detail the numerous studies regarding the application of the Morison equation.

It is obvious that there is a great need for an idealization of the problem, or an experiment which is more manageable (e.g., a sinusoidally oscillating uniform flow). Only in this way can all the complex interactions be separately taken into account.

Engineers faced with the problem of dealing with wave forces on yawed members, having no other recourse, drew upon previous work with steady flow. Hoerner [4] proposed the "independence principle", which stated that the normal pressure forces are independent of the tangential velocity

for subcritical values of Re_n, where Re_n is the Reynolds number based upon the component of the flow velocity normal to the cylinder. This principle allowed the neglecting of the tangential components. Bursnall and Loftin [5] found that the independence principle does not apply to the critical and transcritical flow regimes. Norton, et al. [6] found that the independence principle does apply to the postcritical as well as subcritical flow, but not to the critical and transcritical regions in between. Thus, recent research has shown that the independence principle applies when the boundary layer is wholly laminar (Hoerner) or wholly turbulent (Norton), but its use in the critical and transcritical regions is uncertain.

The designers of offshore structures were thus led to adopt the independence principle for the wave force calculations and, in doing so, to generalize the Morison equation. This has been accepted practice in industry for lack of a better relation. It can be asked what would be anticipated for oscillating flow or waves on the basis of what is known for steady flow. The instantaneous Reynolds number in such a flow will vary from $-Re_{max}$ to $+Re_{max}$ during a complete flow cycle. It could be postulated that the boundary layer would, at times, be fully laminar; at other times fully turbulent; and the rest of the time be in transition. In light of this, it is rather doubtful that the independence principle applies at all to oscillating or wave flow.

The study of forces acting on yawed cylinders can be investigated either by oscillating a yawed cylinder in a tank, using small amplitude waves in a laboratory channel, oscillating the flow about a fixed cylinder, or by using ocean data if available. Oscillating the cylinder has proven to be impractical because of difficulties in accounting for the inertial force acting on the body, producing repeatable oscillations, controlling spurious vibrations in the system, and in measuring the in-line and traverse forces simultaneously. Waves have relatively more-complex flow kinematics due to the orbital motion of particles and the decay of wave amplitude with depth. Ocean data are not available for such a study. Oscillation of the flow past the cylinder has proved to be the most practicable method. By using a sinusoidally oscillating uniform flow (which can be fairly easily produced) the kinematics of the flow are accurately known. Sarpkaya and Isaacson [3] discuss the similarities and differences between such a flow and the flows described by wave theory.

The primary objective of this investigation was to study the forces exerted by a sinusoidally oscillating uniform flow on yawed circular cylinders to determine whether or not the independence principle is applicable. If the principle holds, the force transfer coefficients calculated by Fourier analysis using the normal velocity component should reduce identically to the normal cylinder case at corresponding values of K, Re,

and k/D. If the independence principle does not apply, it is desired to determine what the coefficients are as functions of yaw angle, roughness ratio k/D, Re, and K. It would also be necessary to determine how well Morison's equation works with the new coefficients.

With the foregoing objectives in mind a detailed investigation was undertaken using smooth and rough cylinders of nominal 6-inch, $4\frac{1}{2}$-inch, and 3-inch diameters at yaw angles of 45 degrees, 60 degrees, and 90 degrees (as measured between the ambient flow direction and the cylinder axis). Part of this effort has already been reported [7]. The present study extends the previous work, accomplishes the original objectives of the investigation, and takes a much closer look at the sensitivity of the modified Morison equation and of the measured forces to random external disturbances encountered in nature.

II. EXPERIMENTAL APPARATUS AND CYLINDERS

The experiments were carried out in the large oscillating-flow tunnel at the Naval Postgraduate School. The tunnel was basically unchanged from the configuration described in [8 and 9]. Mounting pads for the strain gage housings were placed on opposite sides of the tunnel in such a manner so as to accommodate the yawed cylinders (Fig. 1). The mounting pad on one side of the tunnel was fitted with a slide so that the pad could be adjusted small distances to exactly match the cylinder length. The force transducers and housings were unchanged from those described in [9].

The cylinders also were similar to those previously reported, except that the ends were cut exactly at the desired angle of yaw. The cylinder ends were parallel to the tunnel walls with a 1/32-inch gap at each end. This gap was filled with a soft foamy material glued to the ends of the cylinder. Ball bearings were mounted in the ends of the cylinder with the outer bearing faces flush with the face of the cylinder.

The cylinders mounted in the tunnel were supported by the pins in the force transducers. The pins were perpendicular to the tunnel wall. Rubber washers were placed behind the pins so that the lateral motion of the cylinders (normal to the tunnel wall) was restrained, but without compressing

the cylinder. The cylinders were free to rotate, but a small clip was placed on one end of the cylinder to restrict the rotation to a very small amount so that the yawed end of the cylinder did not strike the tunnel wall as it rotated. Thus, as mounted, the cylinder was laterally constrained, but free to rotate within a small range. Careful calibration and extensive testing proved that this mounting system allowed accurate and repeatable recording of the normal and transverse forces acting on the cylinder.

Calibration was first conducted in a vertical direction, since yaw would not affect the total force in this direction. Weights were hung from the center of the horizontal cylinder, and calibration factors were obtained by converting the sum of the signals of two force transducers to pounds/mm and pounds/volt. The strain gages were found to be linear throughout the range of expected forces. The horizontal forces normal to the cylinder are related to the streamwise force by the sine of the yaw angle α (as measured between the cylinder axis and ambient flow). A system of supports and pulleys allowed applying horizontal force at the center of the cylinder and normal to it (Fig. 1). The sum of the outputs of the two transducers was recorded on the strip chart recorder, establishing the necessary relationship between the normal in-line force* F and the total electrical

*The force in the plane defined by the velocity vector and the cylinder axis.

output of the gages. The same gages were used to measure the lift force or the in-line force by rotating the gages 90 degrees. It is easy to show that the calibration factor of the lift force (here in the vertical direction, up or down), expressed in terms of pounds or millimeter deflection, is $\sin\alpha$ times the calibration factor for the in-line force. This proved to be true experimentally also and demonstrated independently the validity of the measurement technique.

Raines [7] carried out experiments with the following cylinders:

90 degrees, 5.905 inch, rough and smooth (nominal size 6 inches)

60 degrees, 6.005 inch, rough

45 degrees, 5.923 inch, rough and smooth

45 degrees, 4.42 inch, rough and smooth (nominal size 4.5 inches)

45 degrees, 3.00 inch, rough and smooth (nominal size 3 inches)

The present experiments were carried out with the following cylinders:

60 degrees, 5.965 inch, smooth (nominal size 6 inches)

60 degrees, 4.450 inch, smooth and rough (nominal size 4.5 inches)

60 degrees, 2.985 inch, smooth and rough (nominal size 3 inches)

Relative sand roughness of $k/D = 1/100$ was used for all rough cylinders.

In addition, the foregoing data were complemented with data reported in [10]. These data, taken using 3 inch and 4.5 inch nominal diameter cylinders at 90 degree yaw angle, were used in the analysis and comparison of the entire data.

III. DATA ACQUISITION AND PROCESSING

Data acquisition was accomplished using an HP3052A automatic data acquisition system. The system was configured as described in [9].

The data acquisition system consisted of an HP3495A 20 channel scanner and an HP3437A system voltmeter, both controlled by an HP9845B desk top computer. The in-line or transverse signal, originating as a voltage from the strain gages, was amplified and sent to the strip chart recorder. This amplified signal was also sent to the scanner as one channel of data. The flow amplitude signal originated from a differential pressure transducer, and was similarly amplified and sent to both the strip chart recorder and the scanner as another channel of data. Strip chart data was maintained as a visual record of the flow amplitude and force. The scanner switched between the two channels at designated intervals when triggered by the voltmeter. The voltmeter read each one of these voltage values and transferred them to the computer for immediate calculation of the governing parameters.

At least six cycles of in-line force data, recorded approximately 70 times per cycle, were acquired with the system. The data were then averaged to give one cycle from which the governing parameters were calculated. Ten cycles

of transverse force data, recorded at the same rate, were acquired with the system. The transverse data was not averaged prior to calculating the governing parameters.

The use of the HP3052A system proved highly beneficial for a number of reasons. The calculated parameters were available on a real time basis, allowing for detailed study of anomalies in the force patterns. Taking data over a large number of cycles removes more of the randomness of the flow forces. This was particularly valuable for analyzing the transverse force data.

IV. GOVERNING PARAMETERS

Data reduction for the in-line forces is based on Morison's equation using the normal component of velocity. The derivation of the governing parameters is described in detail in [3 and 9]. Here only a brief description of the parameters will be given.

For a sinusoidally varying flow, Eq. (1) may be written:

$$\frac{2F}{\rho D U_m^2} = \frac{\pi^2}{K} C_m \sin\theta - C_d |\cos\theta| \cos\theta \tag{2}$$

where the flow is represented by $U = -U_m \cos\theta$ with $\theta = 2\pi t/T$. The Fourier averages of C_m and C_d are given as [1]:

$$C_m = \frac{2K}{\pi^3} \int_0^{2\pi} \frac{F_m \sin\theta}{\rho D\, U_m^2} \, d\theta \tag{3}$$

and

$$C_d = -\frac{3}{4} \int_0^{2\pi} \frac{F_m \cos\theta}{\rho D\, U_m^2} \, d\theta \tag{4}$$

where F_m represents the measured force.

As discussed in [9], it would be beneficial to remove the cycle-to-cycle variations in the force. This was accomplished by using the normalized RMS value of the actual force (C_{amrs}). Two new coefficients were defined from this:

$$C^*_{dr} = C_d/C_{rms} \ , \ C_{dr} = C_d/C_{amrs} \tag{5}$$

and

$$C^*_{mr} = C_m/C_{rms} \ , \ C_{mr} = C_m/C_{arms} \tag{6}$$

Using Eq. (2), the rms value of the calculated force can be shown to be:

$$C_{rms} = \sqrt{\frac{3}{8} C_d^2 + \frac{\pi^4 C_m^2}{2K^2}} \tag{7}$$

Transverse force data were represented by the normalized rms value of the measured lift force (C_{lrms}). Previously, some of the lift data were analyzed [7] using a Fourier transform to obtain frequency information. In the present study, this effort was discontinued because the frequency information so far obtained was more than sufficient to draw general conclusions regarding the frequency content of the lift force.

V. EXPERIMENTAL RESULTS

A. PRESENTATION OF THE RESULTS

The force-transfer coefficients (C_m, C_d, C_{arms}, C_{mr}, C_{dr}, C_{lrms}) are presented in graphical form in terms of the governing parameters K, β, α, and k/D in Figs. 2 through 7. The new as well as the previously-obtained data [7 and 10] have been cross-plotted in Figs. 8 through 13 in order to exhibit the effects of the governing parameters.

B. DISCUSSION OF THE RESULTS

1. Inertia and Drag Coefficients

The first indication of the fact that the independence principle is not applicable to yawed cylinders in oscillating flow is seen in Fig. 8a where C_m is plotted as a function of K for β = 4040, k/D = 0.00, and α = 90, 60, and 45 degrees. Evidently, had the independence principle been valid, the three sets of data corresponding to three yaw angles would have collapsed into a single set, thus rendering the C_m versus K relationship independent of the yaw angle (at least within the range of the test parameters and experimental errors). This conclusion is more universal than it may appear at first sight on the basis of Fig. 8a. In fact, Figs. 8b through 8f, presenting C_m versus K for both smooth and rough cylinders of 6, 4.5, and 3 inch nominal diameters, show that C_m varies with the yaw angle as it did in Fig. 8a. Thus, one may conclude

that the independence principle is not valid at least for the inertia coefficient. The recognition of this fact is important for two reasons. Firstly, the inertial force is only part of the total force. Secondly, the significance of the inertial force depends on K. Thus, the failure of the inertia coefficient to obey the independence principle may not by itself be very important if the inertial force is small relative to the total force for the particular case under consideration. Consequently, it is important to examine the variation of the drag coefficient and its relation to the total force and the independence principle.

Figure 9b shows the variation of C_d as a function of K for β = 2345, k/D = 0.00, and α = 90, 60, and 45 degrees. Clearly, the variation of C_d with K and the yaw angle is far more complex than that of C_m. Figures 9a through 9c, depicting C_d versus K for the three smooth cylinders, show that the independence principle does not hold true except at relatively large values of K. The implication of this result is that when the vortex motion about the body becomes extremely turbulent and incoherent, as it would at high K values, the overall effect of yaw becomes less significant. It is also in this region that the force is drag dominated and the drag force may be calculated in terms of the force acting on the projected area. Though the inertia coefficient exhibits strong variation with yaw even at high K values, this variation is of academic interest only since the

contribution of the inertial force to the total force is rather insignificant.

Roughness plays an important and, oddly enough, a unifying role on the drag coefficient. This is somewhat anticipated on the basis of the fact that roughness precipitates earlier transition and greater incoherence in the flow about a yawed cylinder, thereby creating conditions more favorable to the independence principle. Figures 9d through 9f show that the independence principle for rough cylinders is almost valid with the exception of the drag-inertia dominated regime ($8<K<20$).

It is clear from the foregoing discussion of the inertia and drag coefficients that the normal force acting on a yawed cylinder is significantly underestimated through the use of Morison's equation, independence principle, and the drag and inertia coefficients appropriate to the normal cylinder. Only a narrow range of K values (from about 9 to 17), in the drag-inertia dominated regime, that the drag coefficient for a normal cylinder exceeds that for a yawed cylinder. However, the large increase in the inertia coefficient of the yawed cylinder in the same region of K values more than offsets the relatively small decrease in its drag coefficient.

The absence of the inertia crisis, the large increase in the inertia coefficient, the relative decrease in the drag and lift coefficients, all in the drag-inertia dominated

regime, of yawed cylinders are a consequence of the decrease of the spanwise coherence of vortices. In general, the smaller the spanwise coherence, the larger the C_m in this region. It appears that the independence principle or the cosine law, as it is sometimes called, is a gross simplification of the behavior of flow in the near wake. One may, therefore, conclude that the Fourier-averaged drag and inertia coefficients, based on Morison's equation, are unique for each angle of yaw, Reynolds number, Keulegan-Carpenter number, and the relative roughness.

2. RMS Values of the Inertia and Drag Coefficients

It has already been shown [7] that the normalized rms values of the inertia or drag coefficients remove significantly the scatter from the data and establish clearer relationships between these coefficients and the governing parameters. The same rms coefficients are used here to examine the effect of yaw and experimental error. Figures 11a through 11f show $C_{mr} = C_m/C_{arms}$ as a function of K. Clearly, C_{mr} is independent of Reynolds number (or β), yaw angle, and the roughness for K smaller than about 8. For smooth cylinders, C_{mr} is nearly independent of yaw for K larger than about 20. Additionally, for rough cylinders C_{mr} is least dependent on yaw for relatively low values of Re.

The drag coefficient C_{dr} exhibits similar characteristics (see Figs. 12a through 12f). The scatter in C_{dr} is considerably less than that in C_d primarily because of the

fact that the variations in C_d as a consequence of the random disturbances imposed on the measured force are smoothened out by the variations in the corresponding C_{arms} values. This fact has been substantiated through numerous examples by examining the relative variations of C_d, C_m, and C_{arms}. As K increases C_{dr} reaches its theoretical value of 1.63, as seen from Eq. (7). Finally, roughness tends to decrease the dependency of C_{dr} on Re (see Figs. 12d through 12f).

3. Transverse (Lift) Force

The lift force data are presented in terms of the normalized rms values of the measured lift force in Figs. 13a through 13c for the three smooth cylinders. These figures show that C_{lrms} is largest for the 90-degree cylinders, as one would expect, and decreases rapidly with yaw. However, the variation of C_{lrms} with the yaw angle (60 and 45 degrees) is not as large as that with the Reynolds number. The lift coefficient increases rapidly as K increases from about 6 to 12. Then, C_{lrms} again decreases rapidly due to the increased lack of coherence of the vortices. Similar observations may be made for rough cylinders (see Figs. 13d through 13f). It suffices to note that the yaw has an immediate effect on the coherence of vortices and on the lift coefficient, particularly in the drag-inertia dominated regime. For large values of K or Re, the irregularity of the vortex shedding even for a 90-degree cylinder obscures the yaw effect. It is then rather difficult to distinguish

between the lift coefficients of cylinders at various yaw angles. In the ocean environment, one is more likely to find a confused vortex shedding with very small coherence length. Thus, one may safely state that the inclined members subjected to the wave motion in the ocean environment will experience considerably less lift force than those normal to the waves.

VI. SENSITIVITY ANALYSIS

A. PHASE SHIFT EFFECTS

It has been known since the inception of Morison's equation in 1950 that the phase change between the maximum force and the maximum velocity may lead to varying degrees of error, depending on the governing parameters. This phase shift may arise due to electronic or numerical filtering of the force and velocity data or due to variations in the coherence of the vortices along a given separation line. Even though it is not yet possible to attribute a given fraction of the estimated error to a specific cause, it is most desirable to examine in detail the isolated effects of such things as an imposed phase shift and/or a random disturbance of a given amplitude and frequency. Eventually, such information will show the region of sensitivity of the force coefficients and Morison's equation to the disturbances imposed by the environmental conditions and will lead to a more rational interpretation of the causes of large scatter observed in the results of ocean tests.

The effects of phase shift on the force-transfer coefficients have been examined as follows. For a given K, β, k/D, and yaw angle the drag and inertia coefficients have been calculated from Eqs. (3) and (4). These coefficients correspond to cases where there was no phase

shift as ascertained by the manner in which the experiments were carried out. Then the force was recalculated through the use of Morison's equation and the above coefficients. The calculated force was then given a phase shift and a new set of force coefficients were calculated through the use of Eqs. (3) and (4). The method was repeated for representative values of K and reasonable phase angles.

Figures 14a through 14e show the results for five coefficients. Clearly, the phase angle has significant effect on all of these coefficients with the exception of C_{arms}. Concentrating attention on C_m and C_d it is noted that C_m decreases and C_d increases with increasing phase angle (where the force curve is shifted forward in time). The relative rate of decrease or increase of these two coefficients certainly depends on the particular values of the governing parameters. For example, for K = 6.66 (Fig. 14a) C_m decreases rather gradually whereas C_d increases rapidly with increasing phase angle. The reason for this is that for values of K less than about 8 the fluid force is inertia dominated and the inertia coefficient is not very sensitive to small disturbances imposed on it. In mathematical terms the foregoing simply means that the force curve is like a sine curve and that when it is shifted right or left by some amount and then multiplied with $\sin\theta$, as in Eq. (3), the integral could not be too sensitive to the phase difference. The drag coefficient, on the other hand,

is extremely sensitive to small phase shifts in the inertia dominated region simply because a small phase shift in a "sine-like" curve multiplied with $|\cos\theta|\cos\theta$, as in Eq. (4), produces large changes.

In the drag-inertia dominated regime (K ranging from about 8 to 20) both C_d and C_m are affected, as seen in Figs. 14c and 14d. In the drag dominated regime, however, C_d is hardly affected by phase shifts; whereas C_m shows a dramatic drop with increasing phase angle (Fig. 14e). The reason for this is easily explainable in a manner similar to that previously presented in connection with Fig. 14a.

The overall conclusion to be drawn from the foregoing is that there is *no* flow regime where one or the other coefficients is not effected by the phase shift. In fact, if a constant phase shift of ± 5 degrees were to be randomly imposed on a series of data obtained with K values ranging from 5 to 100 one would have observed large scatter in C_d and small scatter in C_m for K smaller than about 8; large scatter in both C_d and C_m for K from about 8 to 20; and large scatter in C_m and small scatter in C_d for K larger than about 20. These scatter patterns are invariably observed in the data obtained in the ocean environment. As noted earlier, not all of the phase shift is due to electronic filtering of the data. Some of the phase shift comes from the reduction of the coherence length of the vortices by the disturbances ever-present in the wave field.

Thus the purpose of the foregoing is not to suggest that all phase shifts could be avoided or eliminated but rather to quantify the effects of the phase shift in terms of the expected variation of the force coefficients in order to have a better grasp of the meaning of the observed scatter.

B. RANDOM SQUARE WAVE EFFECTS

The experiments conducted under controlled laboratory conditions are immune to practically all of the disturbances encountered in the ocean environment. Consequently, the vortices have larger coherence lengths and these give rise to maximum values of the semi-peak-to-peak force coefficient $C_F(spp)$.* In the ocean environment, however, the variable wave direction, change of wave velocity with depth, effect of secondary waves with all sorts of harmonics, irregular surface roughness, and numerous other stochastic variables give rise to varying degrees of scatter in the force coefficients based on ocean data. It is important from the engineering point of view to examine the collective impact of these disturbances on the force coefficients. It is understood that very high frequency disturbances imposed on the measured force cannot significantly affect C_d and C_m. On the other hand, disturbances which simulate either in part

---

*This does not imply that perfect coherence leads to maximum values of C_d and C_m. In fact, a force trace resulting from a perfect coherence can be rendered incoherent by a random square wave. The new force trace yields a larger C_m and a smaller C_d.

or in combination a "sine like" or a "cosine like" wave are most effective in causing large changes in C_d and C_m. This follows from the very definition of the inertia and drag coefficients as in Eqs. (3) and (4). Clearly one must examine the effect of randomly imposed disturbances of given frequency and phase shift on the variation of the force coefficients. Such an extensive analysis has been carried out in a manner described as follows. A frequency ratio of f_{sw}/f_t was chosen where f_{sw} is the frequency of the square wave and f_t is the frequency of the periodic oscillation of the flow in the tunnel. Then the square wave was assigned a random amplitude and initial phase shift through the use of a built-in random number generator. The maximum of the disturbance was taken to be the absolute of C_F(spp) (almost equal to the absolute maximum of the measured force). This procedure varied the amplitude of each disturbance by multiplying a random number between +1 and -1 with C_F(spp). Calculations have been performed 1000 times for a given frequency ratio and force trace. Each calculation started with a randomly selected phase angle and followed with square wave fluctuations whose amplitude varied randomly as noted above and whose frequency was fixed by the frequency ratio. Figures 15a through 15e show sample plots of the original force, the disturbed force, and the square wave disturbance. These figures are presented here for the purpose of illustration and not necessarily for the

quantification of the boundaries of the sensitivity envelope.

Figure 16a shows the results obtained in the manner described previously. The two symbols in this figure represent the relative changes in C_m and C_d. The computer program was directed to identify the particular cases in 1000 runs which gave the largest changes in C_m and the corresponding changes in C_d. It is important to emphasize that the change in C_d in Fig. 16a is not the maximum possible change that could have taken place with a suitable square wave disturbance. Thus, Fig. 16a shows that there are certain frequency ratios which cause a large change in C_m with very little change in the corresponding C_d. As expected, disturbances with a frequency ratio of 1.0 yield the largest $\Delta C_m/C_m$ since this nearly corresponds to a sine function. Surprisingly enough, high frequency disturbances have very little effect on the inertia coefficient, at least in the drag-inertia dominated regime (see Fig. 16a). Thus, one can filter out such high frequency disturbances without materially affecting the determination of the force-transfer coefficients.

A similar calculation has been performed with the force trace corresponding to Fig. 16a to determine the maximum change in C_d and the corresponding change in C_m for representative frequency ratios. Figure 16b shows the results obtained in this manner. Several facts are

immediately apparent. C_d is not as sensitive as C_m to the randomly imposed disturbances in the drag-inertia regime even though $\Delta C_d/C_d$ is quite appreciable. This is directly related to the stability of the integral representing C_d, i.e., $|\cos\theta|\cos\theta$ times a square wave.

Figures 17a and 17b show the effect of the disturbances on C_m and C_d in the inertia dominated regime and Figs. 18a and 18b illustrate the similar effects in the drag-inertia dominated regime. It is clear from all of the figures pertaining to the sensitivity of the drag and inertia coefficients that it is not the dominance of the drag or inertia in a given regime that determines the sensitivity of a given coefficient. To be sure, the said effect is present in Figs. 16a through 18b. However, the most significant elements of a disturbance are its frequency and relative magnitude. Disturbances imposed on the force at a frequency ratio of about one or unity will cause major changes in both C_d and C_m irrespective of the flow regime. As to the amplitude of the disturbances, they may depend on a number of parameters such as K, Re, turbulence in ambient flow, interference of other bodies, etc. In the present analysis the maximum amplitude of the disturbances at any frequency were taken to be equal to C_F(spp) of the measured force. Since this coefficient decreases with increasing K, it is easy to understand that at high K values $\Delta C_m/C_m$ or $\Delta C_d/C_d$

will result in values as large as those encountered at smaller K values (see Figs. 16a through 18b).

The significance of these results will be illustrated with a numerical example. Assume K = 14.08, Beta = 4040 (as in Fig. 16a), for which $C_m = 0.61$, $C_d = 1.63$ and $C_F(spp) = 1.66$. For a frequency ratio of $f_{sw}/f_t = 1.0$, one has $\Delta C_m/C_m = 2.7$ and $\Delta C_d/C_d = 0.91$ from Figs. 16a and 16b. Assuming a disturbance amplitude equal to 10 percent of $C_F(spp)$, one has:

$$C_d(\text{perturbed value}) = (1 \pm \Delta C_d/C_d * \%C_F(spp)) * C_d(\text{original value})$$

$$= (1 \pm 0.91 * 0.10) * 1.63 = \begin{matrix} 1.78 \\ 1.48 \end{matrix}$$

and

$$C_m(\text{perturbed value}) = (1 \pm \Delta C_m/C_m * \%C_F(spp)) * C_m(\text{original value})$$

$$= (1 \pm 2.7 * 0.10) * 0.61 = \begin{matrix} 0.77 \\ 0.45 \end{matrix}$$

The foregoing examples show that a random disturbance of frequency ratio 1.0, imposed on a particular force, may have resulted in relatively large cycle to cycle variations of the force coefficients. Here C_d varies from a minimum

value of 1.48 to a maximum value of 1.78 and C_m varies from a minimum value of 0.45 to a maximum value of 0.77. These are relatively large changes and show clearly the importance of the following two factors. First, it is not possible to obtain scatter-free data in the ocean environment even for a single K and Re because of the ever-present random disturbances emanating from various sources. Secondly, a structure cannot be designed to withstand the maximum forces predicted on the basis of idealized laboratory experiments because the maximum forces may occur only in a small fraction of the lifespan of the structure. Clearly, beyond this point one has to make subjective decisions regarding the probability of the occurrence of maximum force. Figures similar to 16a through 18b enable one to predict the force coefficients which would have prevailed under less favorable conditions (reduced coherence, directional waves, body interference, etc.).

VII. CONCLUSIONS

The forces acting on yawed smooth and rough circular cylinders in sinusoidally oscillating uniform flow have been extensively investigated, and the following conclusions have been reached:

1. The independence principle does not apply over significant portions of the range of K values investigated. The drag and inertia coefficients differ significantly from those deduced from the 90-degree case for all 45-degree and 60-degree smooth and rough cylinder cases.

2. The effect of roughness is to bring the yawed and unyawed cylinder force-coefficients closer, except in the drag-inertia dominated regime.

3. Yaw has a very strong effect on the coherence of vortices and hence on the transverse force coefficient, particularly in the drag-inertia dominated regime. The lift coefficient is largest for the 90-degree cylinder, as might have been expected, and decreases sharply with yaw.

4. An extensive sensitivity analysis has shown that the force-transfer coefficients are affected by the phase shift between force and velocity to various amounts dependent on the flow regime and the magnitude of the phase shift.

5. Finally, the results have shown that the force coefficients and the validity of the Morison equation are

sensitive to disturbances imposed on the in-line force, particularly in the frequency range where the disturbance frequency matches the wave frequency. The stability envelope has been delineated through extensive calculations to enable one to interpret the scatter of the data obtained in the ocean environment.

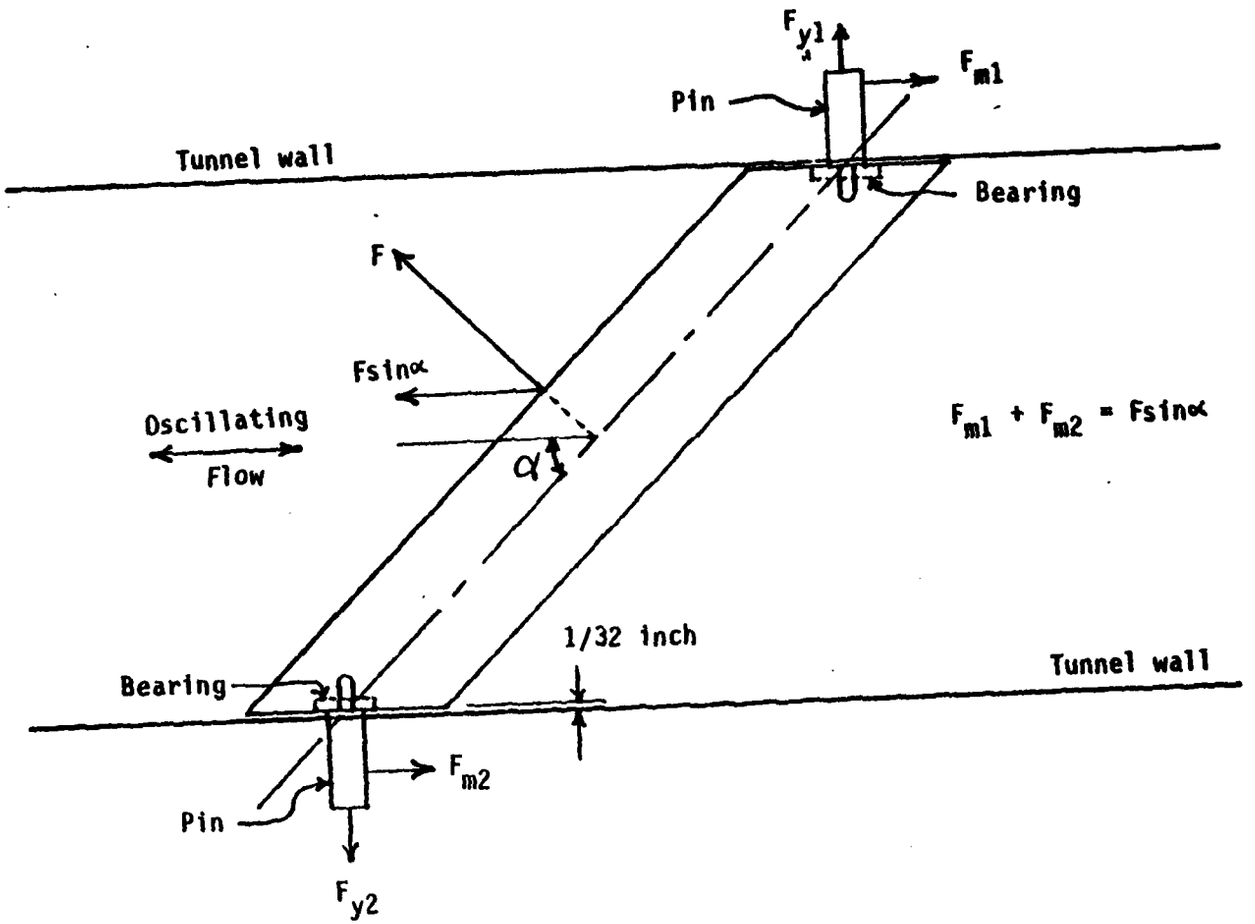

Figure 1. Schematic of Cylinder Installation and Calibration.

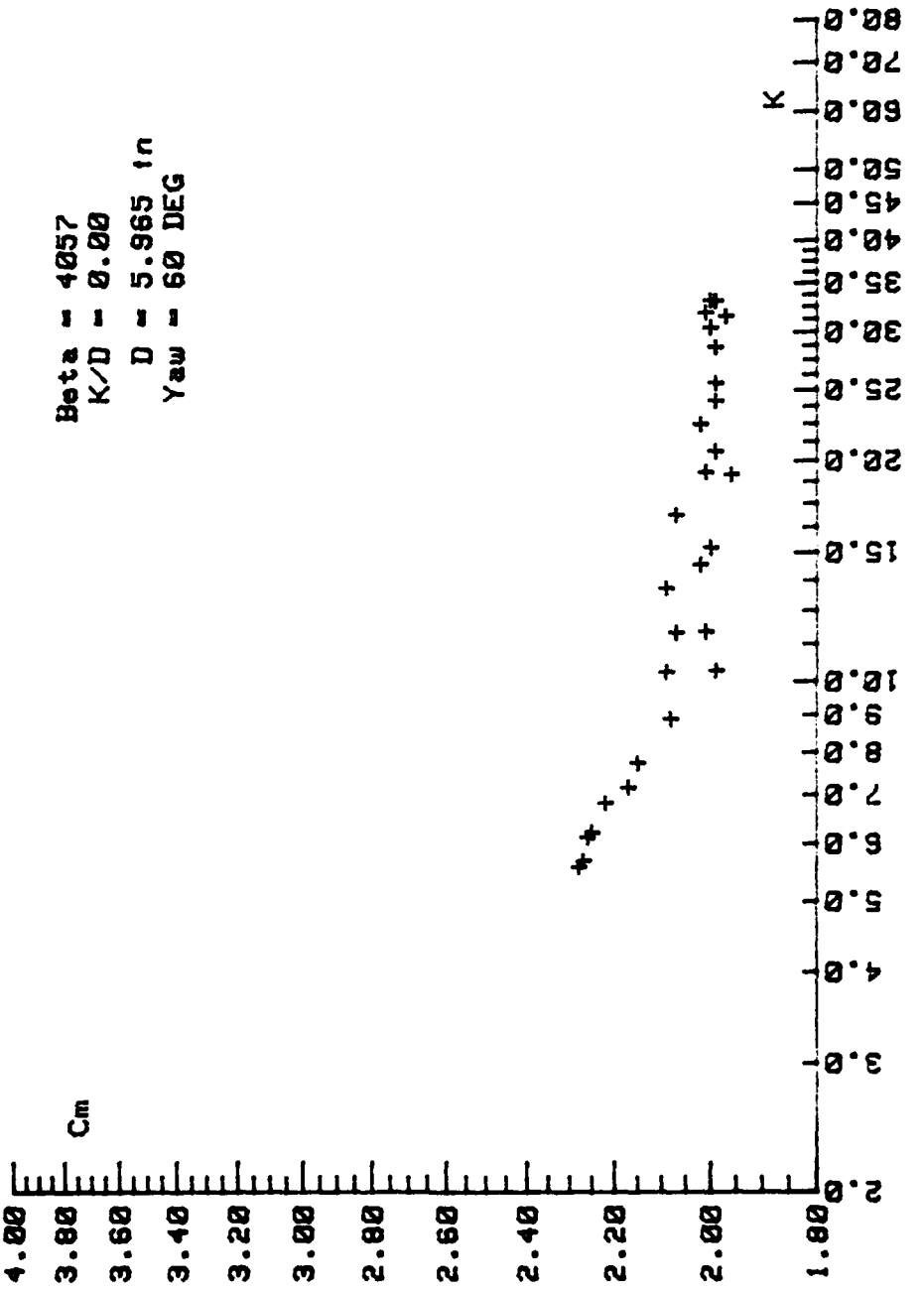

Figure 2a. C_m Versus K for β = 4057, α = 60 Deg., k/D = 0.00.

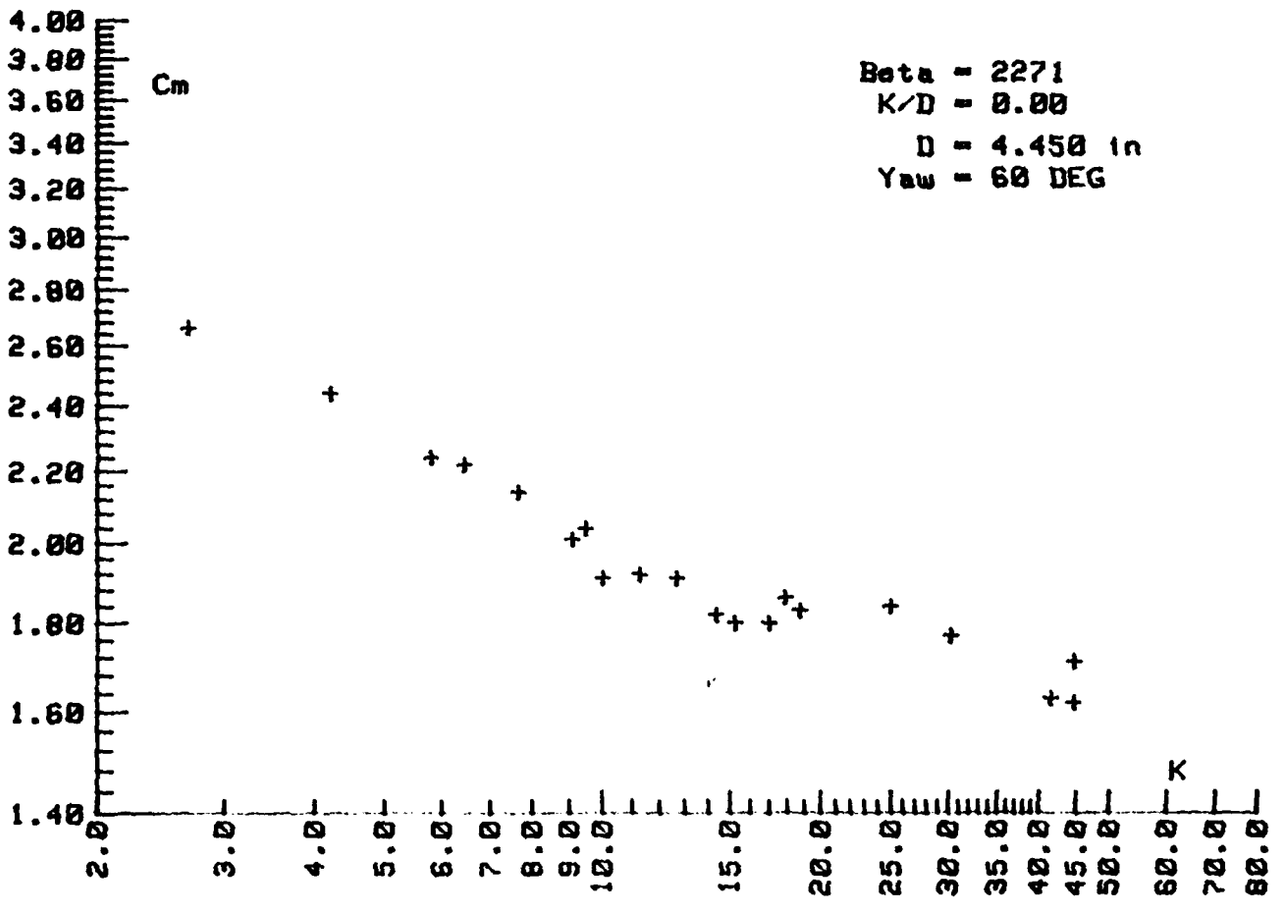

Figure 2b. C_m Versus K for β = 2271, α = 60 Deg., k/D = 0.00.

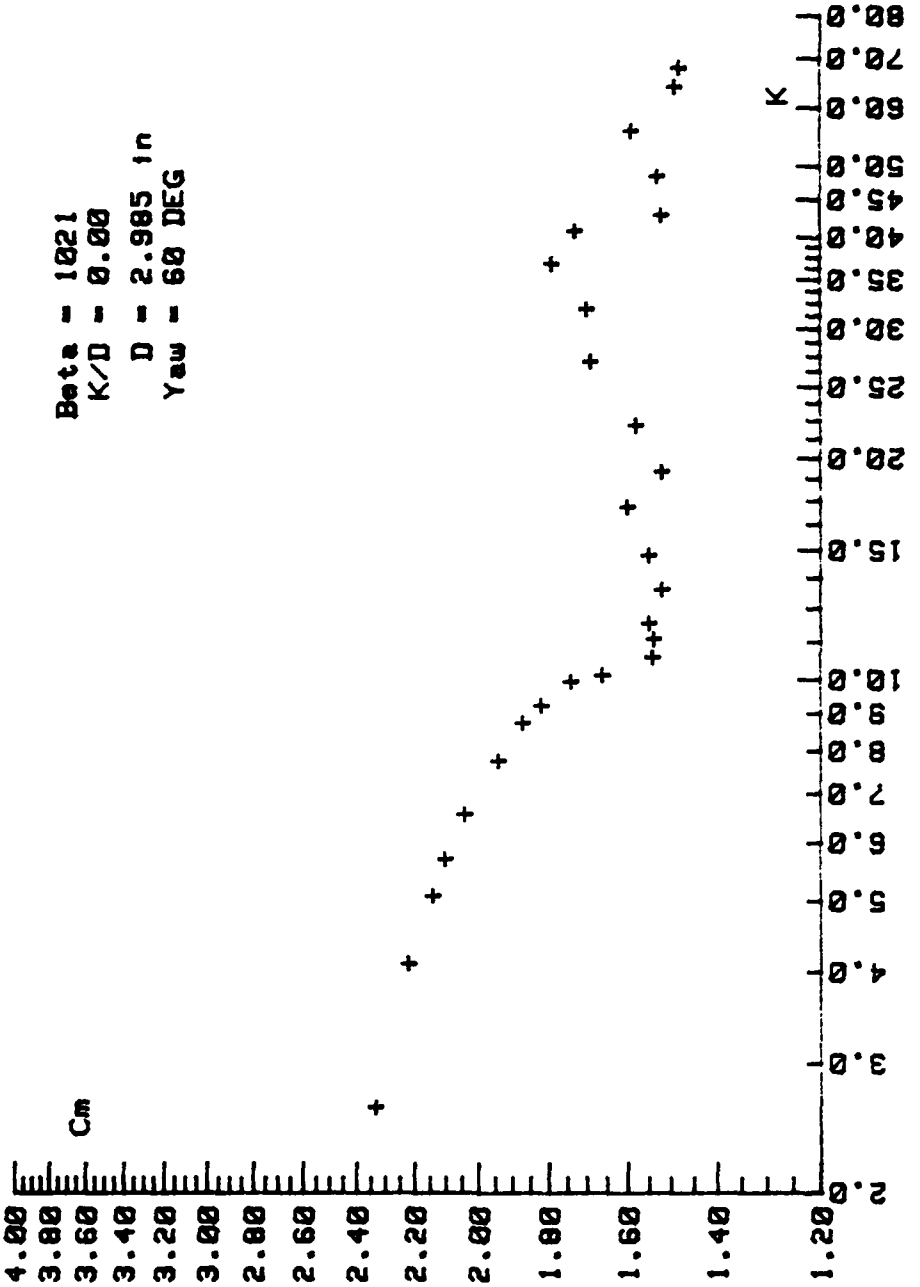

Figure 2c. C_m Versus K for β = 1021, α = 60 Deg., k/D = 0.00.

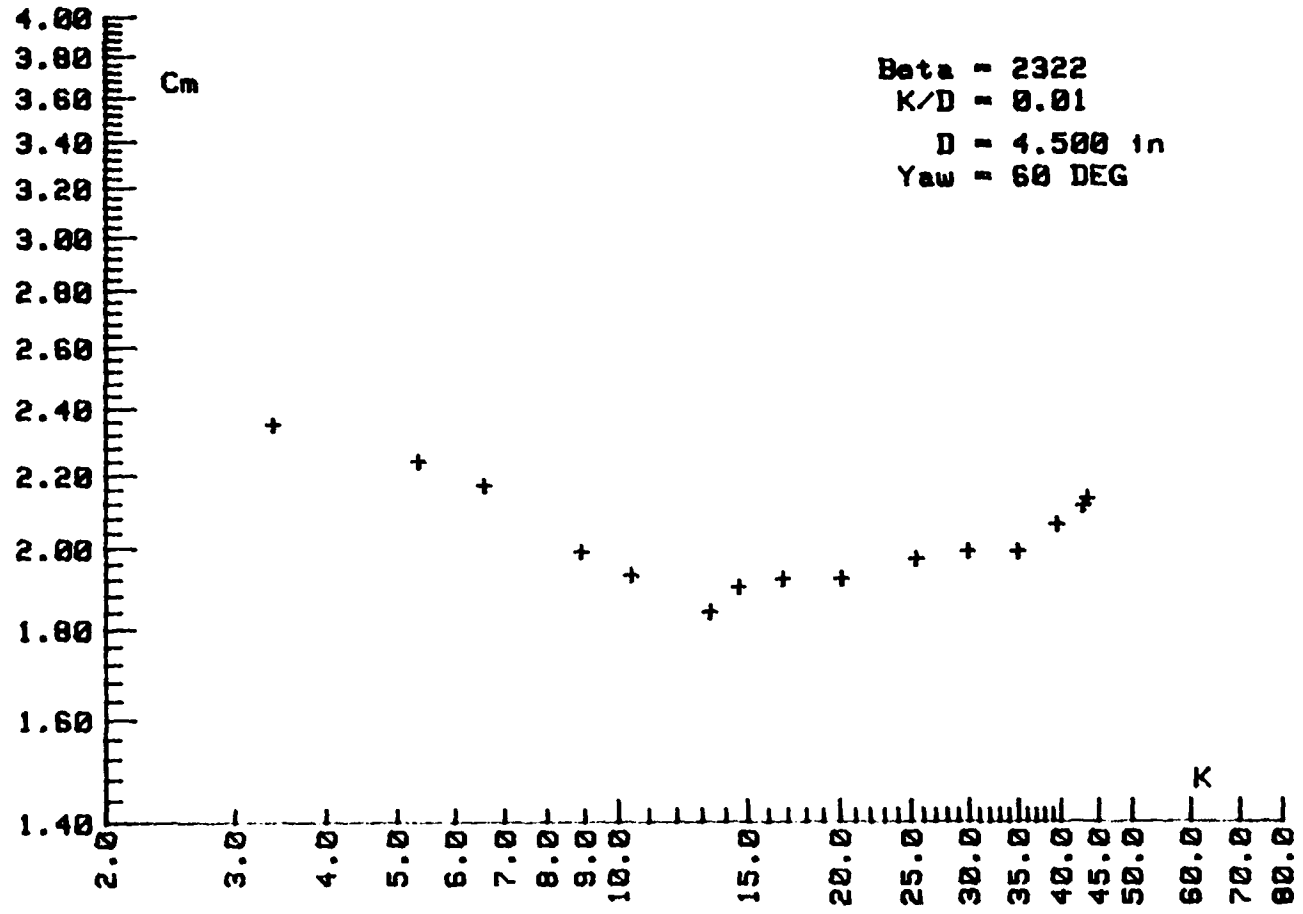

Figure 2d. C_m Versus K for β = 2322, α = 60 Deg., k/D = 0.01.

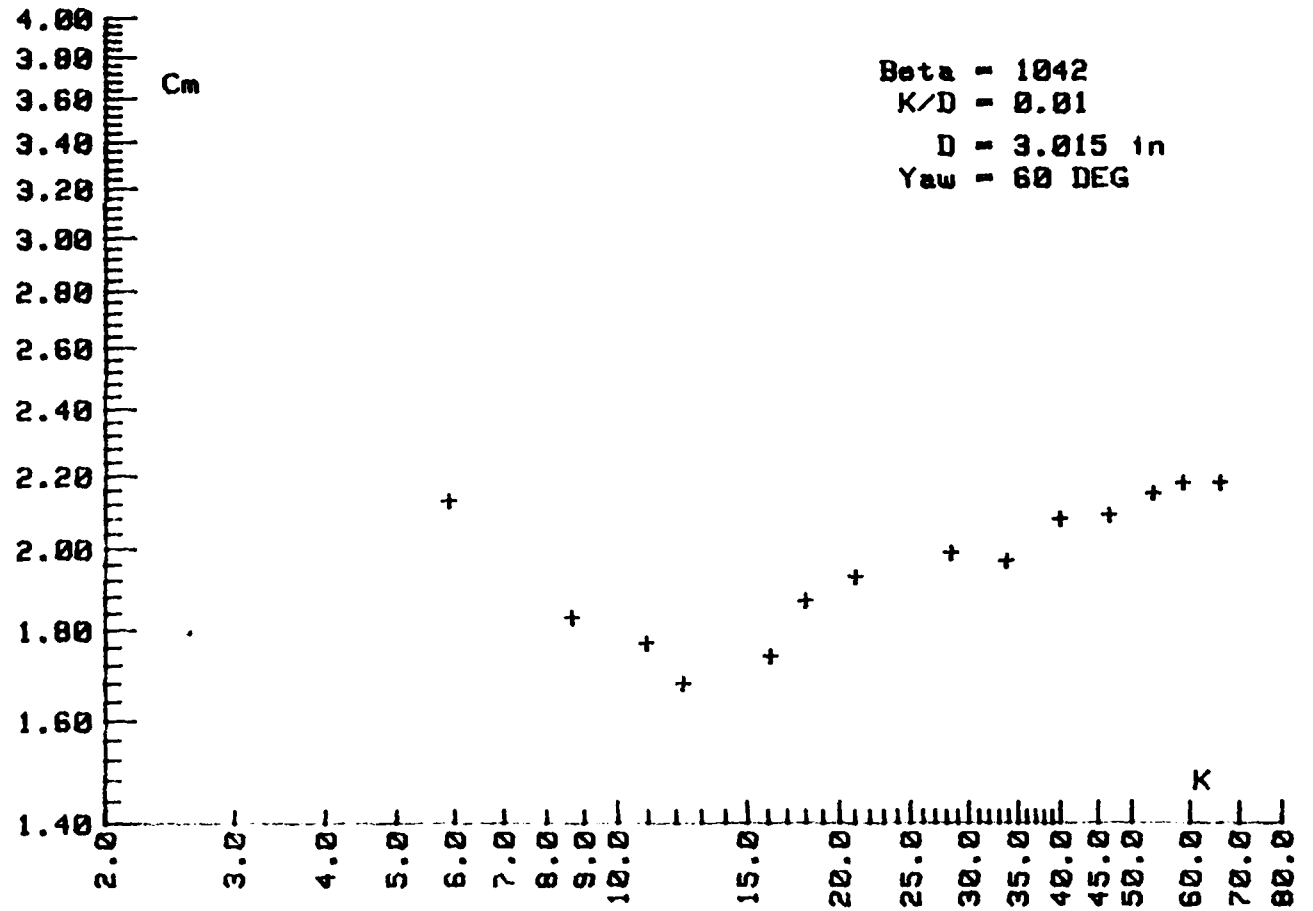

Figure 2e. C_m Versus K for β = 1042, α = 60 Deg., k/D = 0.01.

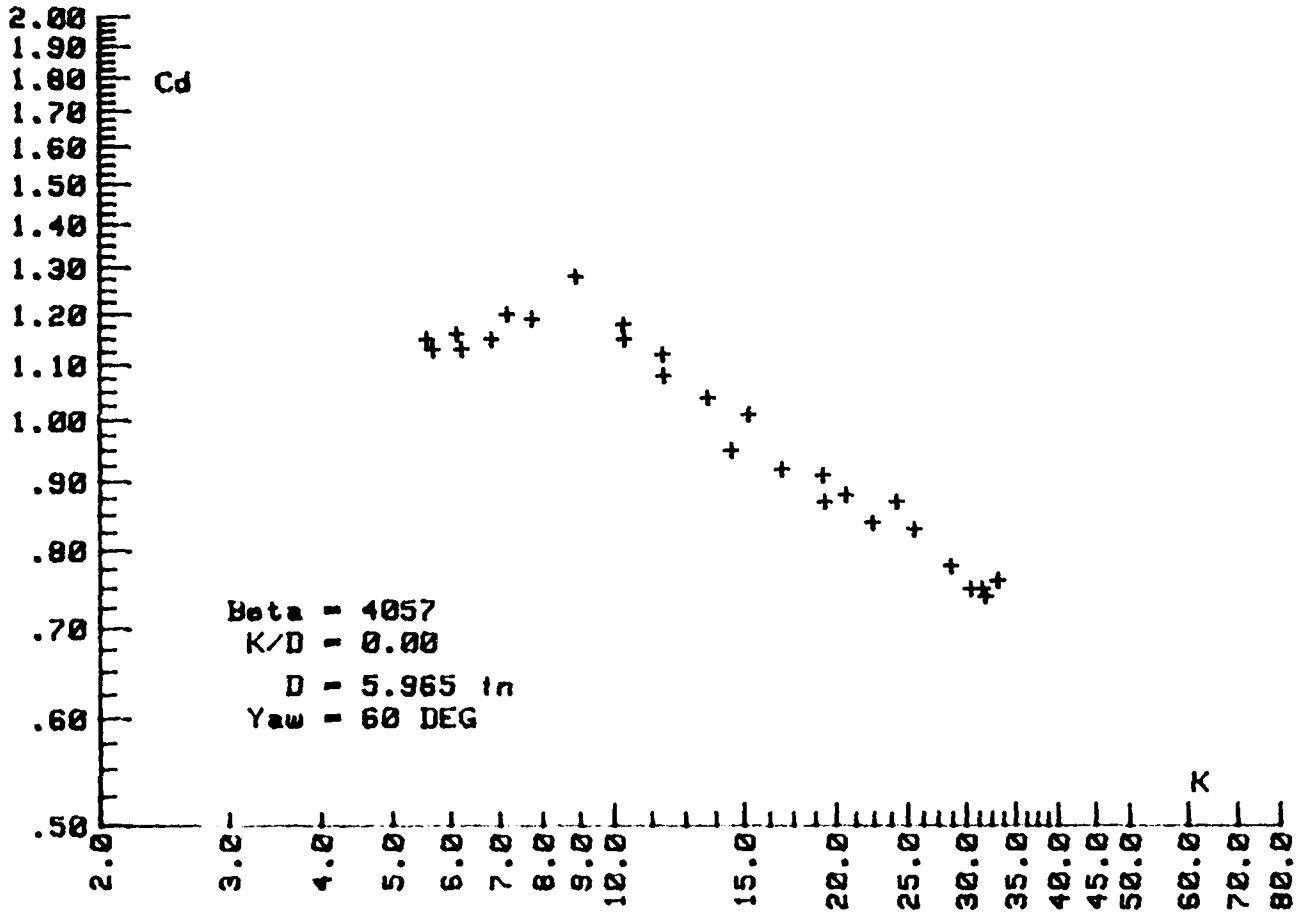

Figure 3a. C_d Versus K for β = 4057, α = 60 Deg., k/D = 0.00.

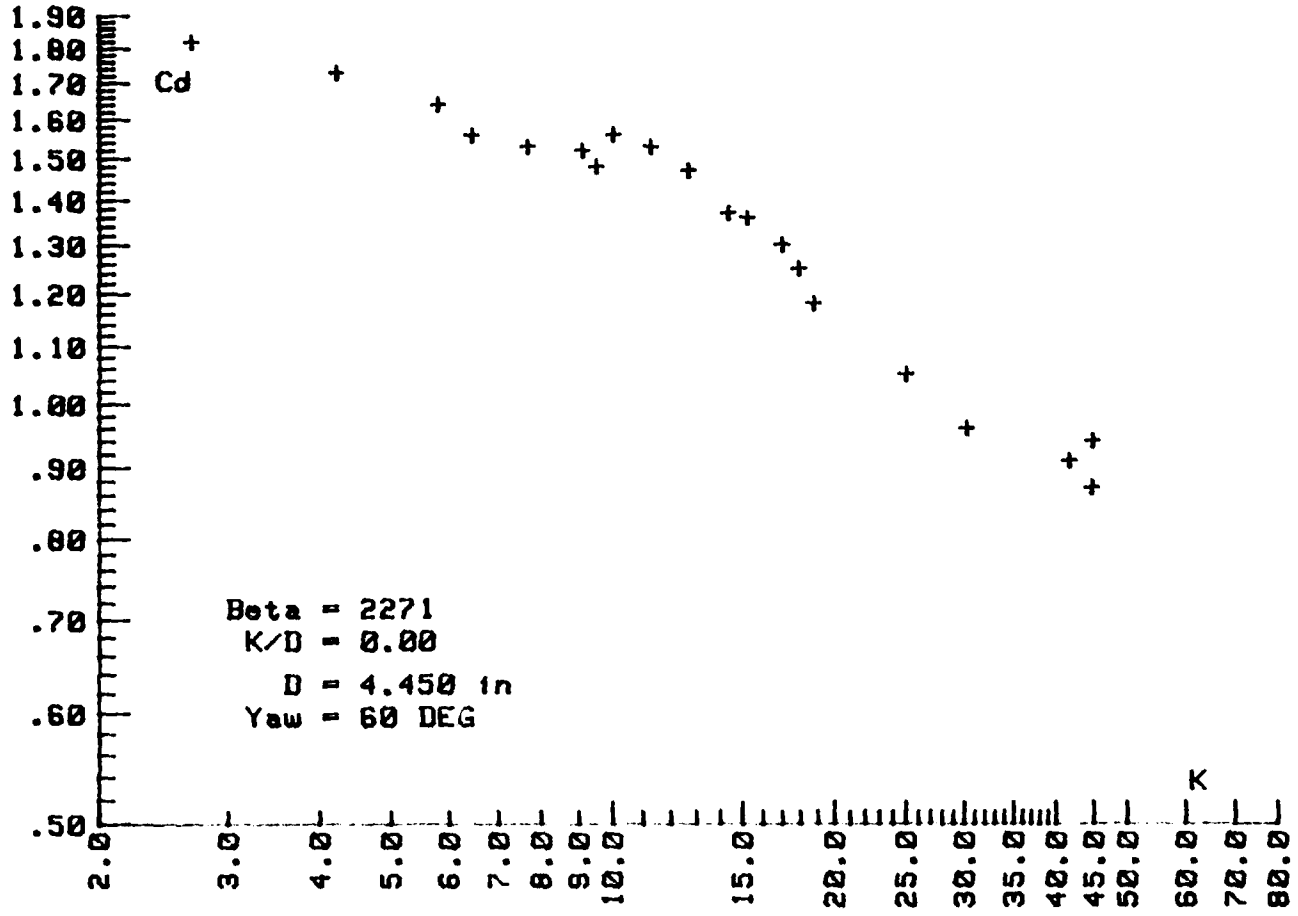

Figure 3b. C_d Versus K for β = 2271, α = 60 Deg., k/D = 0.00.

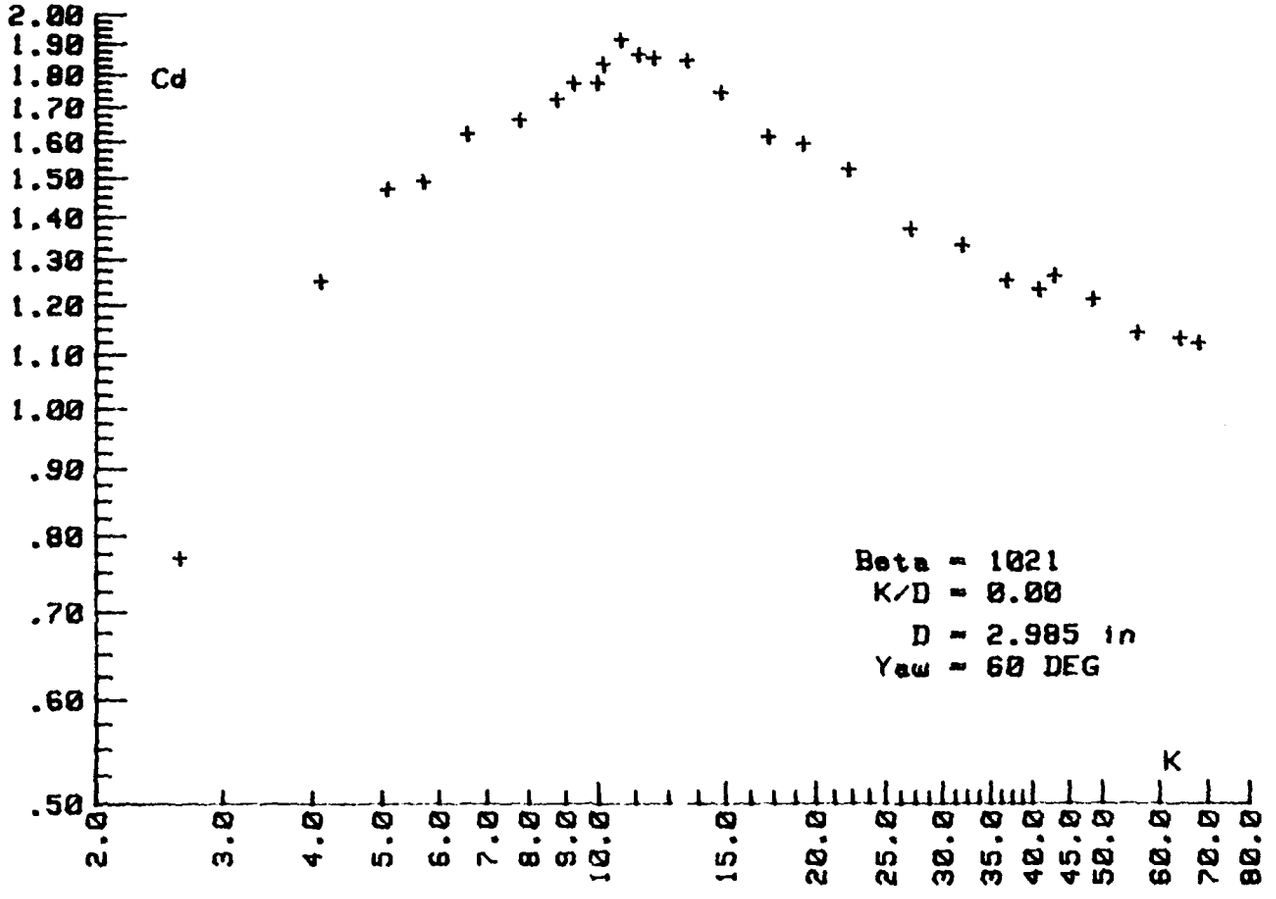

Figure 3c. C_d Versus K for β = 1021, α = 60 Deg., k/D = 0.00.

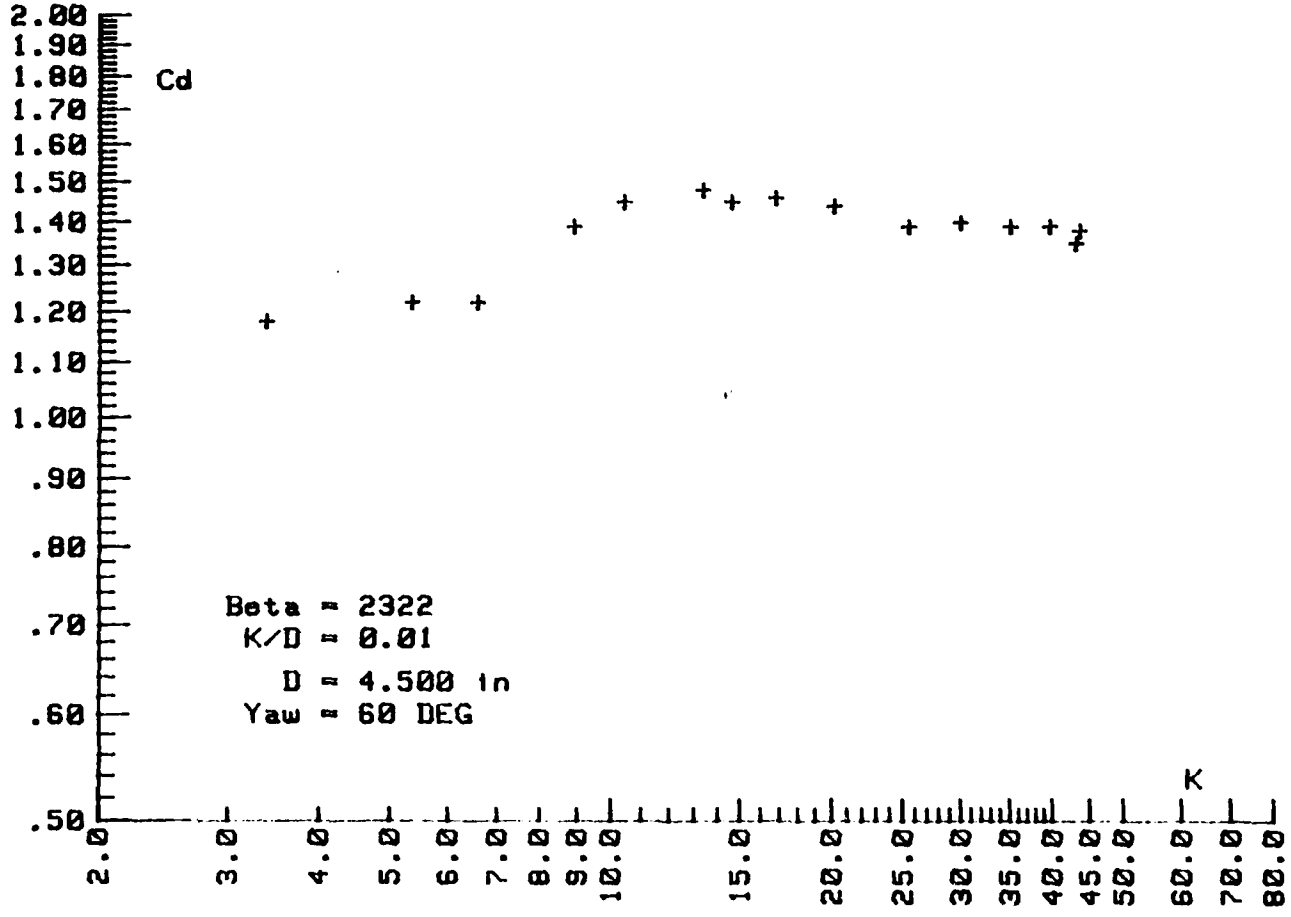

Figure 3d. C_d Versus K for β = 2322, α = 60 Deg., k/D = 0.01.

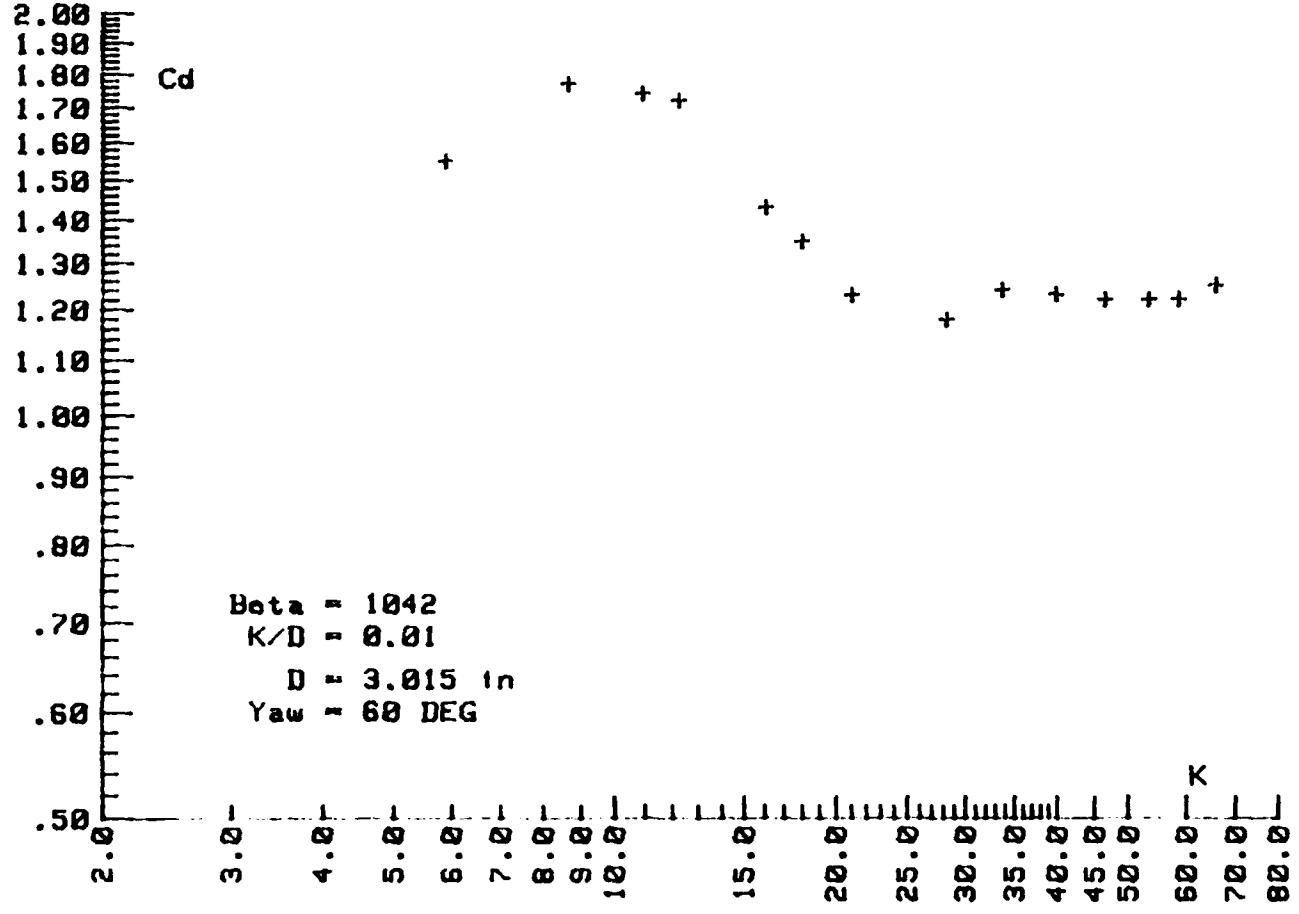

Figure 3e. C_d Versus K for β = 1042, α = 60 Deg., k/D = 0.01.

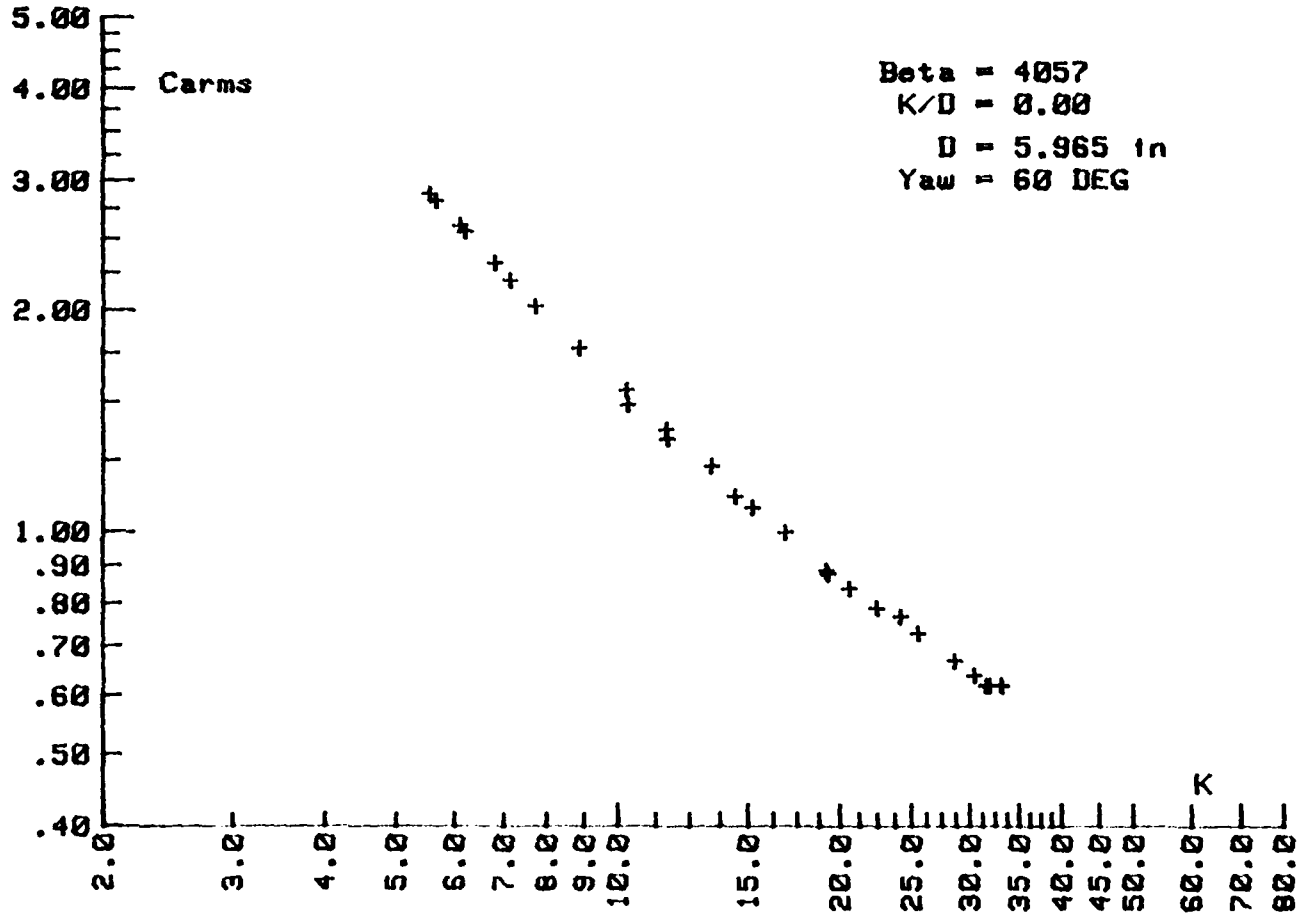

Figure 4a. C_{arms} Versus K for β = 4057, α = 60 Deg., k/D = 0.00.

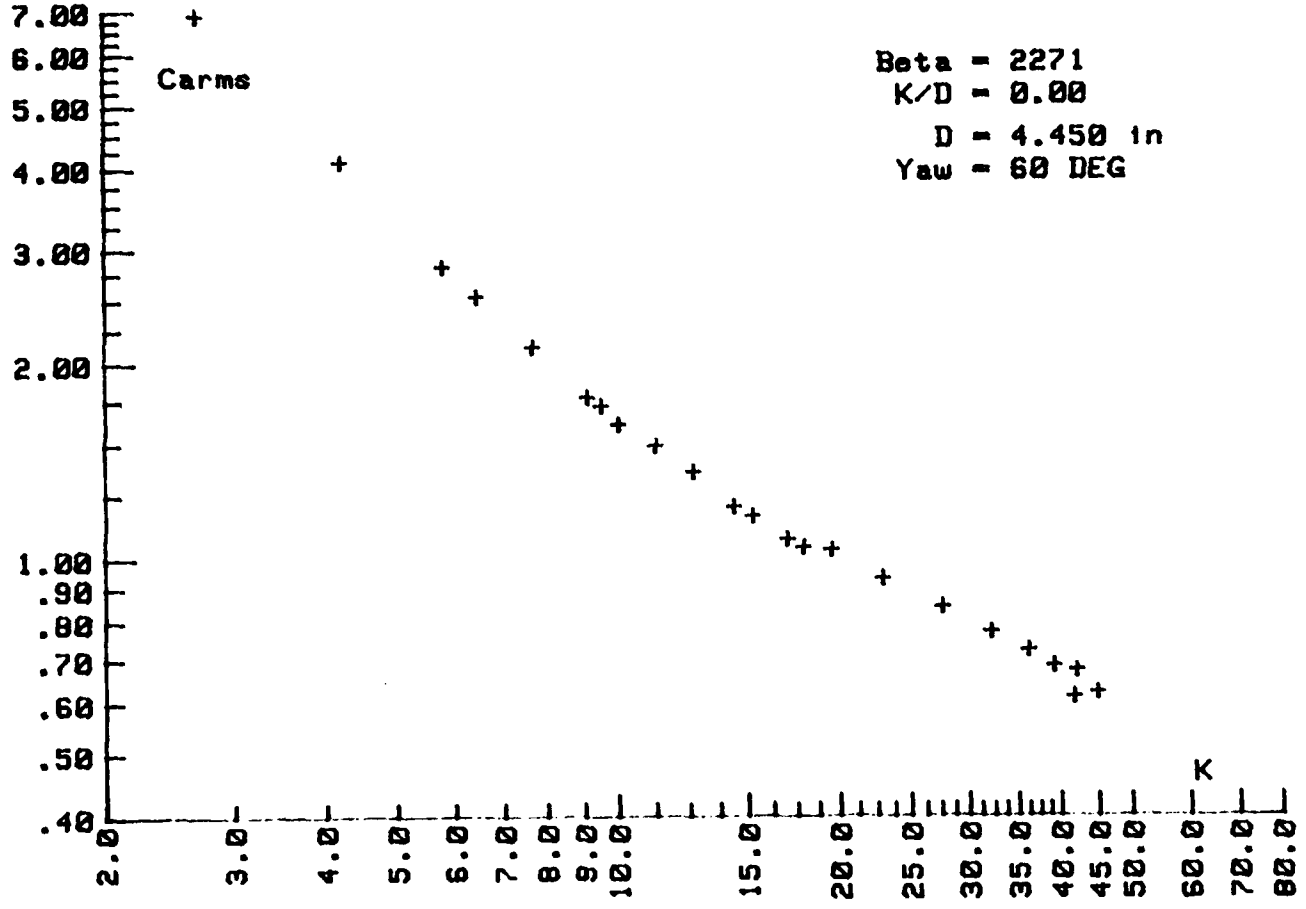

Figure 4b. C_{arms} Versus K for β = 2271, α = 60 Deg., k/D = 0.00.

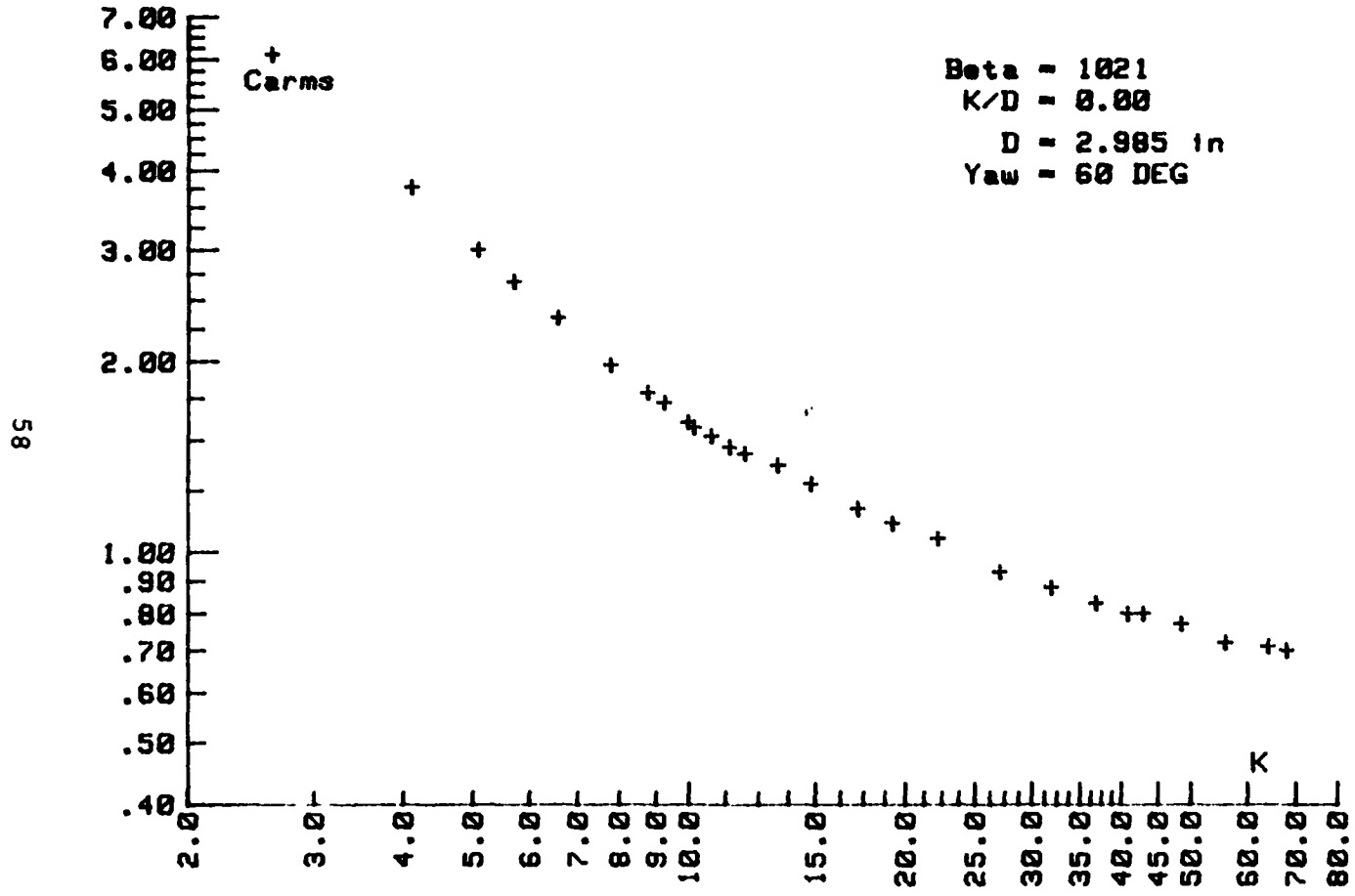

Figure 4c. C_{arms} Versus K for β = 1021, α = 60 Deg., k/D = 0.00.

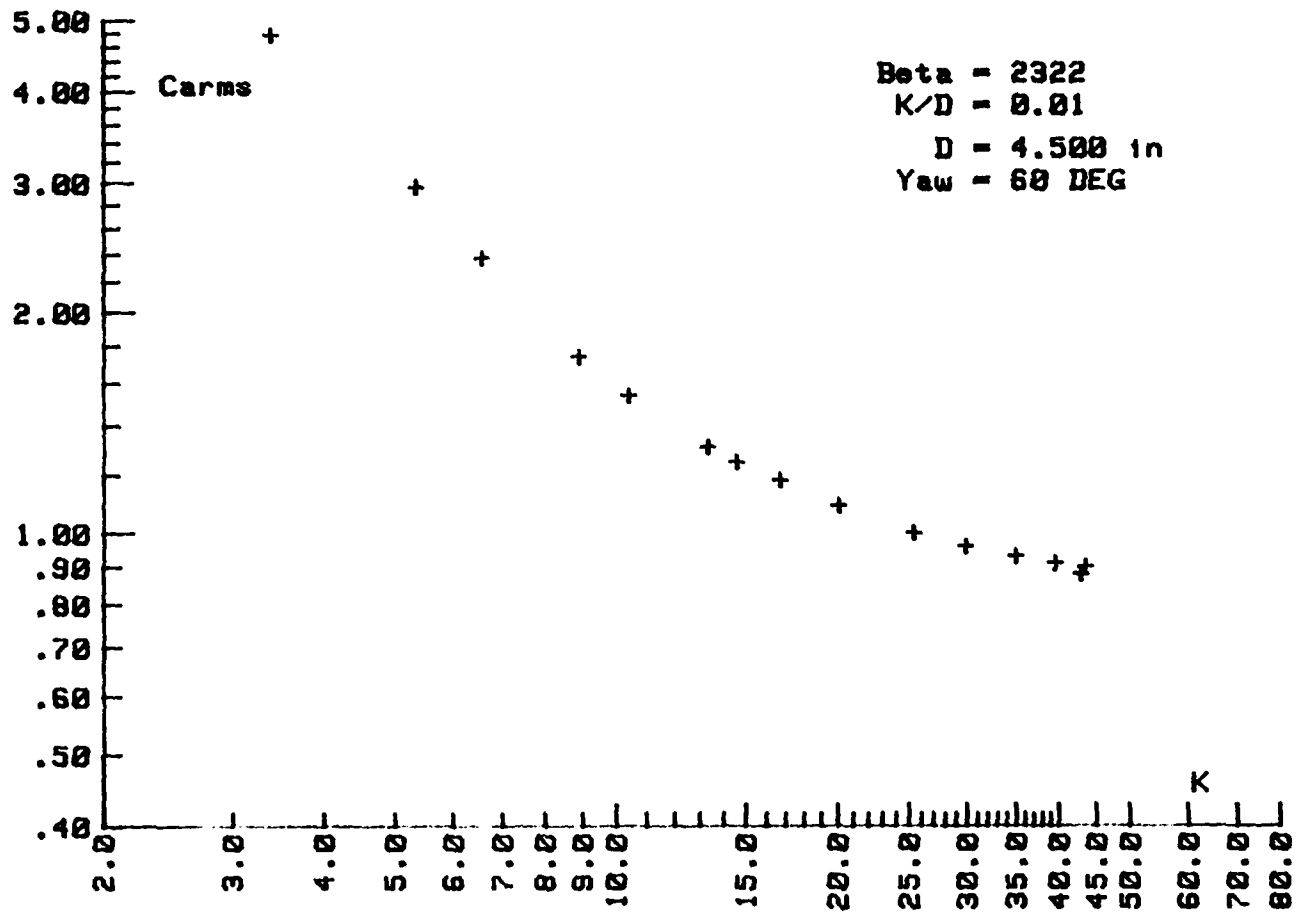

Figure 4d. C_{arms} Versus K for β = 2322, α = 60 Deg., k/D = 0.01.

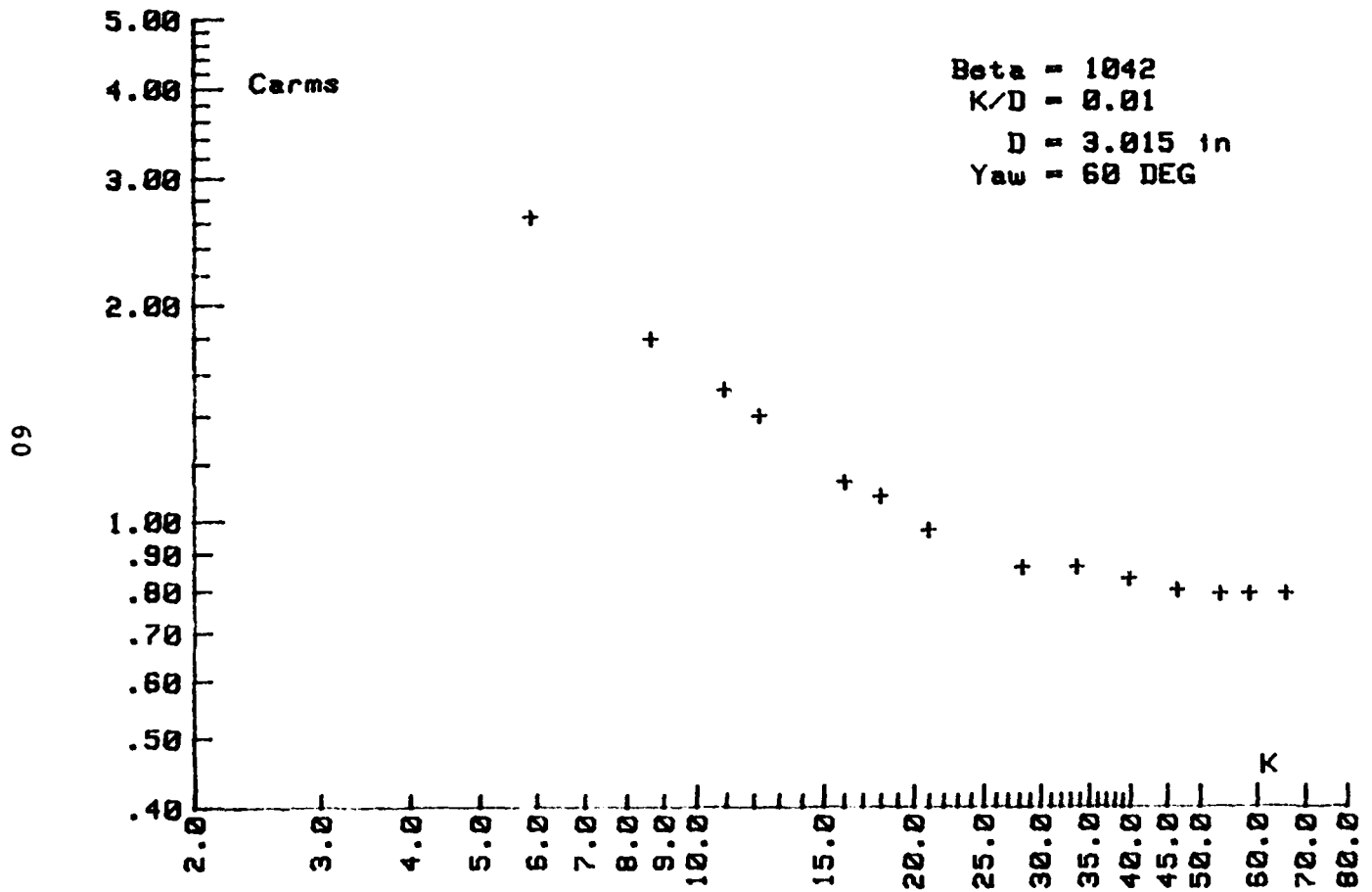

Figure 4e. C_{arms} Versus K for β = 1042, α = 60 Deg., k/D = 0.01.

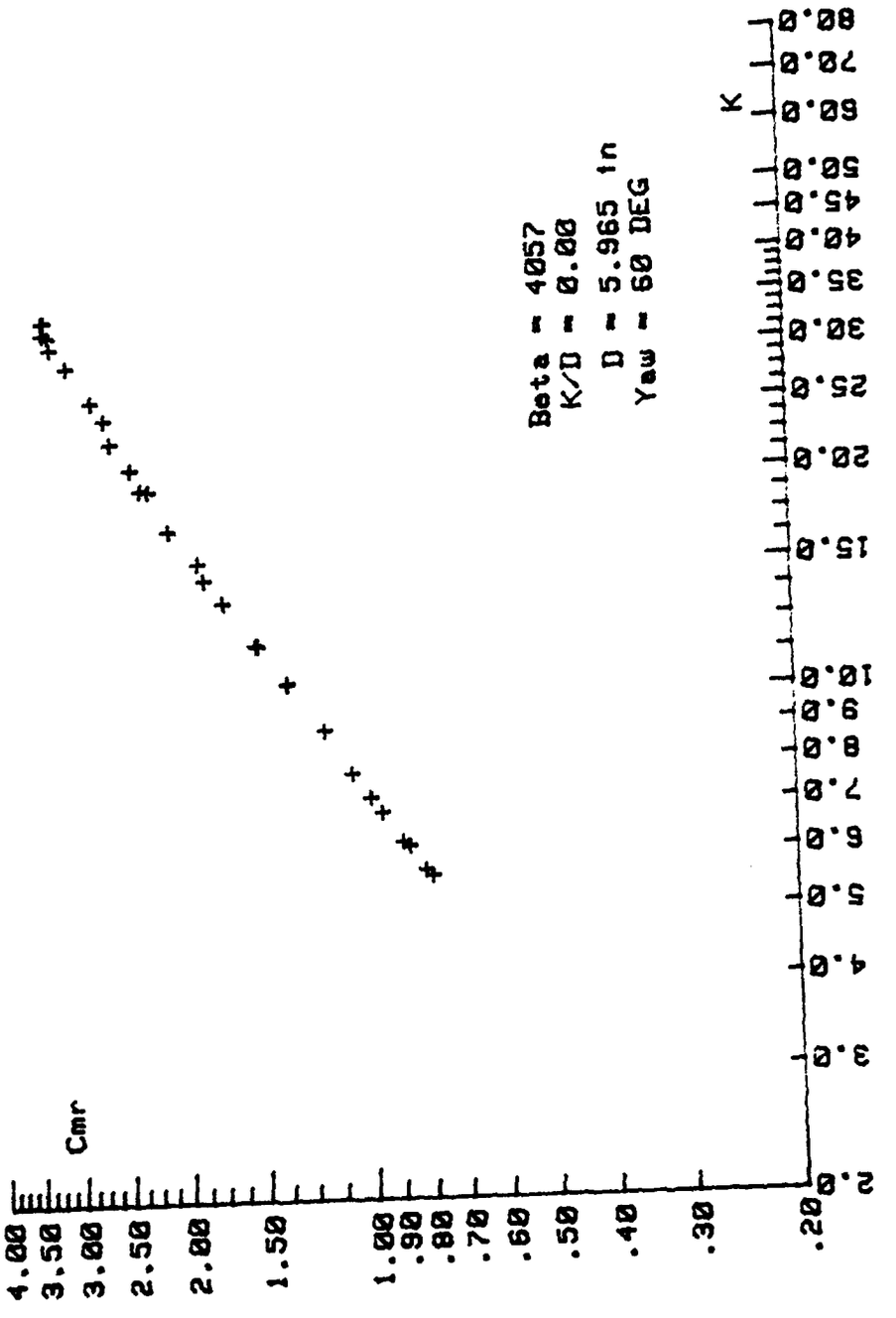

Figure 5a. C_{mr} Versus K for β = 4057, α = 60 Deg., k/D = 0.00.

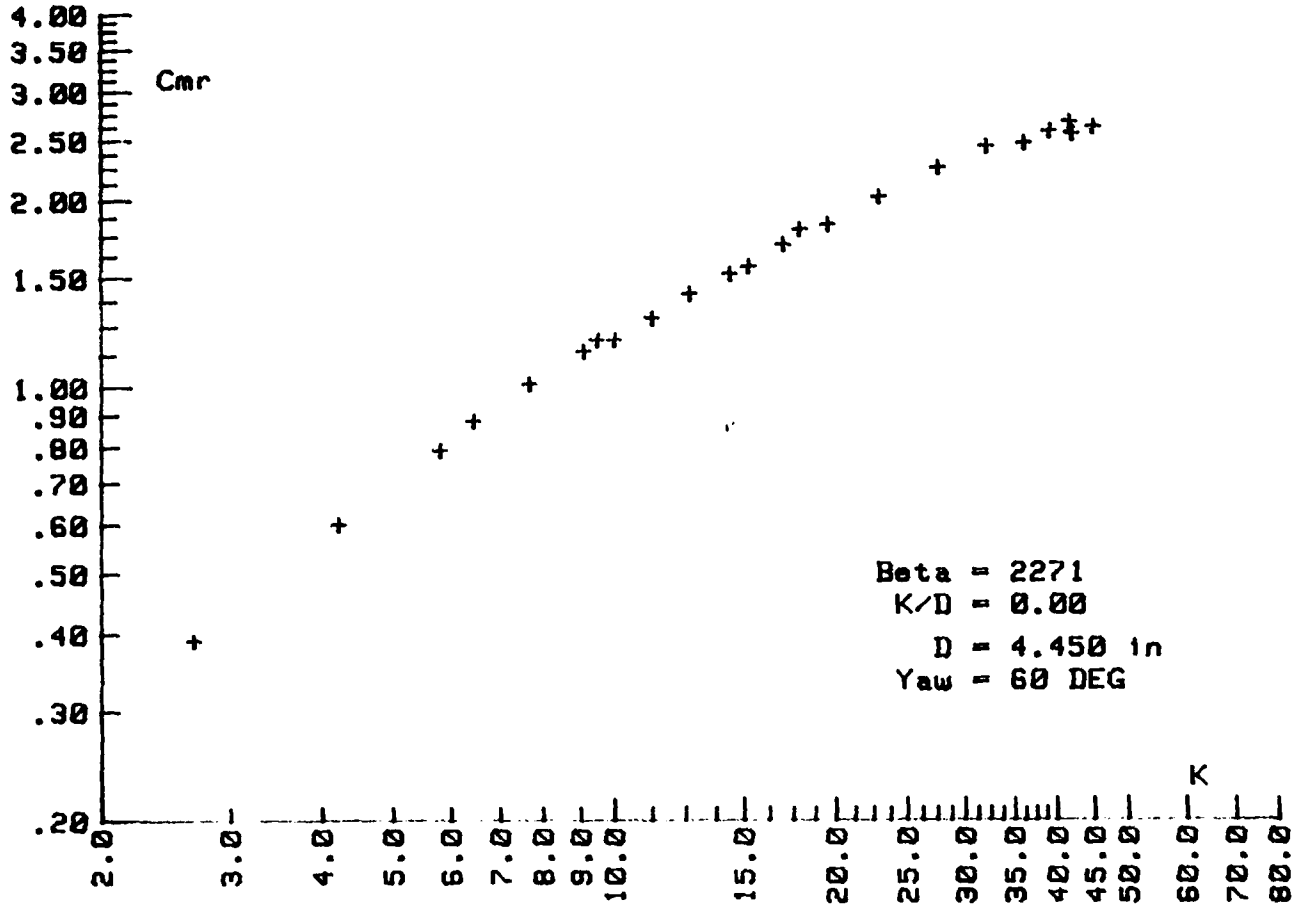

Figure 5b. C_{mr} Versus K for β = 2271, α = 60 Deg., k/D = 0.00.

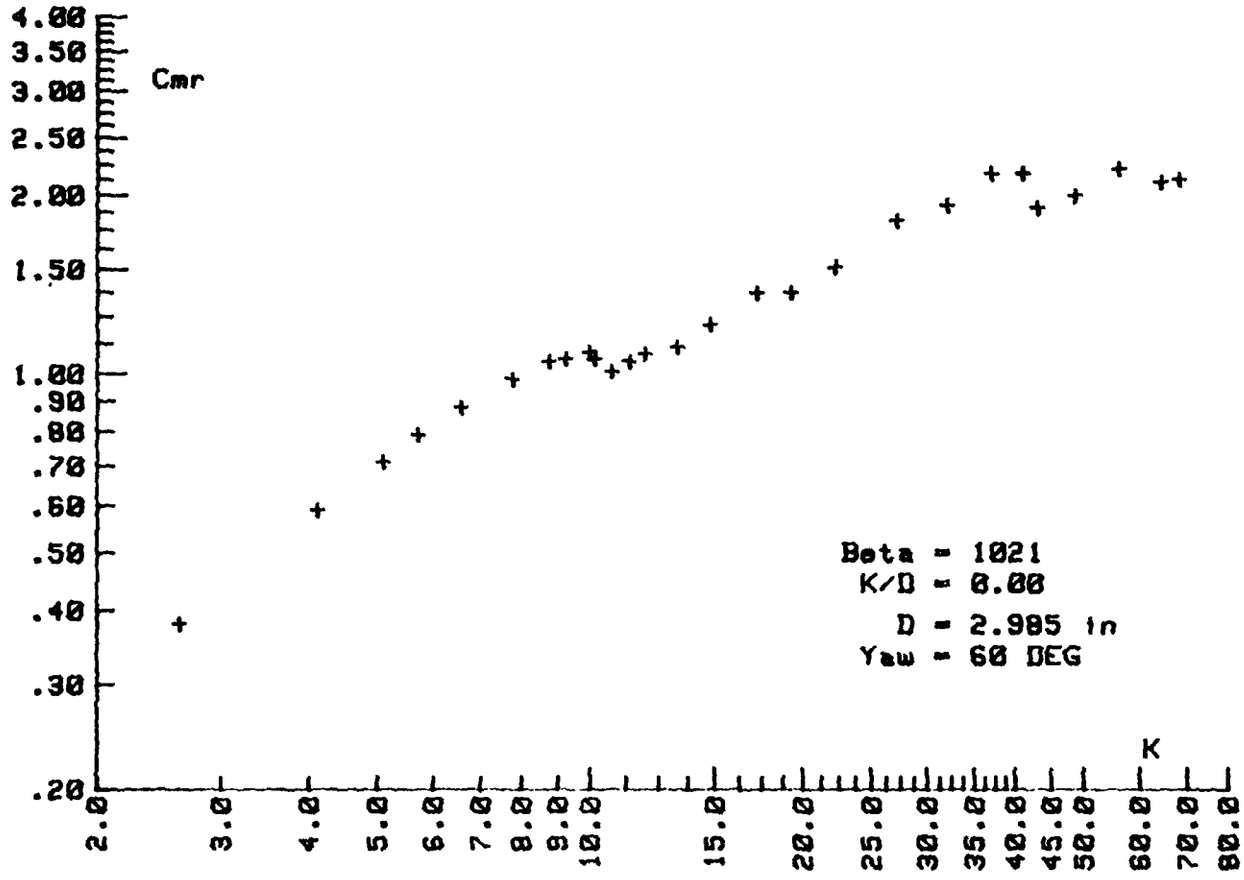

Figure 5c. C_{mr} Versus K for β = 1021, α = 60 Deg., k/D = 0.00.

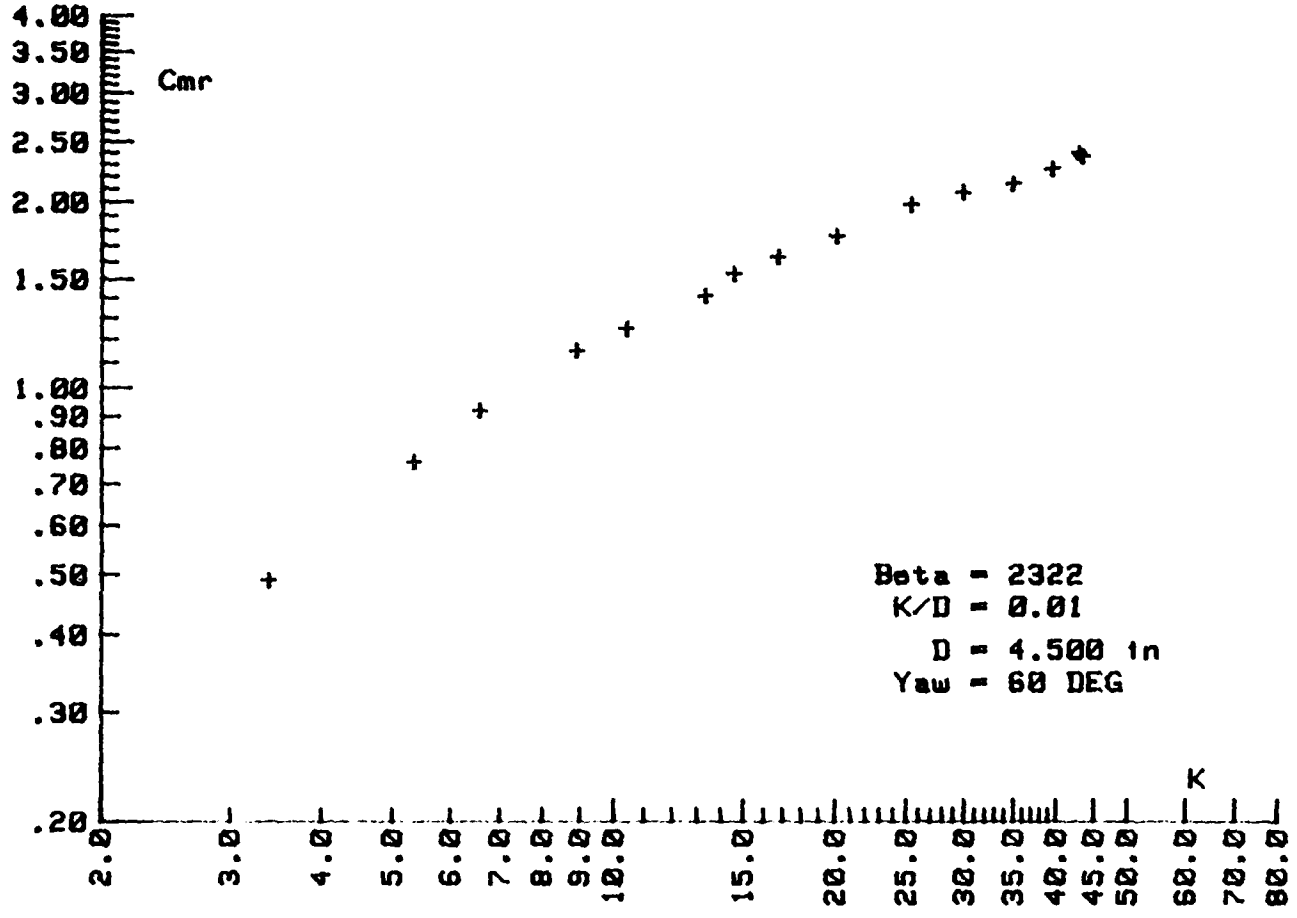

Figure 5d. C_{mr} Versus K for β = 2322, α = 60 Deg., k/D = 0.01.

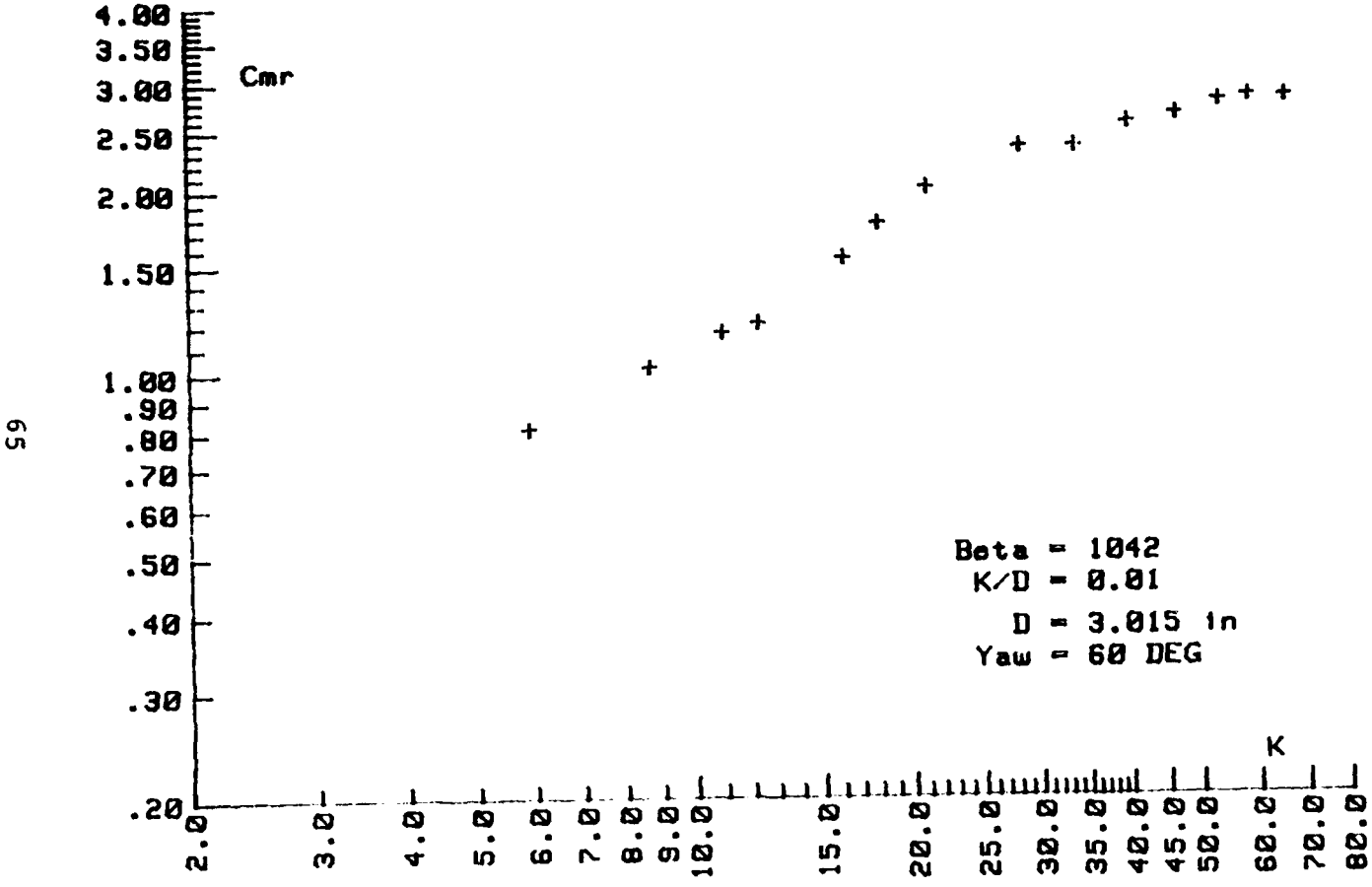

Figure 5e. C_{mr} Versus K for β = 1042, α = 60 Deg., k/D = 0.01.

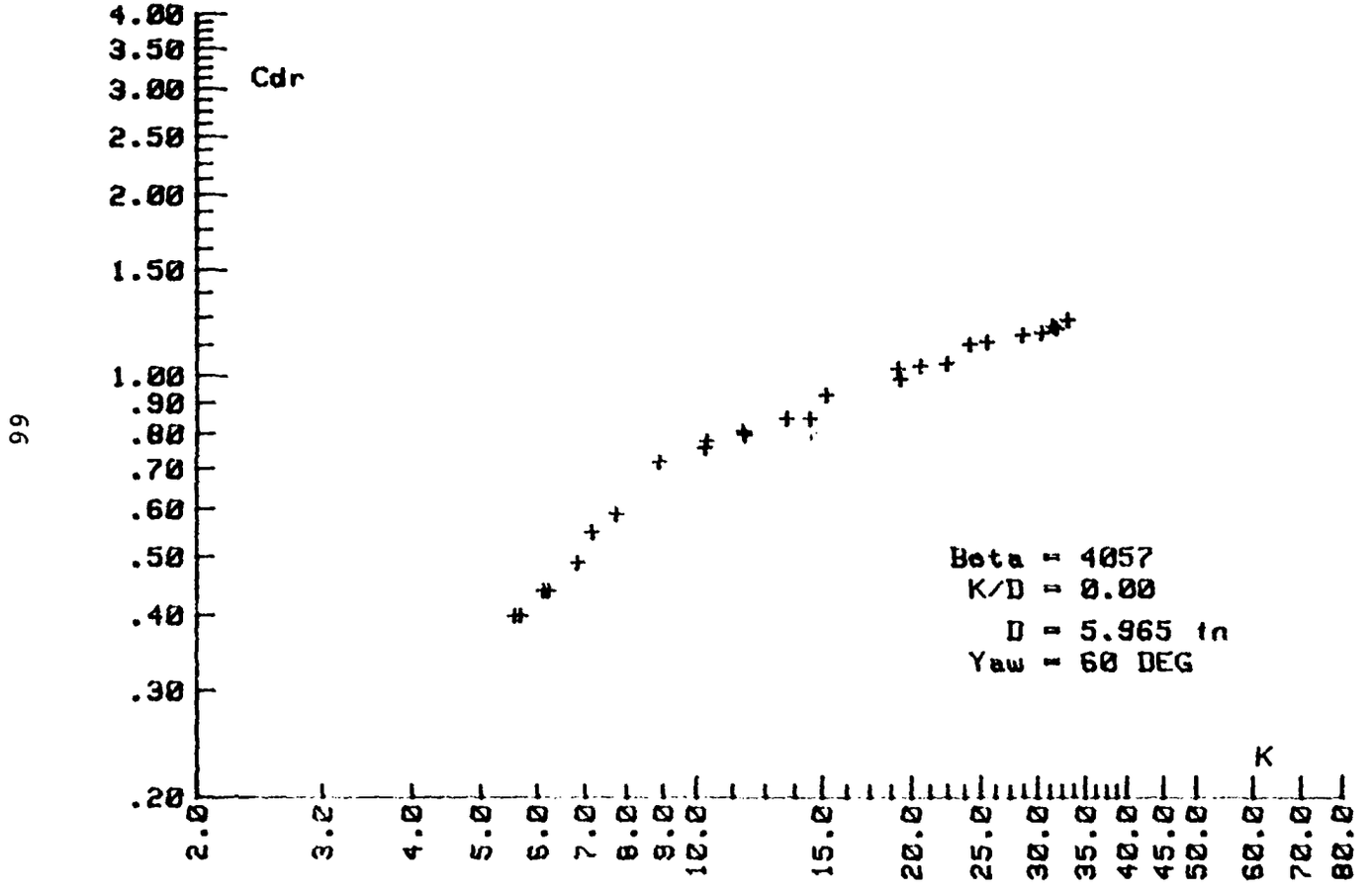

Figure 6a. C_{dr} Versus K for β = 4057, α = 60 Deg., k/D = 0.00.

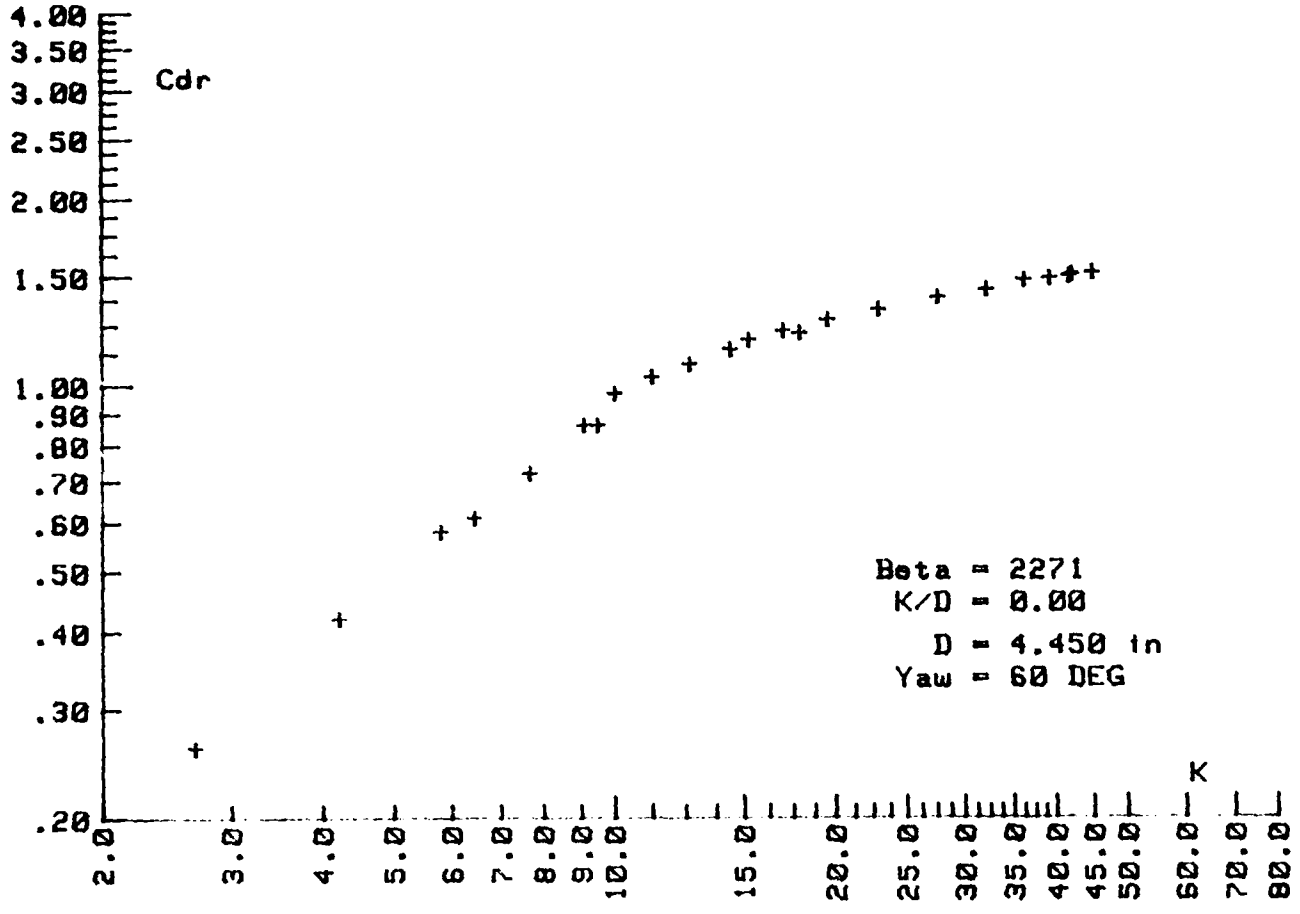

Figure 6b. C_{dr} Versus K for β = 2271, α = 60 Deg., k/D = 0.00.

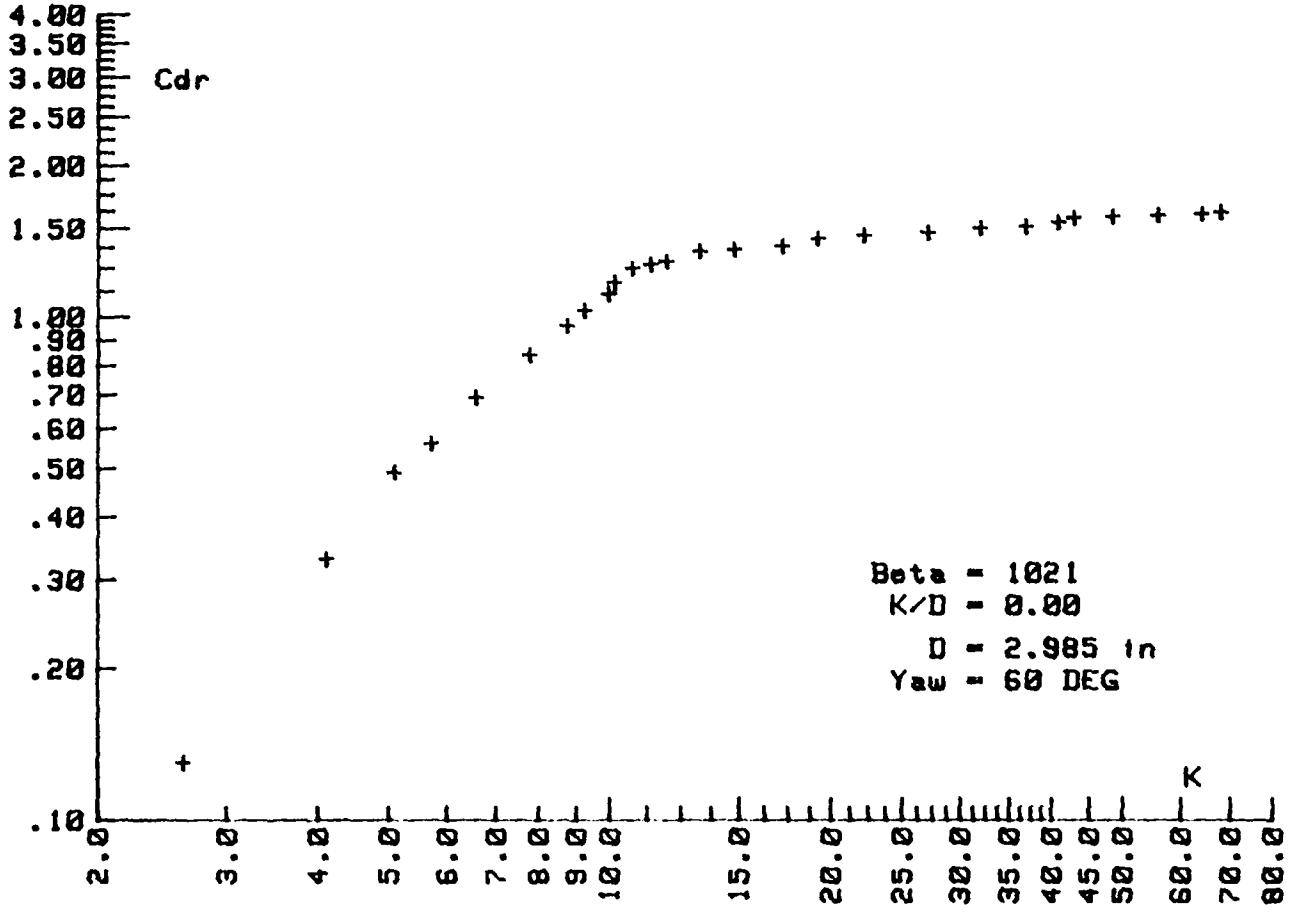

Figure 6c. C_{dr} Versus K for β = 1021, α = 60 Deg., k/D = 0.00.

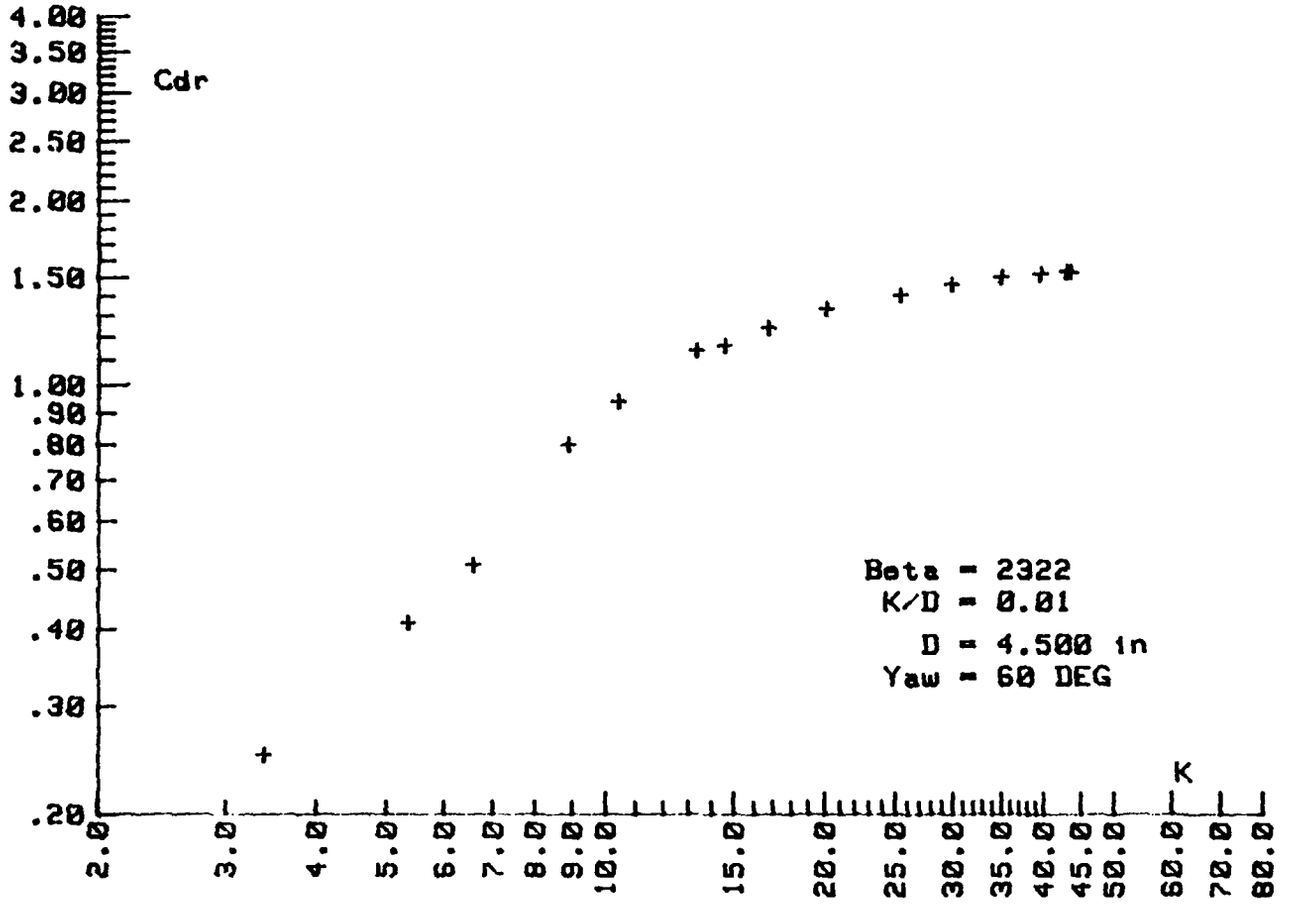

Figure 6d. C_{dr} Versus K for β = 2322, α = 60 Deg., k/D = 0.01.

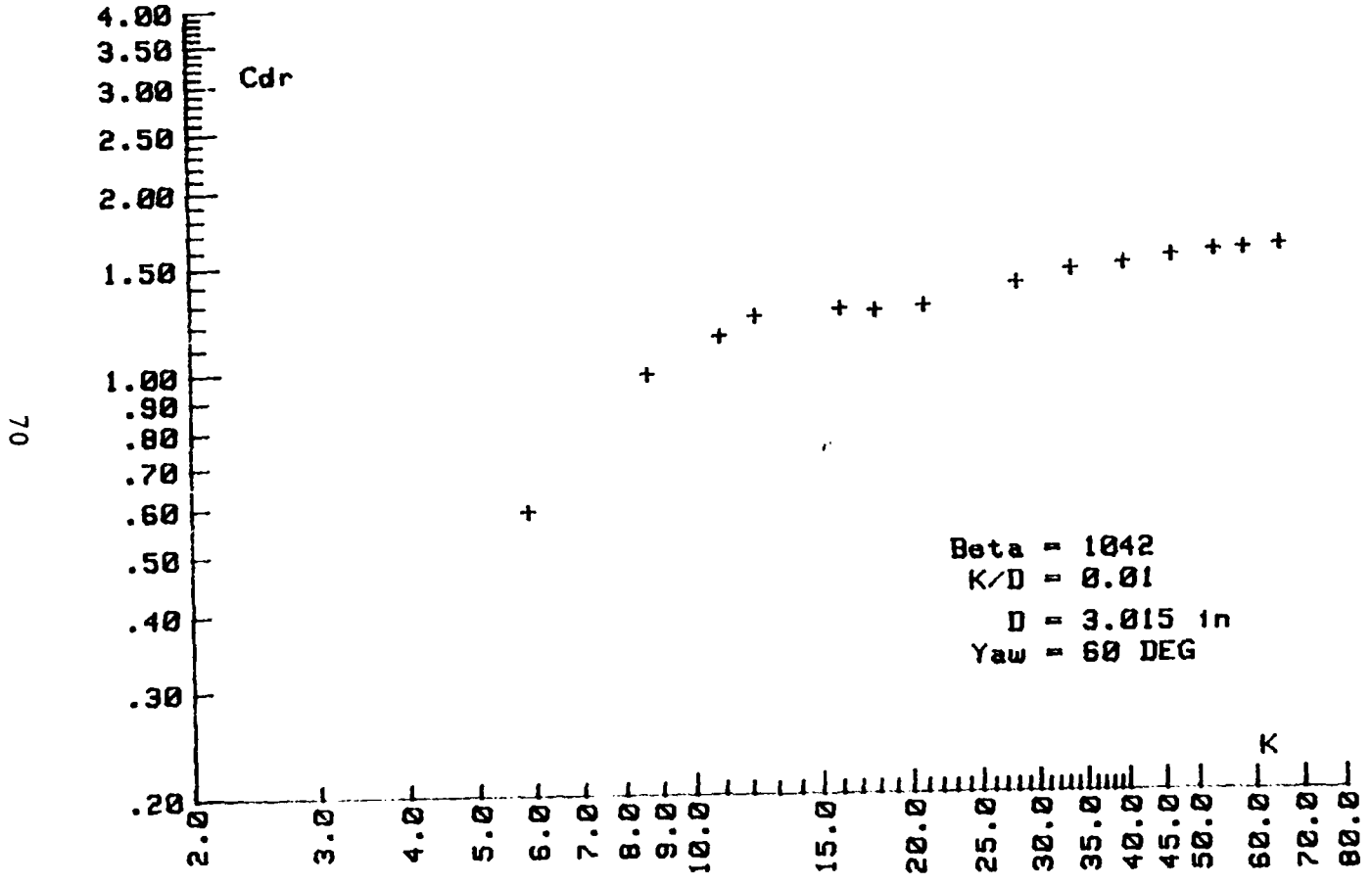

Figure 6e. C_{dr} Versus K for β = 1042, α = 60 Deg., k/D = 0.01.

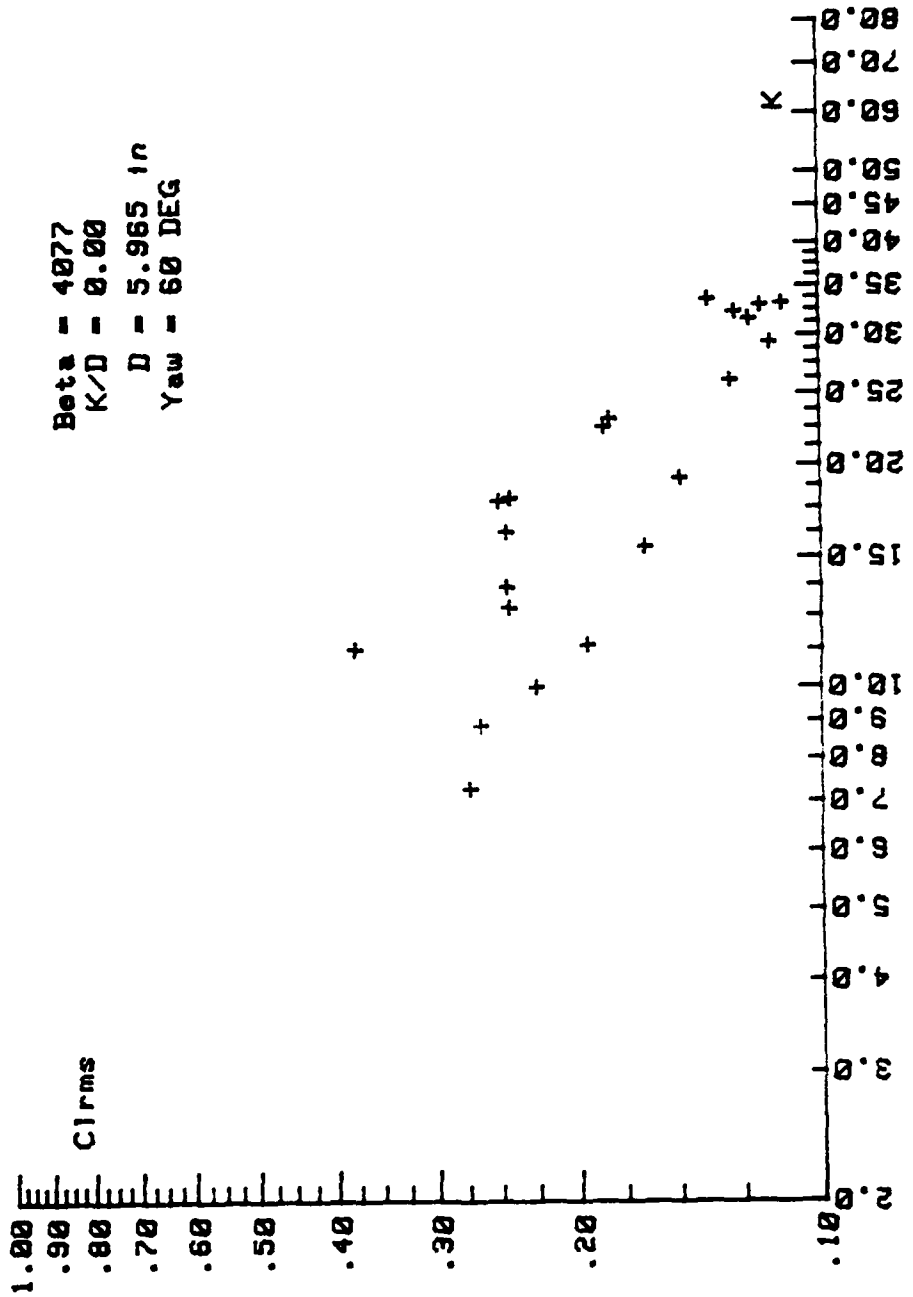

Figure 7a. C_{lrms} Versus K for β = 4077, α = 60 Deg., k/D = 0.00.

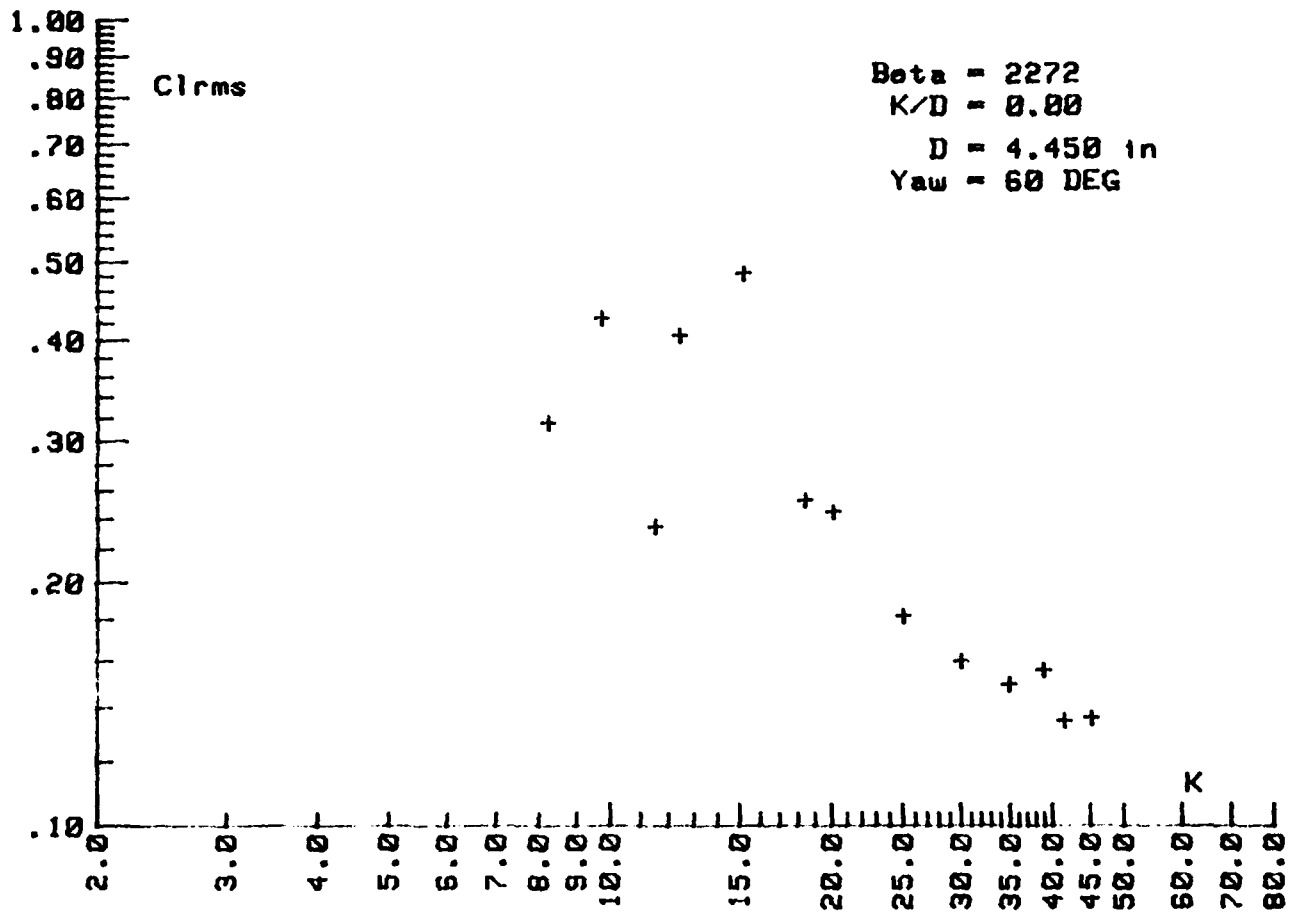

Figure 7b. C_{lrms} Versus K for β = 2272, α = 60 Deg., k/D = 0.00.

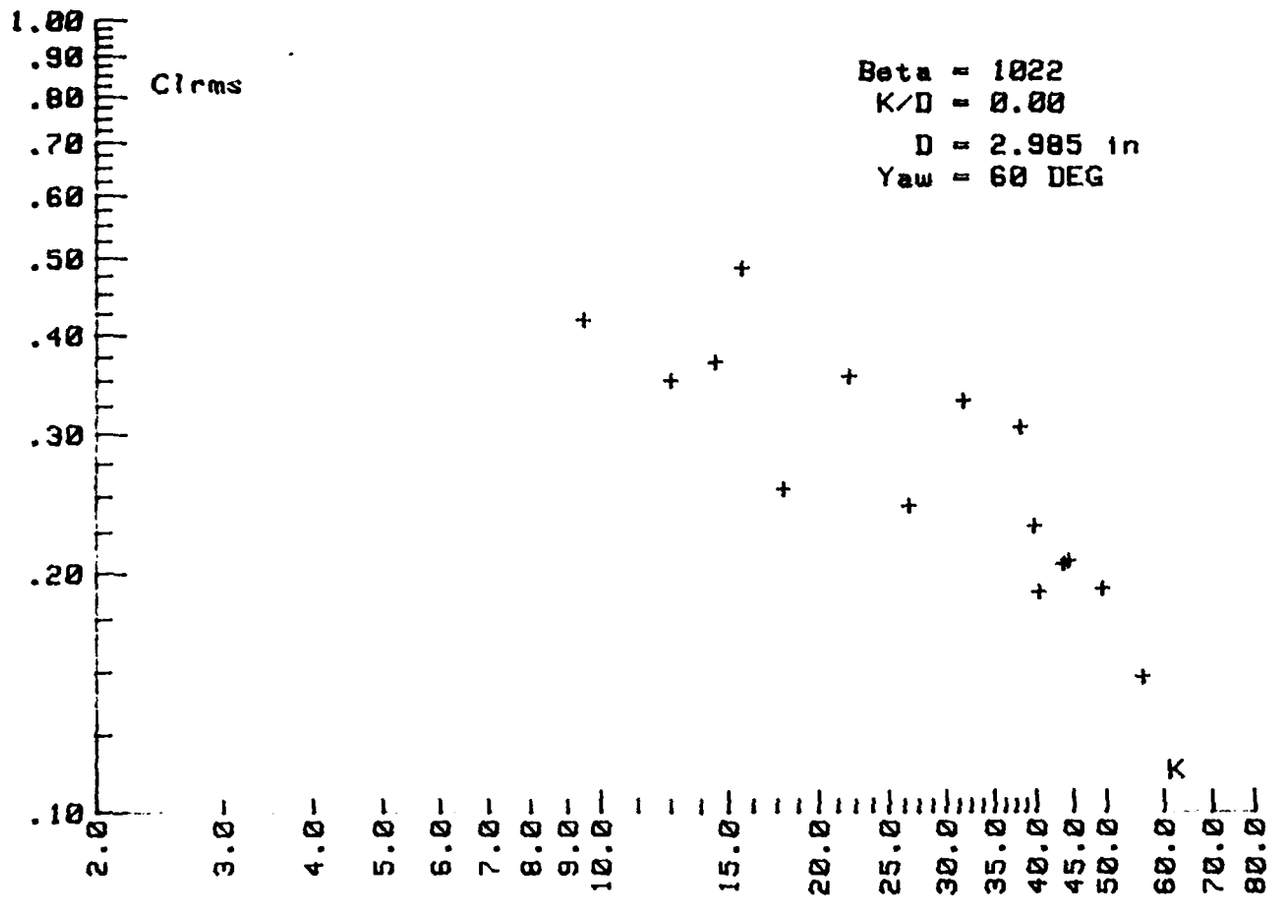

Figure 7c. C_{lrms} Versus K for β = 1022, α = 60 Deg., k/D = 0.00.

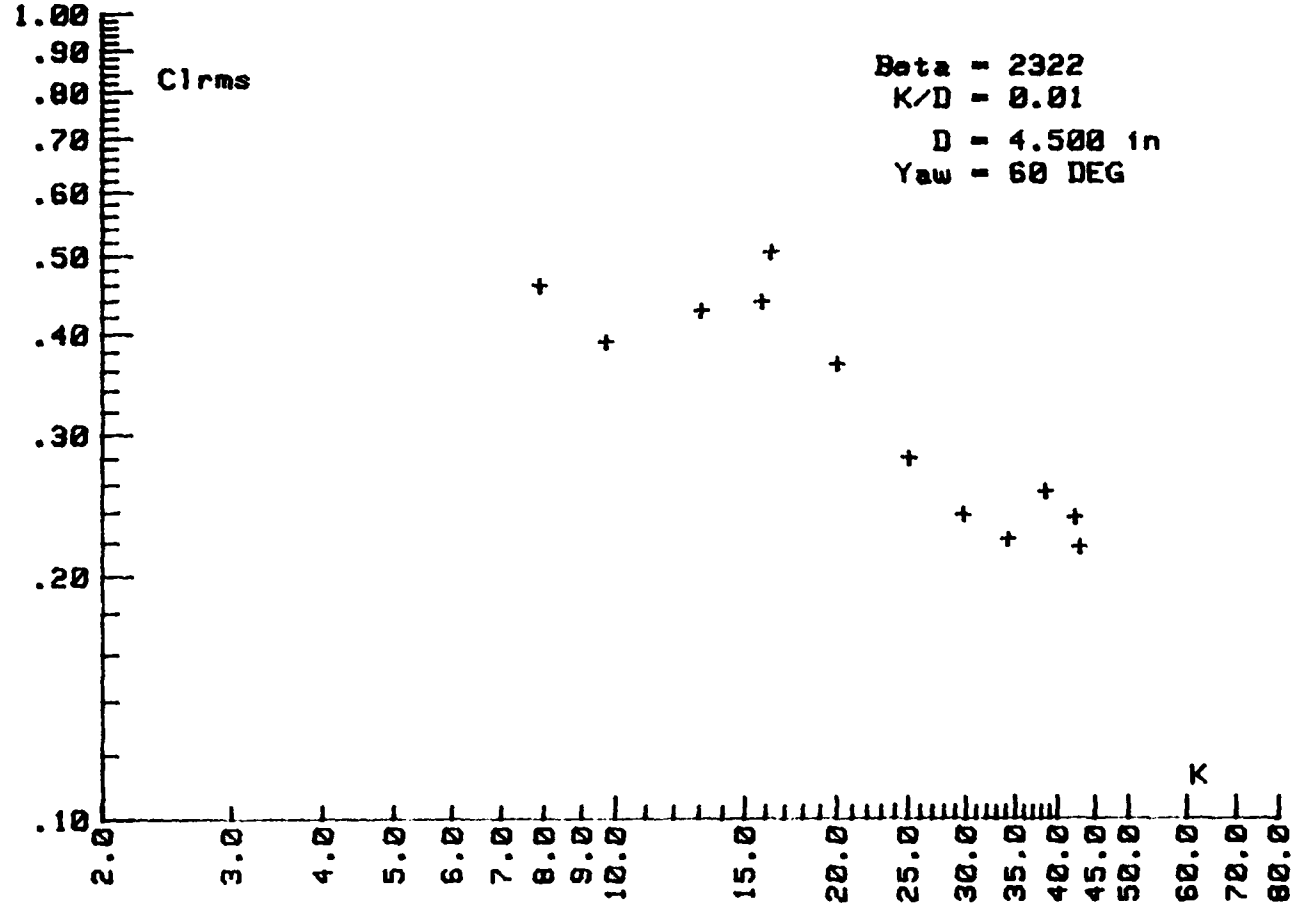

Figure 7d. C_{lrms} Versus K for β = 2322, α = 60 Deg., k/D = 0.01.

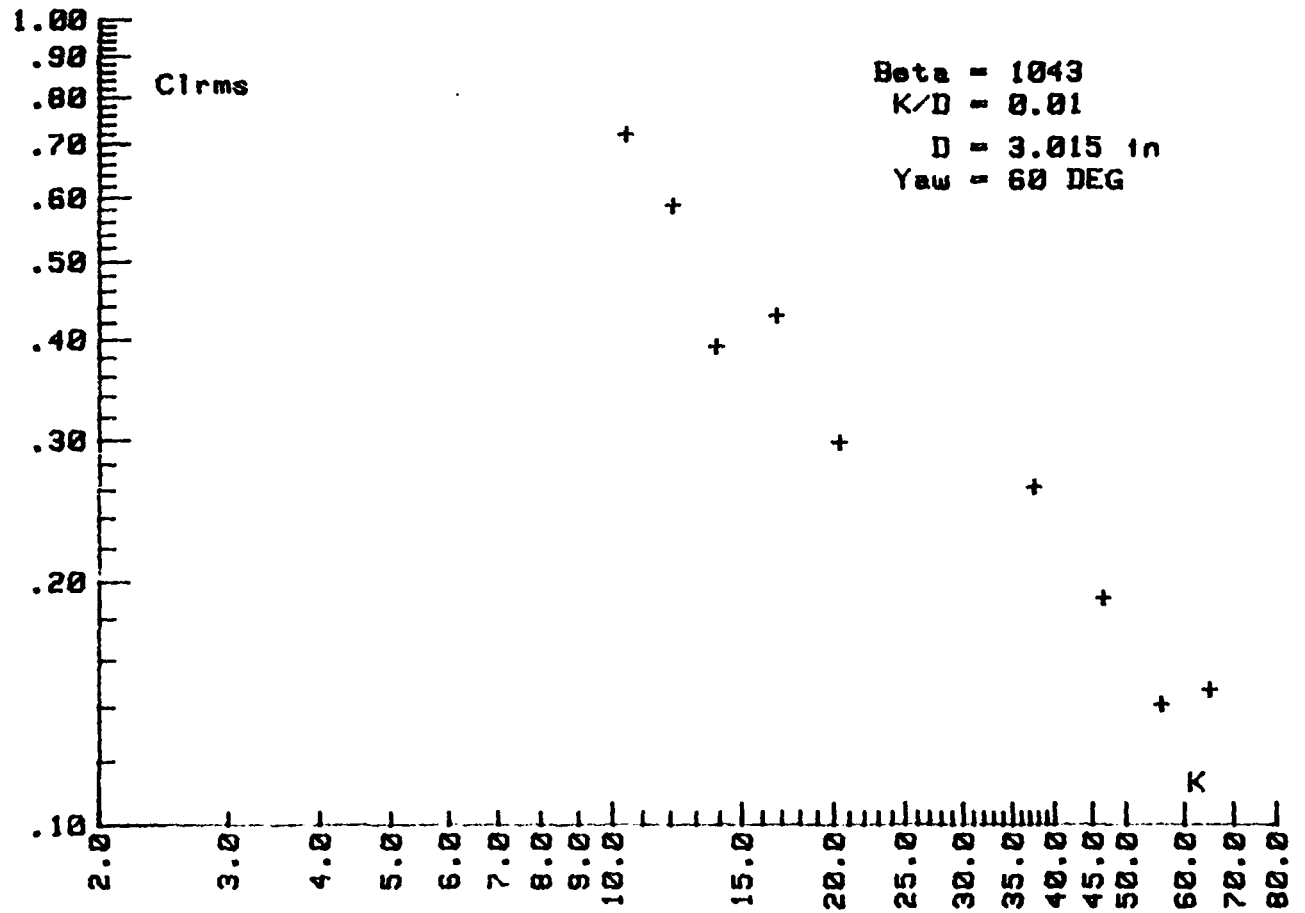

Figure 7e. C_{lrms} Versus K for β = 1043, α = 60 Deg., k/D = 0.01.

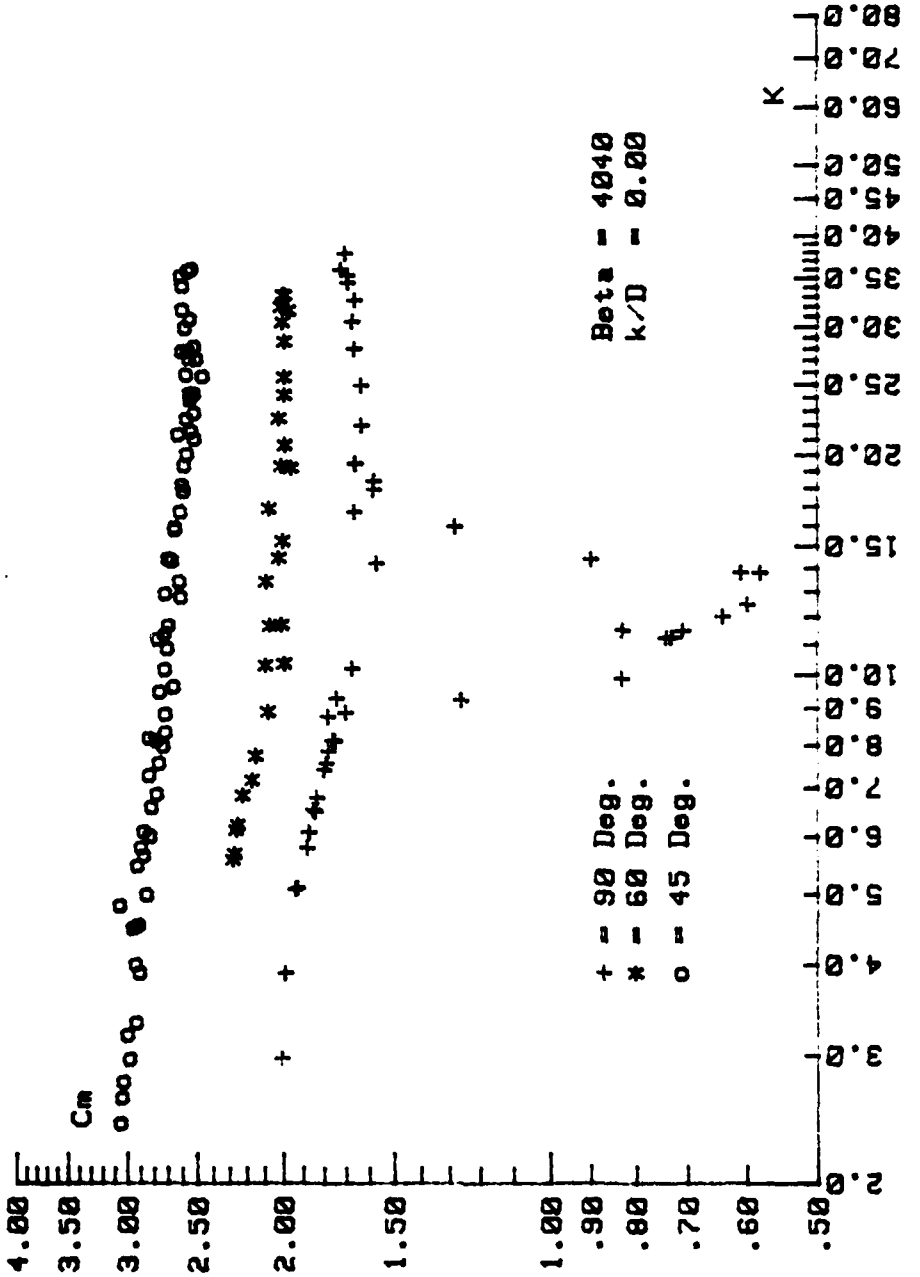

Figure 8a. Comparison of C_m Versus K for β = 4040, k/D = 0.00, α = 90, 60, and 45 Deg.

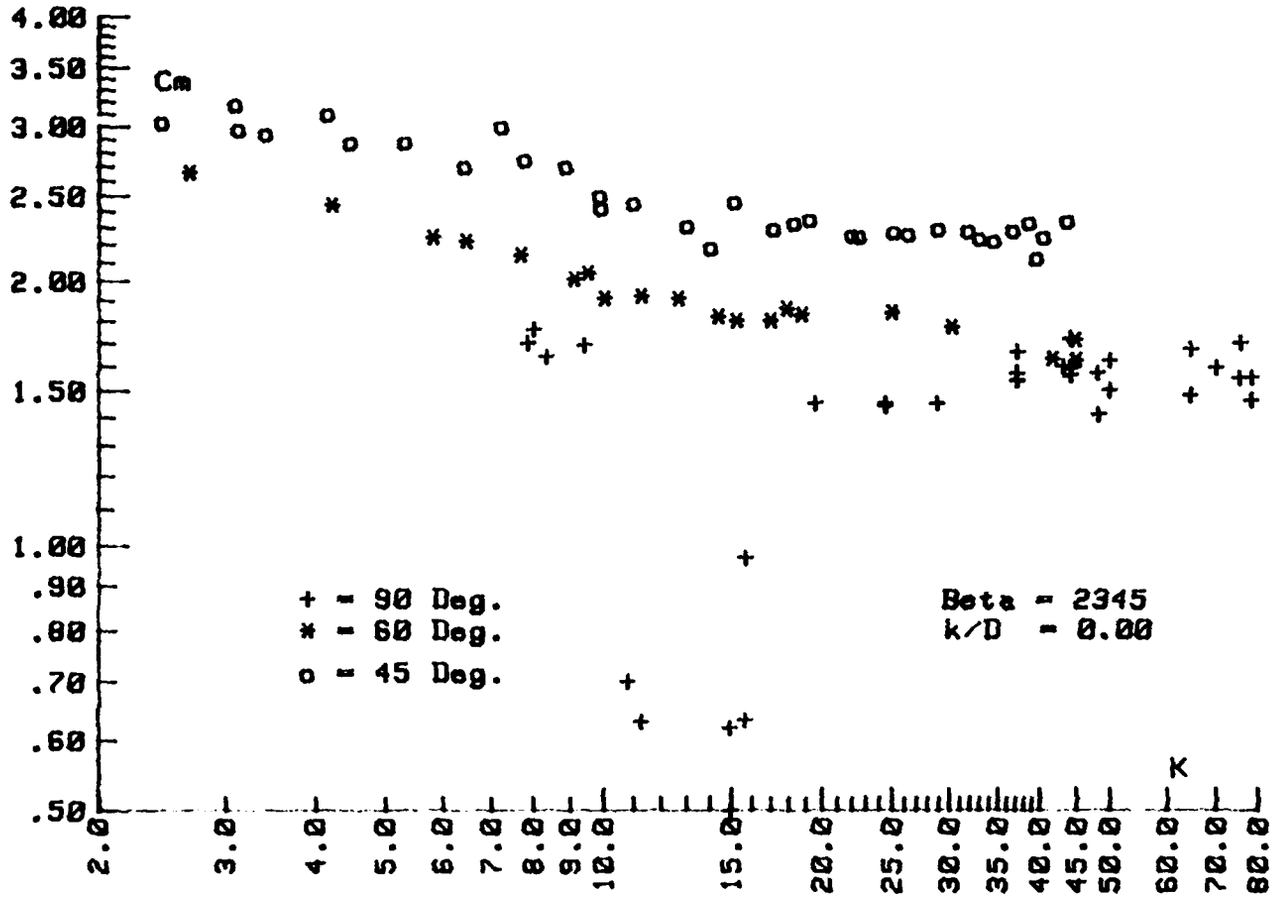

Figure 8b. Comparison of C_m Versus K for β = 2345, k/D = 0.00, α = 90, 60, and 45 Deg.

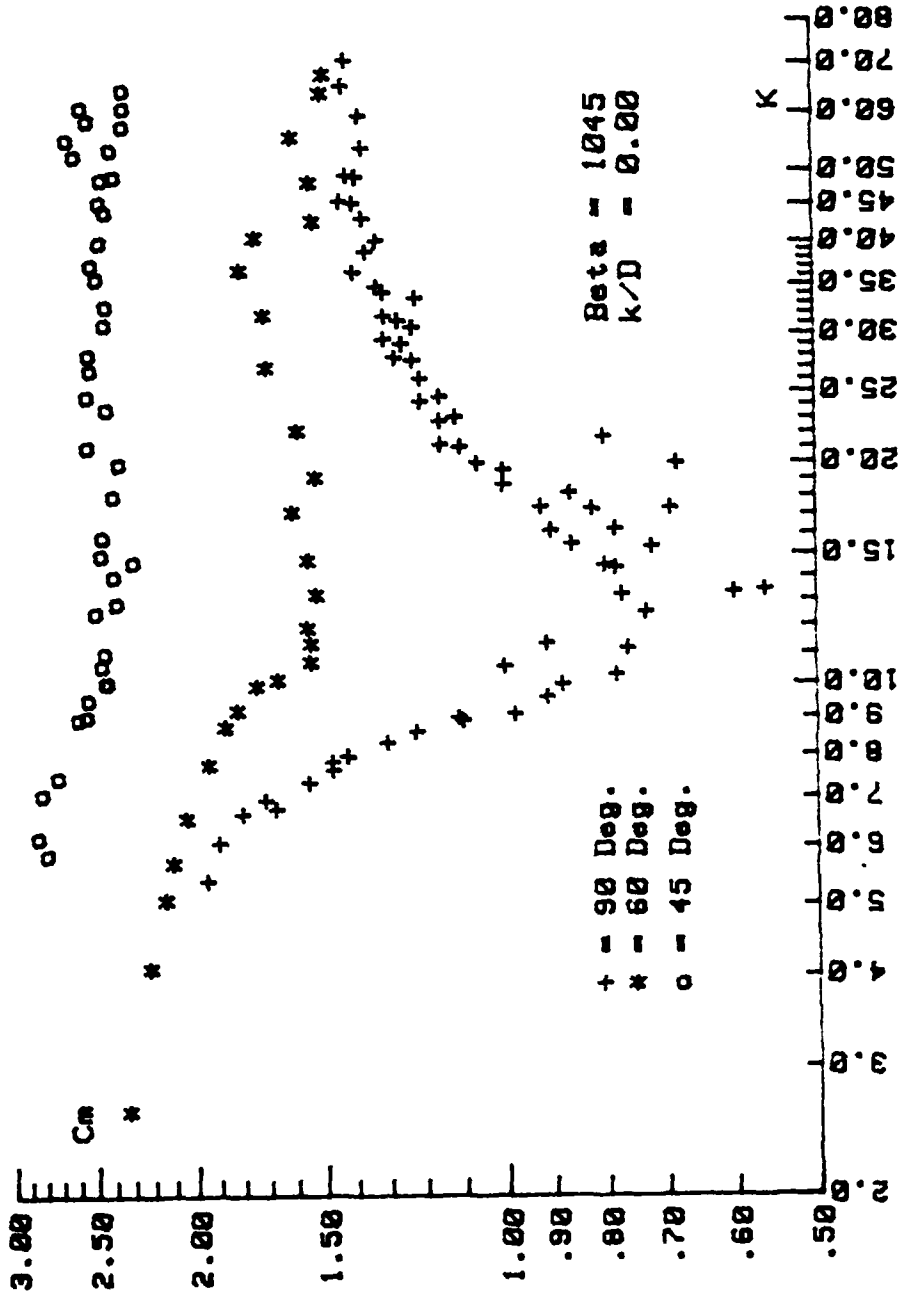

Figure 8c. Comparison of C_m Versus K for β = 1045, k/D = 0.00, α = 90, 60, and 45 Deg.

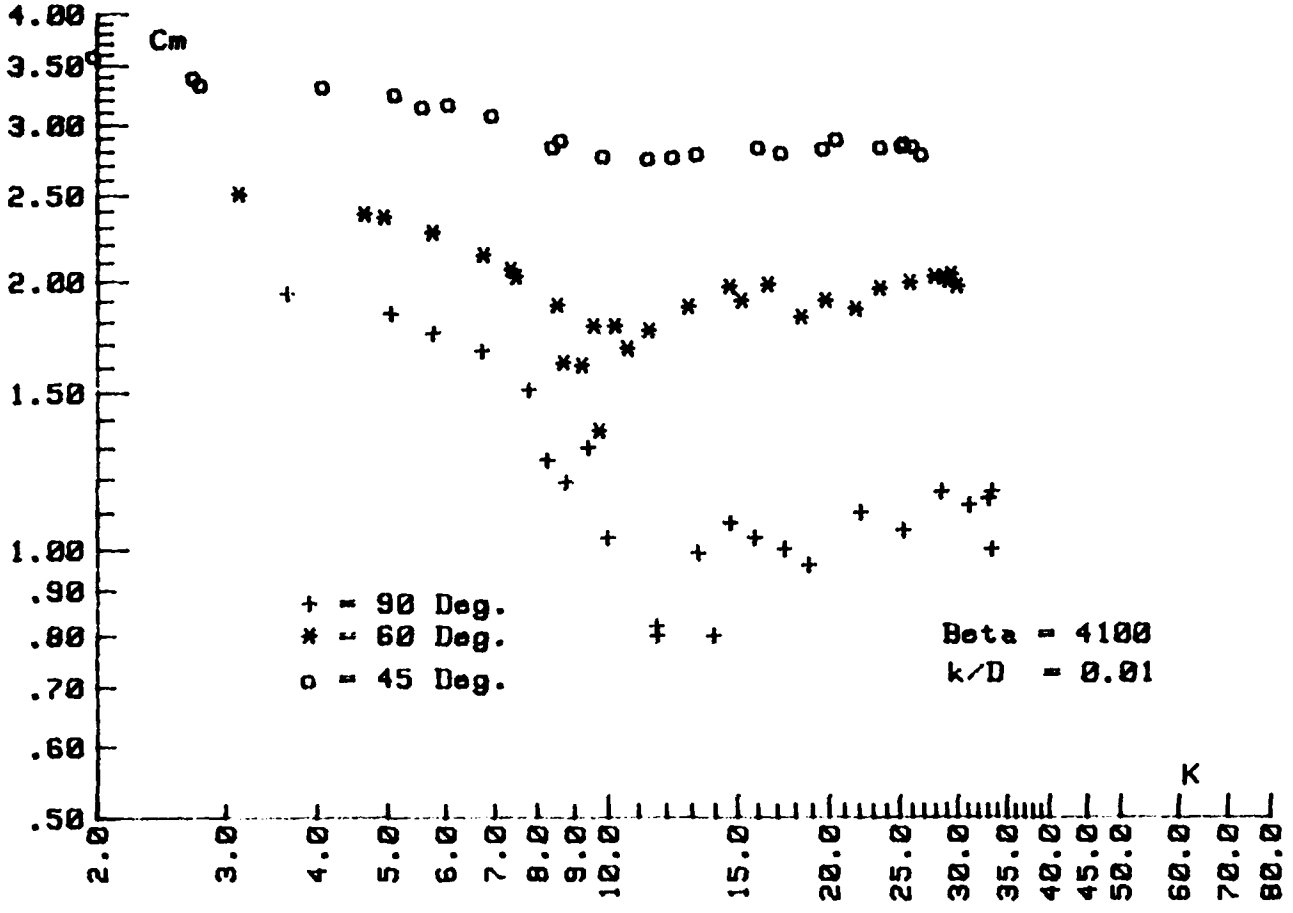

Figure 8d. Comparison of C_m Versus K for β = 4100, k/D = 0.01, α = 90, 60, and 45 Deg.

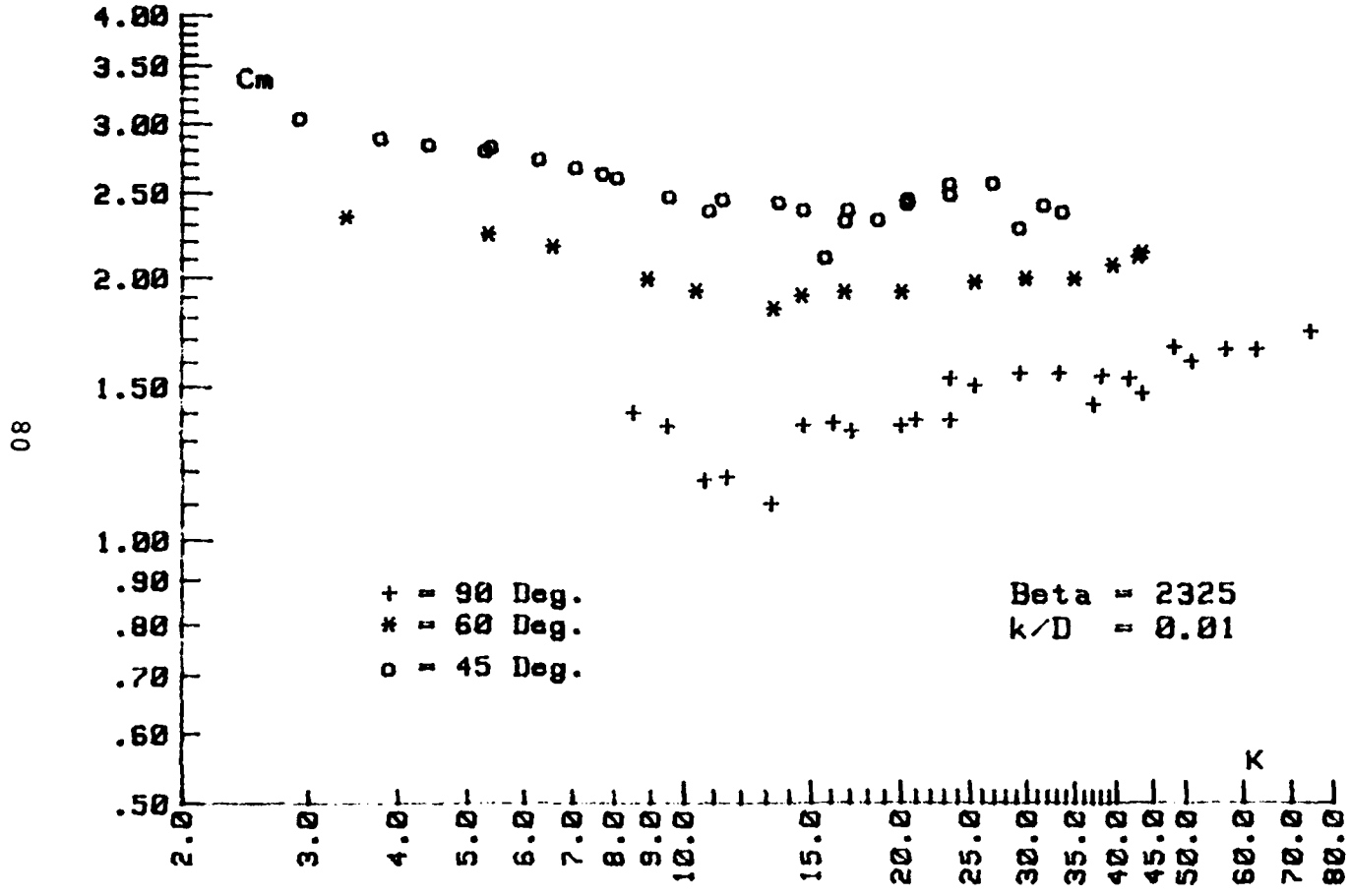

Figure 8e. Comparison of C_m Versus K for β = 2325, k/D = 0.01, α = 90, 60, and 45 Deg.

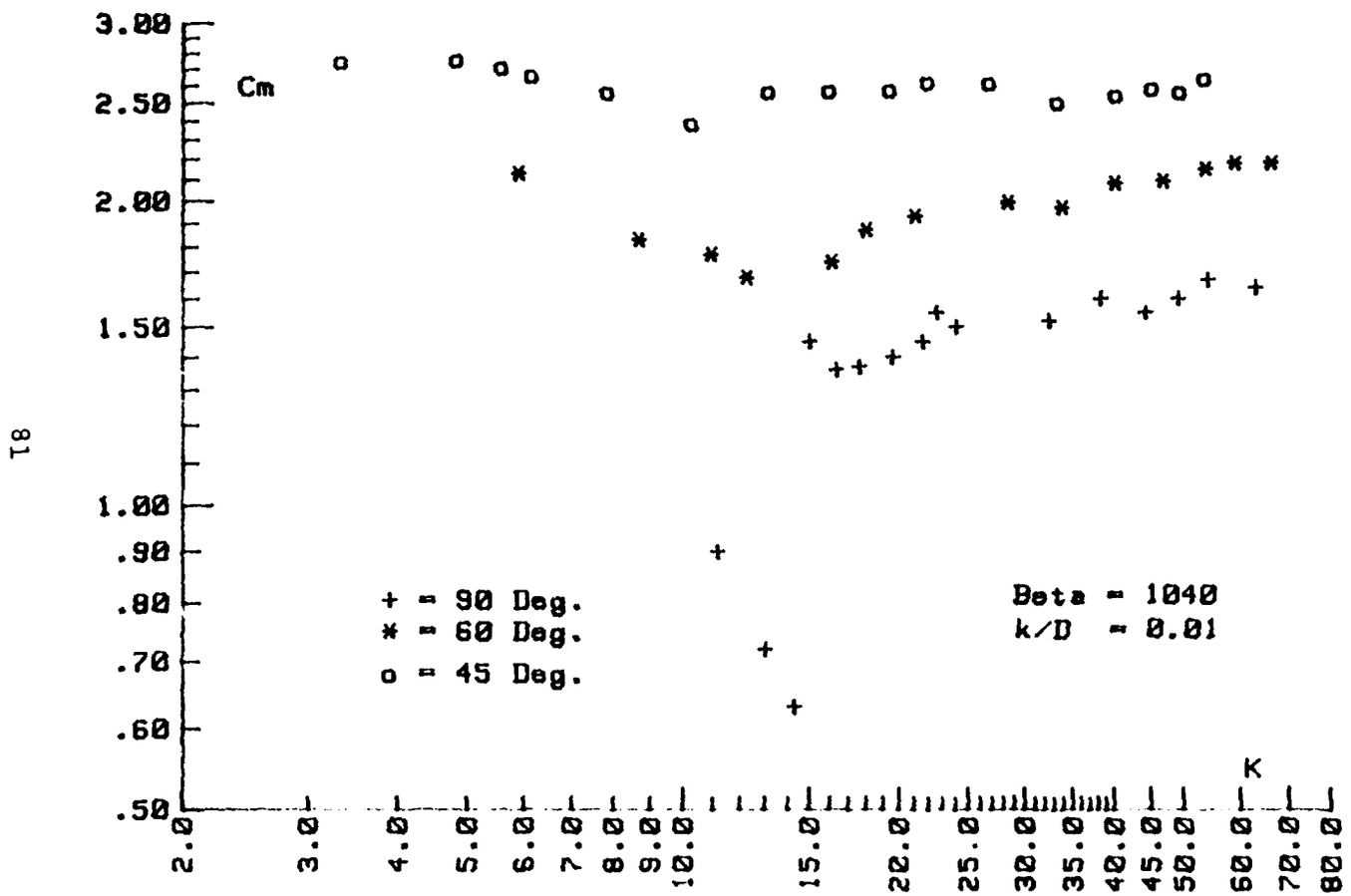

Figure 8f. Comparison of C_m Versus K for β = 1040, k/D = 0.01, α = 90, 60, and 45 Deg.

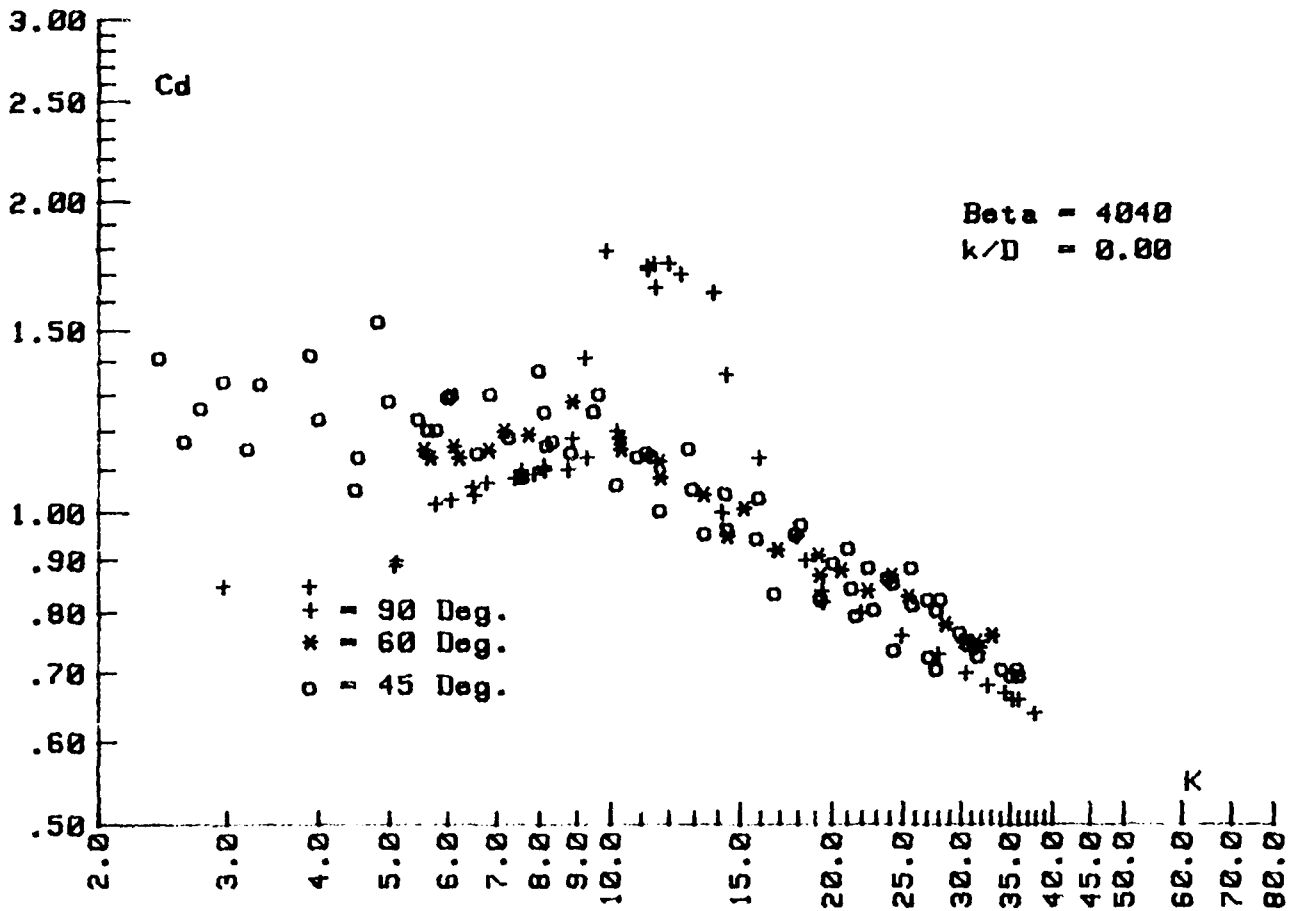

Figure 9a. Comparison of C_d Versus K for β = 4040, k/D = 0.00, α = 90, 60, and 45 Deg.

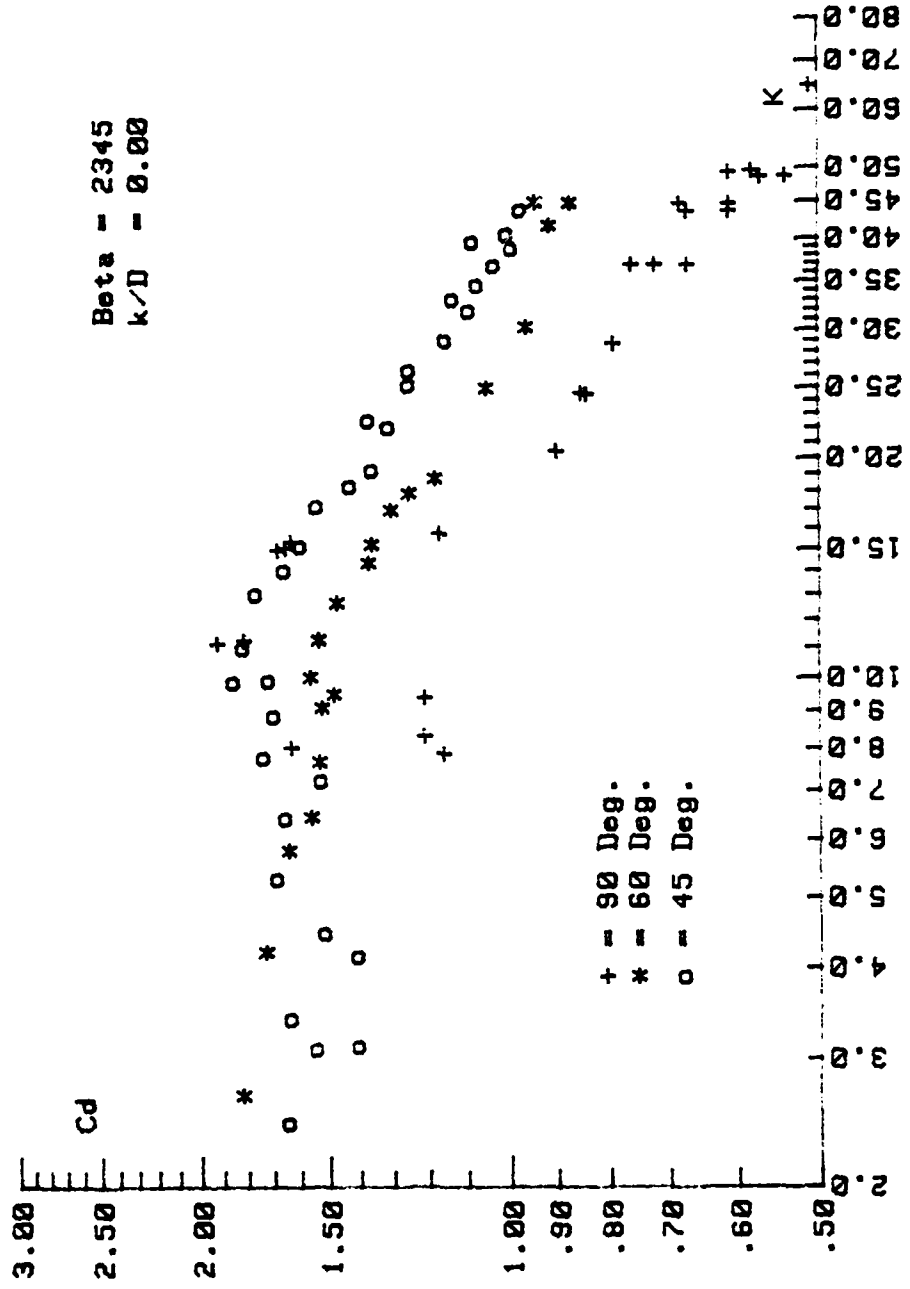

Figure 9b. Comparison of C_d Versus K for β = 2345, k/D = 0.00, α = 90, 60, and 45 Deg.

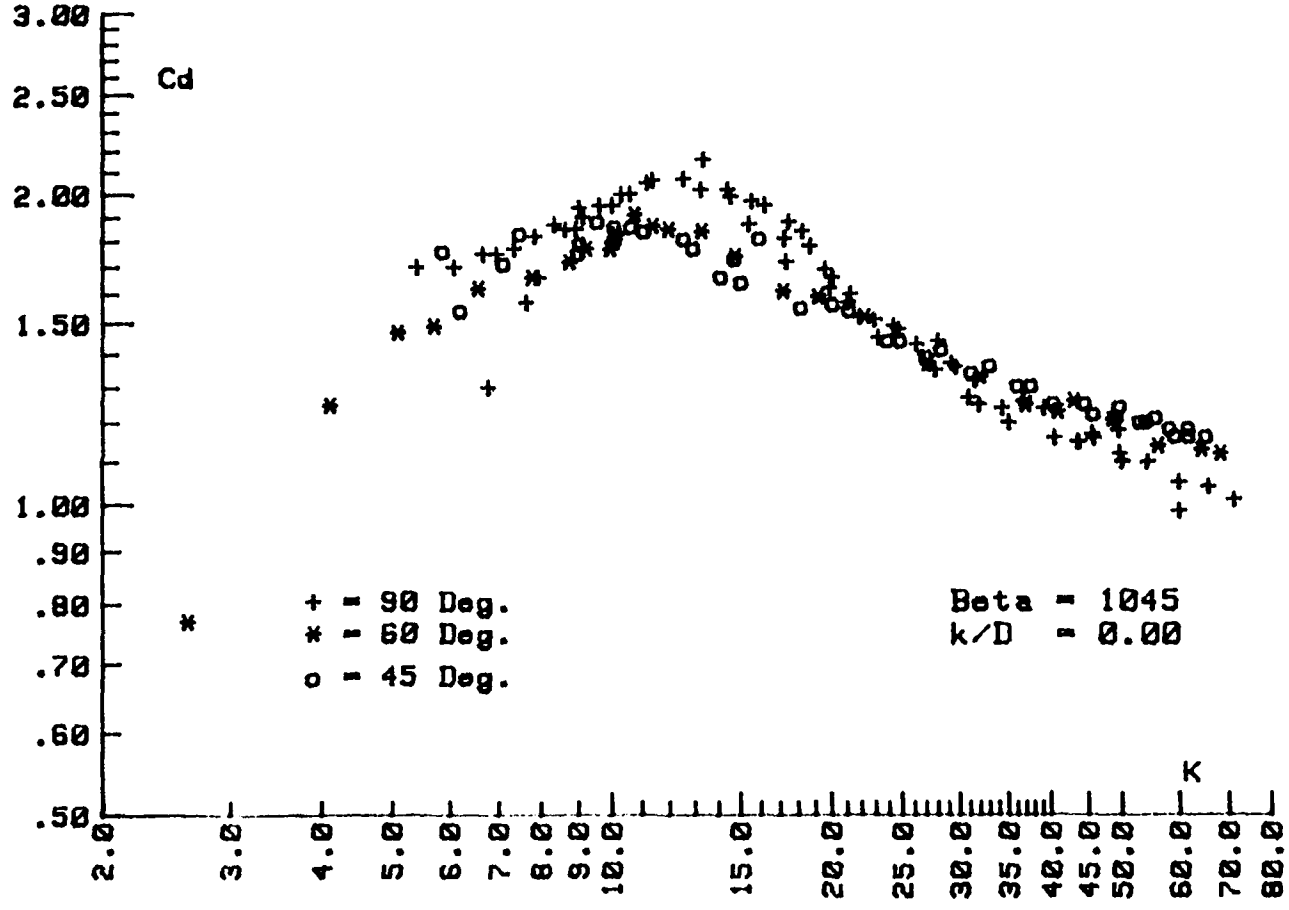

Figure 9c. Comparison of C_d Versus K for β = 1045, k/D = 0.00, α = 90, 60, and 45 Deg.

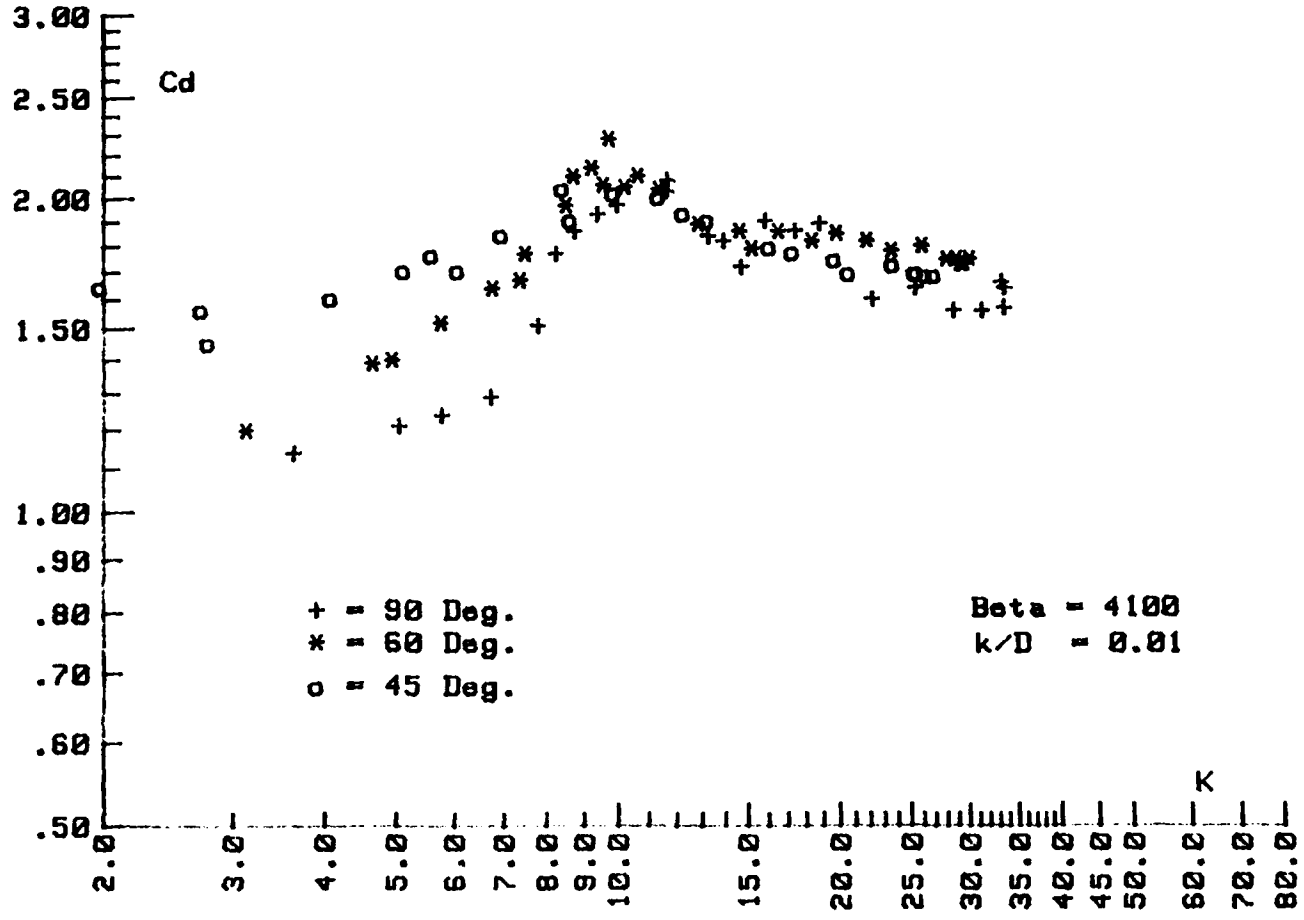

Figure 9d. Comparison of C_d Versus K for β = 4100, k/D = 0.01, α = 90, 60, and 45 Deg.

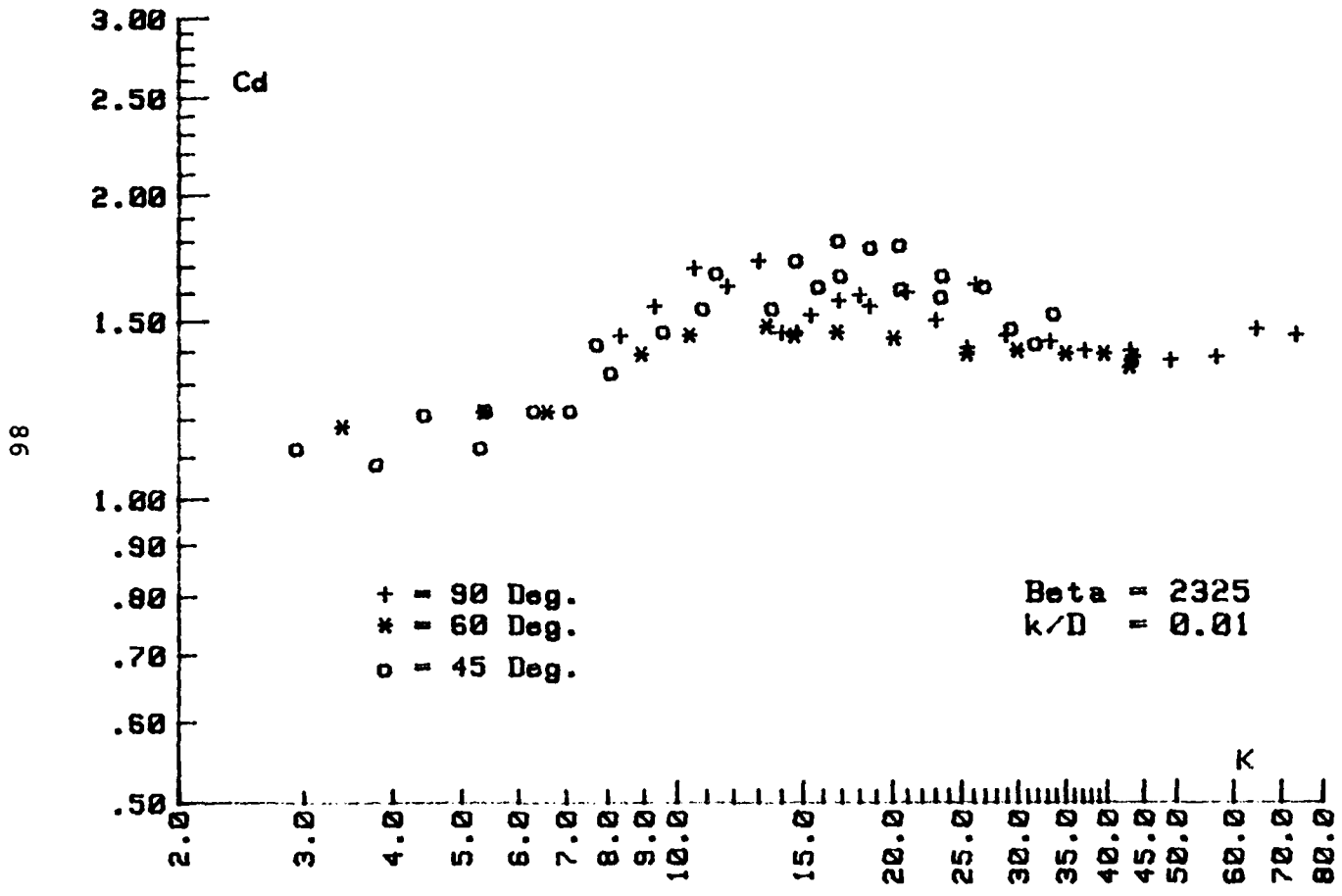

Figure 9e. Comparison of C_d Versus K for β = 2325, k/D = 0.01, α = 90, 60, and 45 Deg.

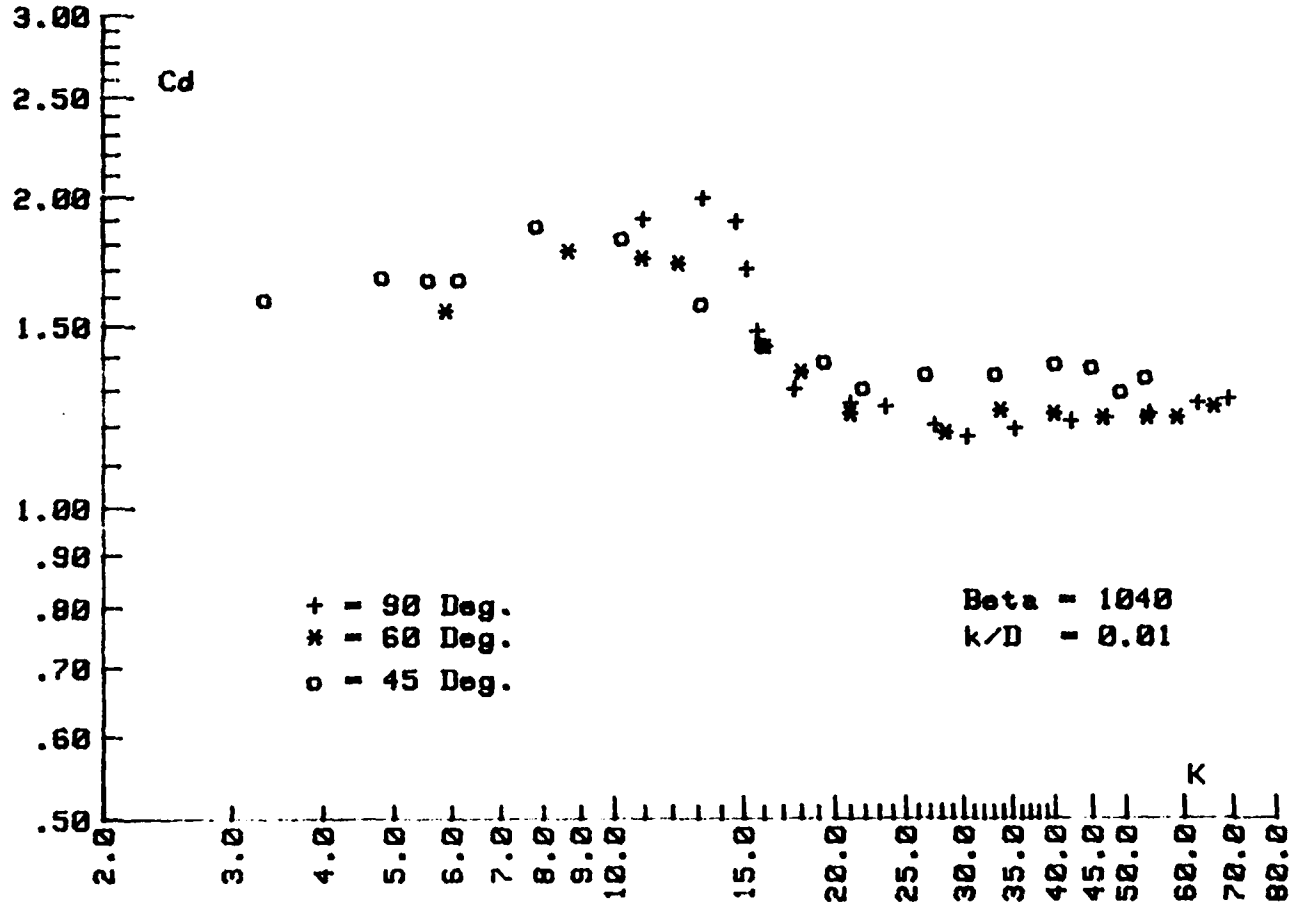

Figure 9f. Comparison of C_d Versus K for β = 1040, k/D = 0.01, α = 90, 60, and 45 Deg.

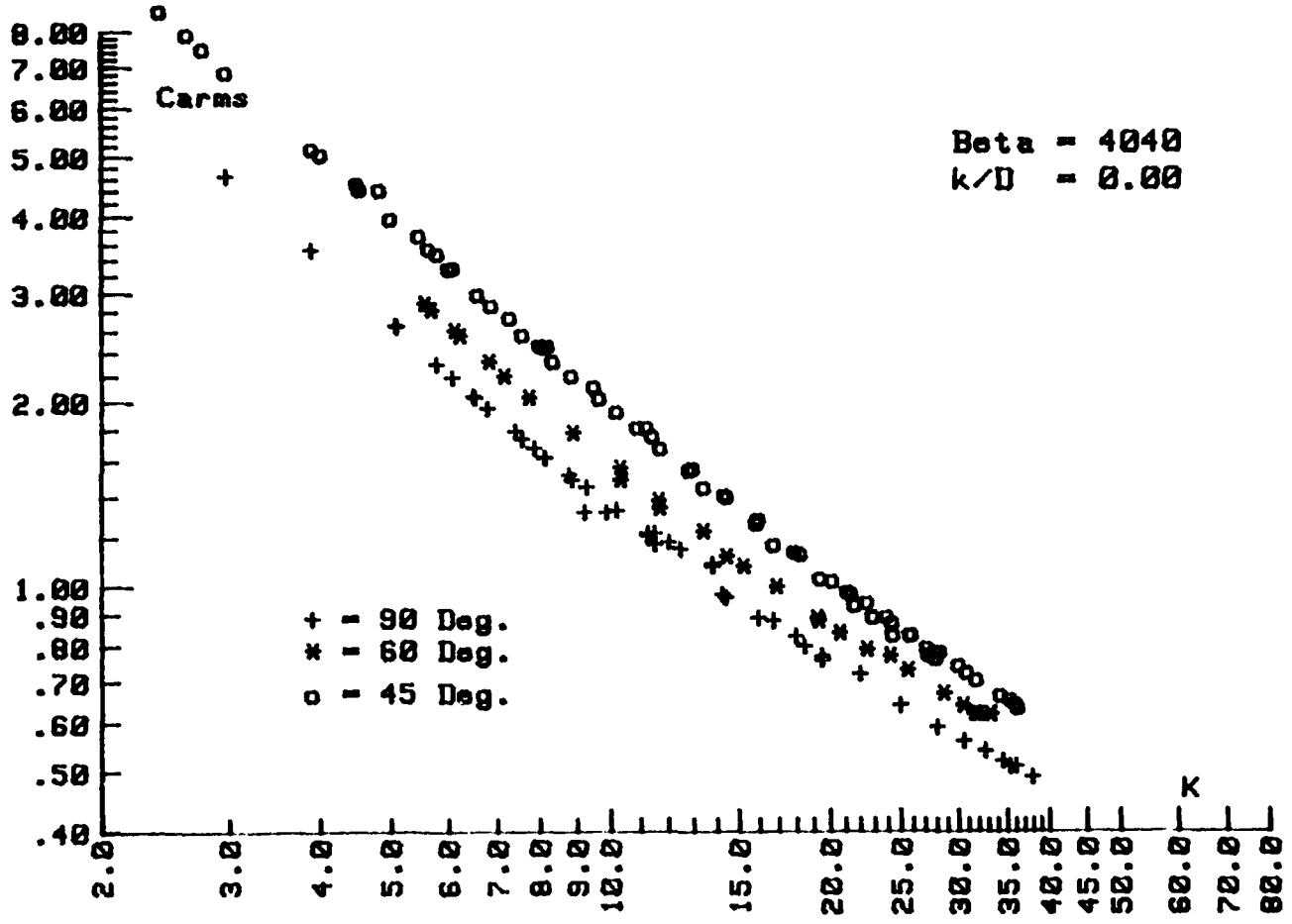

Figure 10a. Comparison of C_{arms} Versus K for β = 4040, k/D = 0.00, α = 90, 60, and 45 Deg.

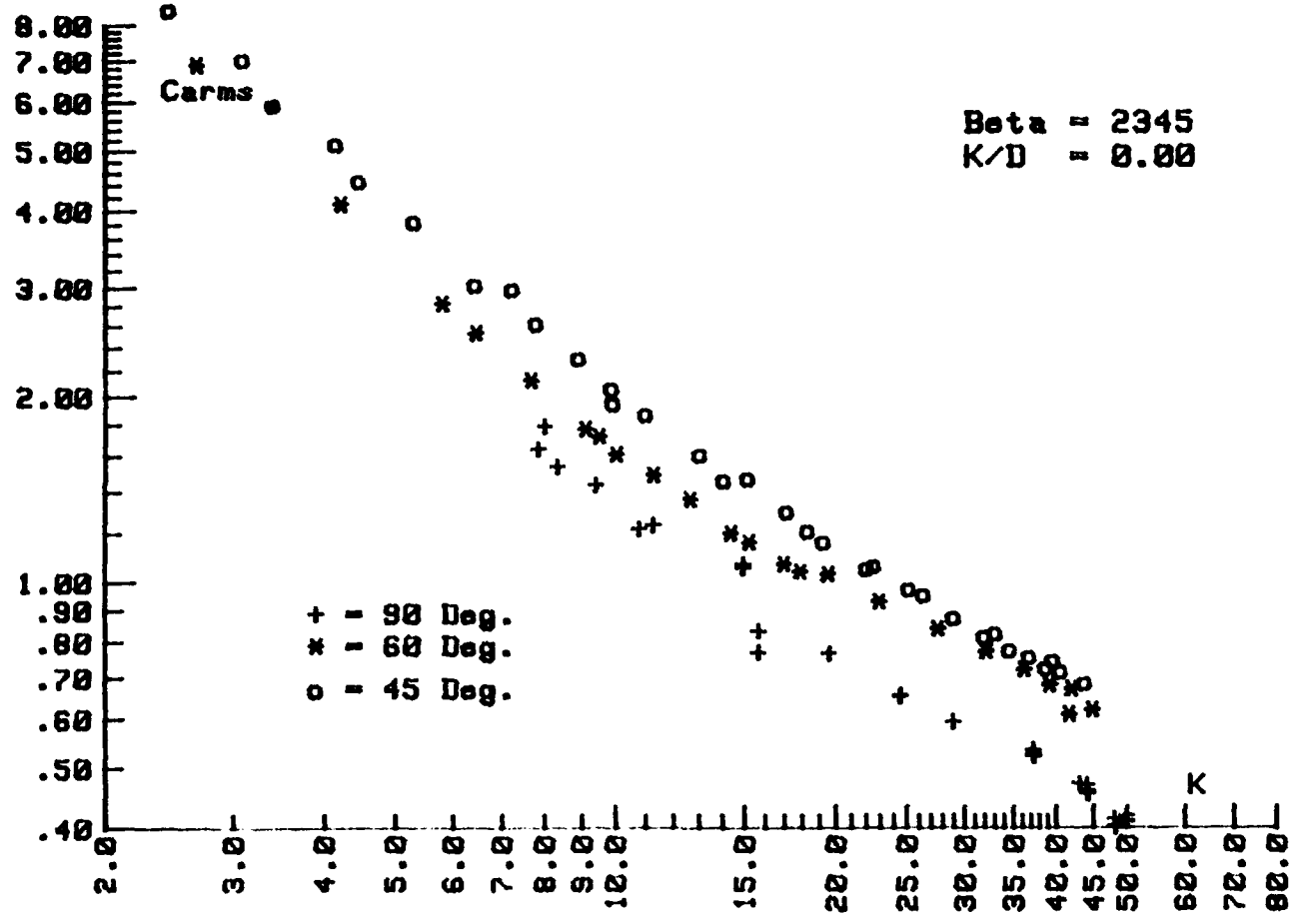

Figure 10b. Comparison of C_{arms} Versus K for β = 2345, k/D = 0.00, α = 90, 60, and 45 Deg.

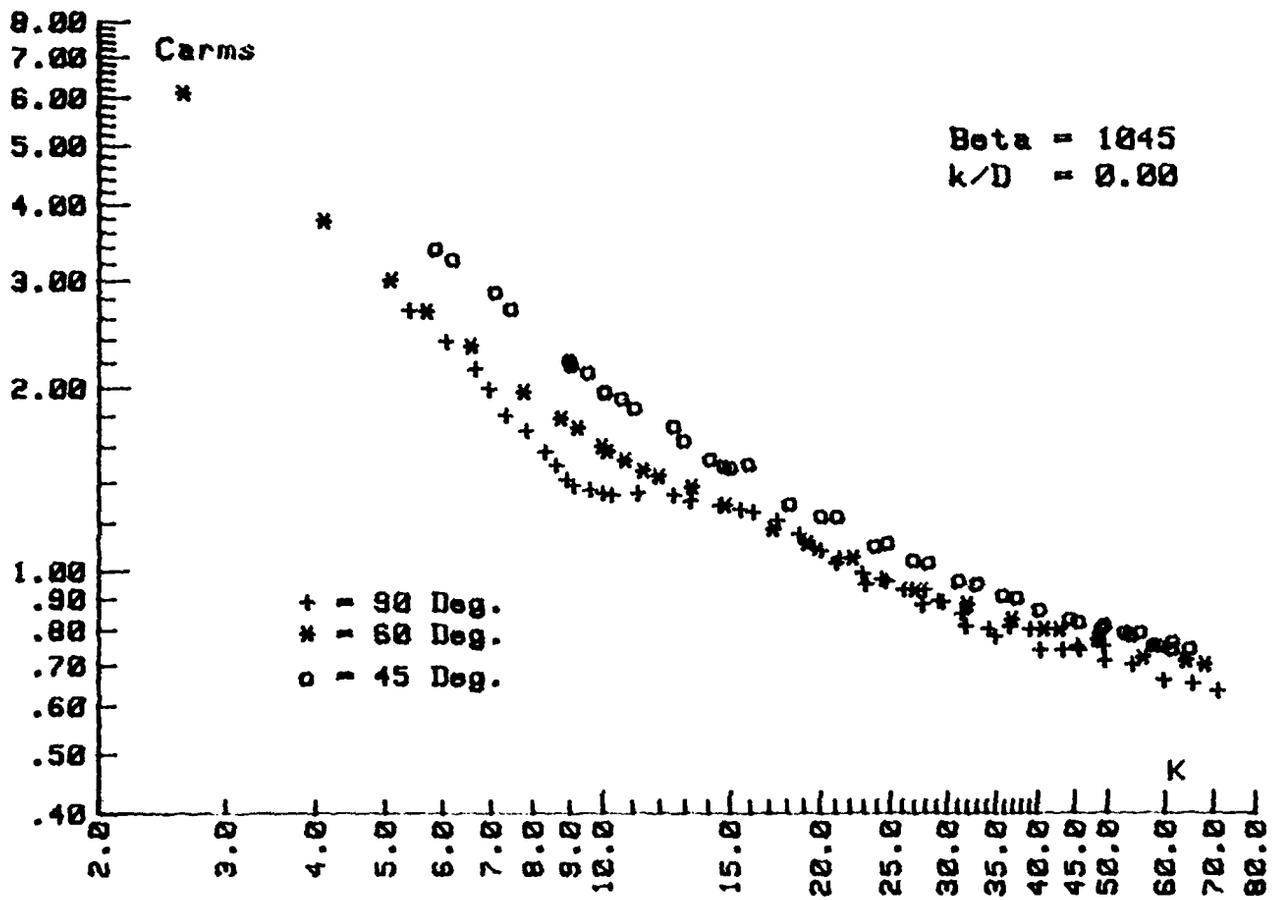

Figure 10c. Comparison of C_{arms} Versus K for β = 1045, k/D = 0.00, α = 90, 60, and 45 Deg.

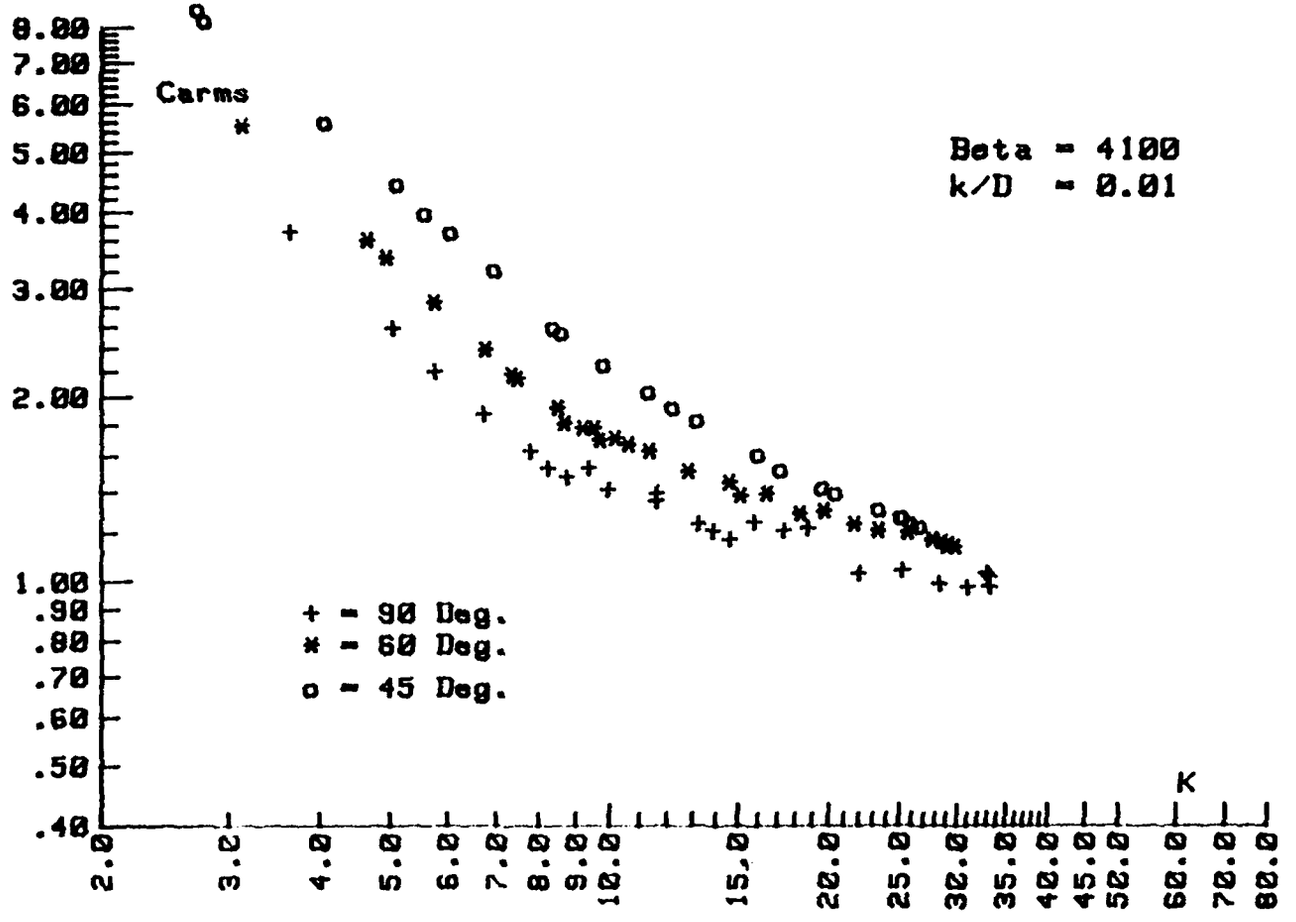

Figure 10d. Comparison of C_{arms} Versus K for β = 4100, k/D = 0.01, α = 90, 60, and 45 Deg.

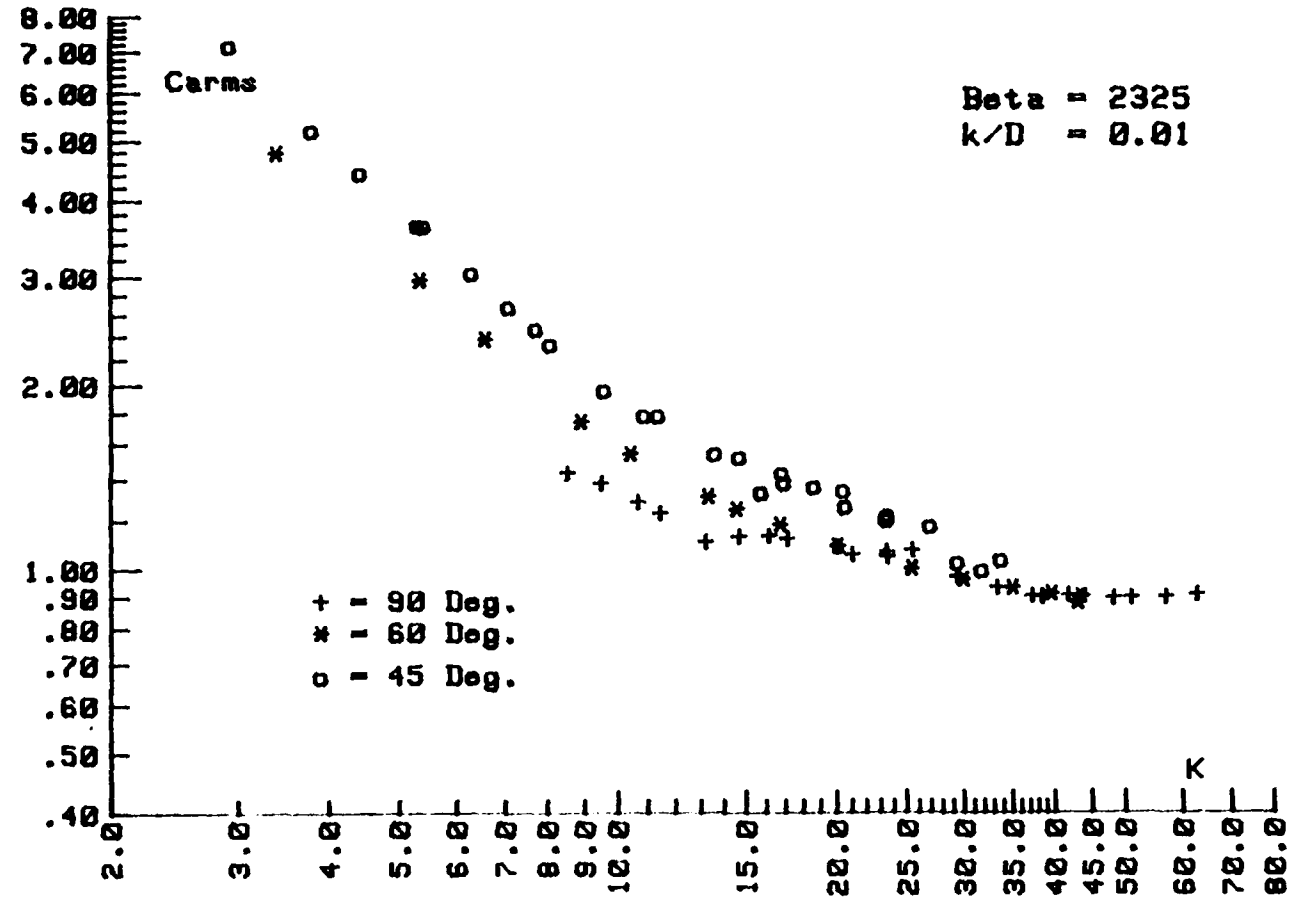

Figure 10e. Comparison of C_{arms} Versus K for β = 2325, k/D = 0.01, α = 90, 60, and 45 Deg.

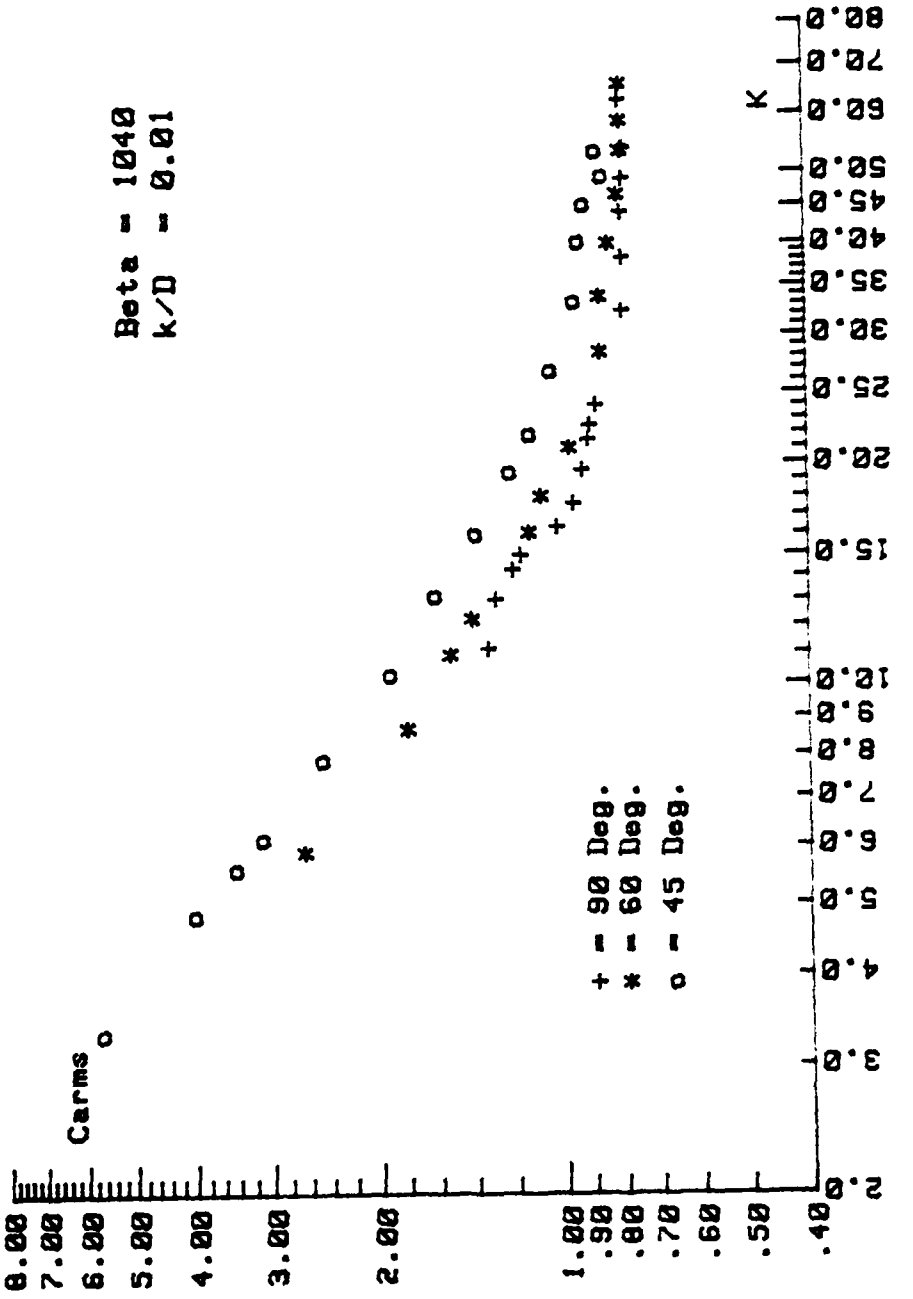

Figure 10f. Comparison of C_{arms} Versus K for β = 1040, k/D = 0.01, α = 90, 60, and 45 Deg.

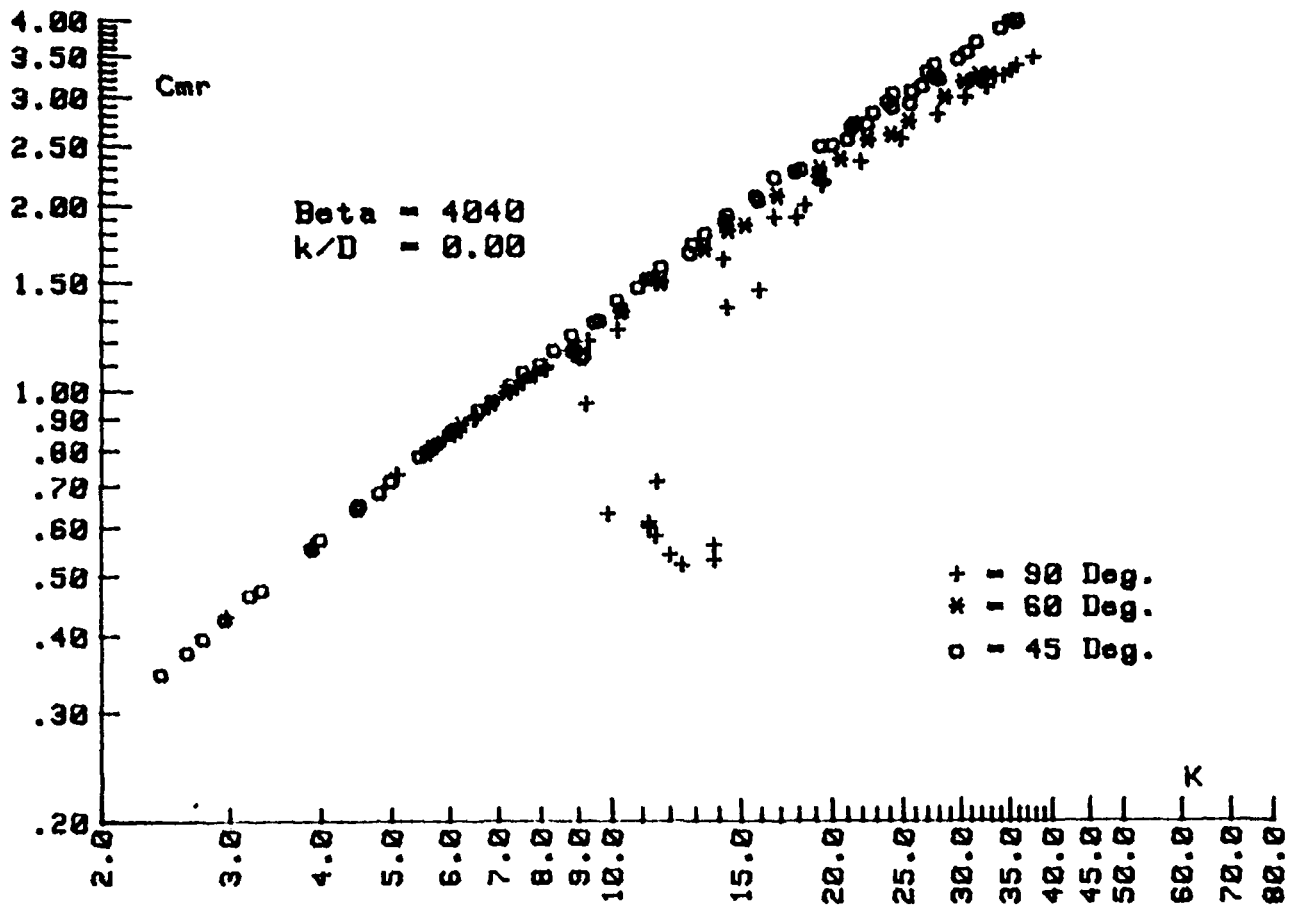

Figure 11a. Comparison of C_{mr} Versus K for β = 4040, k/D = 0.00, α = 90, 60, and 45 Deg.

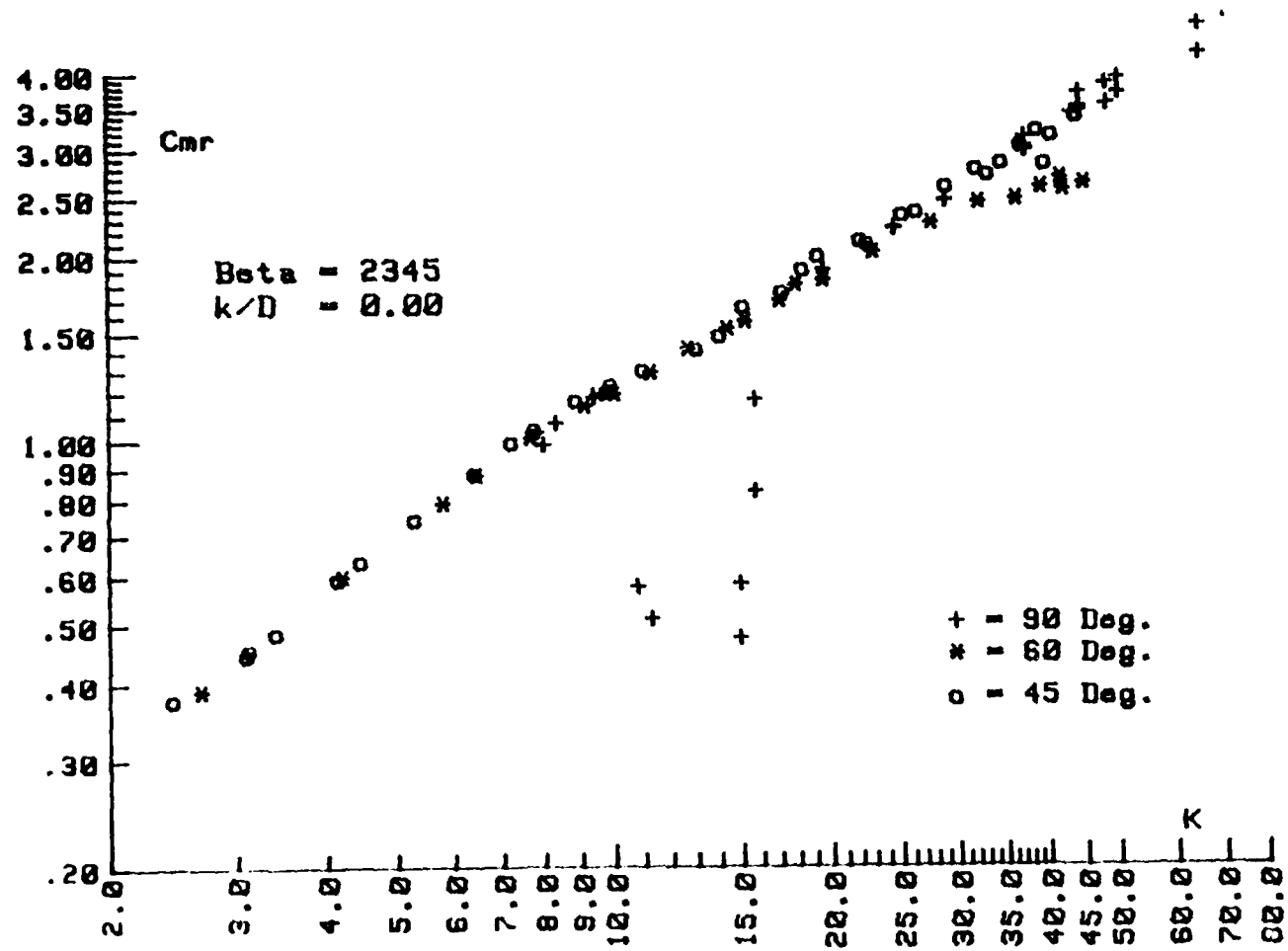

Comparison of C_{mr} Versus K for β = 2345, k/D = 0.00, 90, 60, and 45 Deg.

AD-A118 212 NAVAL POSTGRADUATE SCHOOL MONTEREY CA F/G 20/4
OSCILLATING FLOW ABOUT YAWED CYLINDERS.(U)
MAR 82 D O TRYTTEN

UNCLASSIFIED NL

2 OF 2
AD A
118212

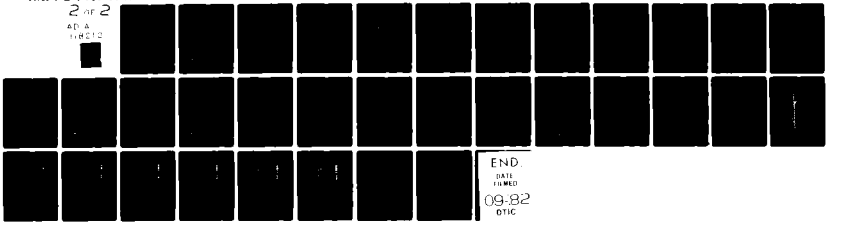

END
DATE FILMED
09-82
DTIC

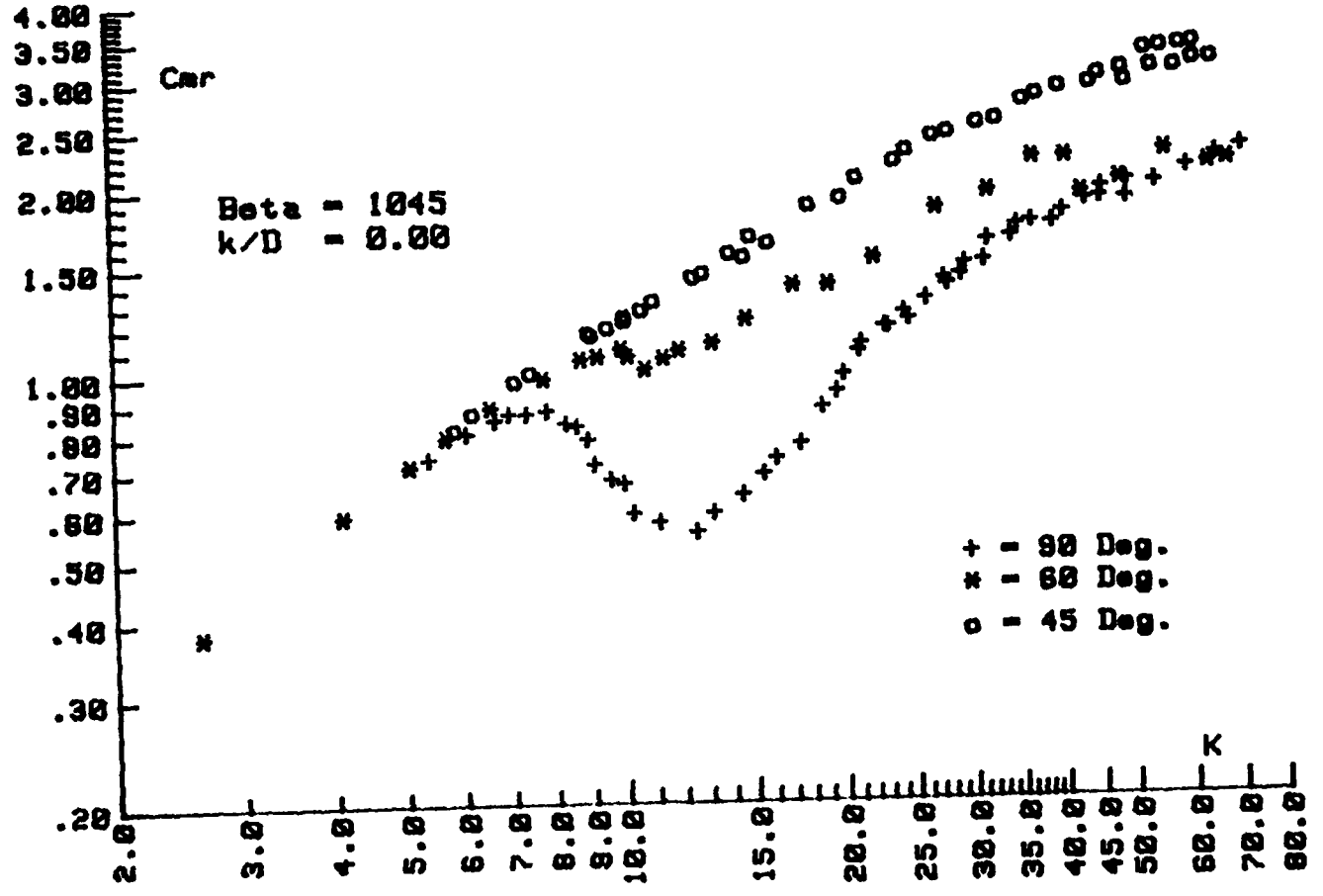

Figure 11c. Comparison of C_{mr} Versus K for β = 1045, k/D = 0.00, α = 90, 60, and 45 Deg.

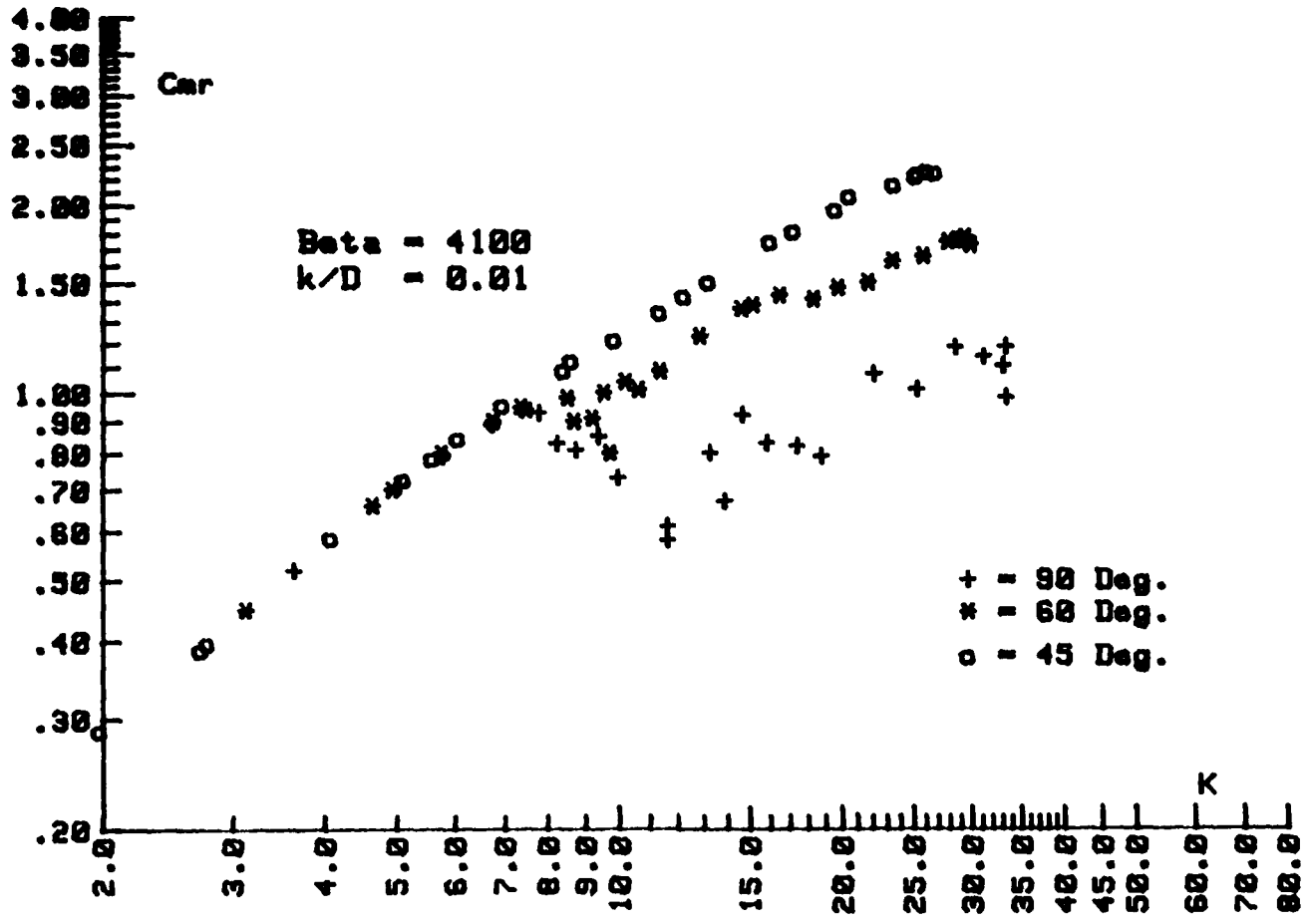

Figure 11d. Comparison of C_{mr} Versus K for β = 4100, k/D = 0.01, α = 90, 60, and 45 Deg.

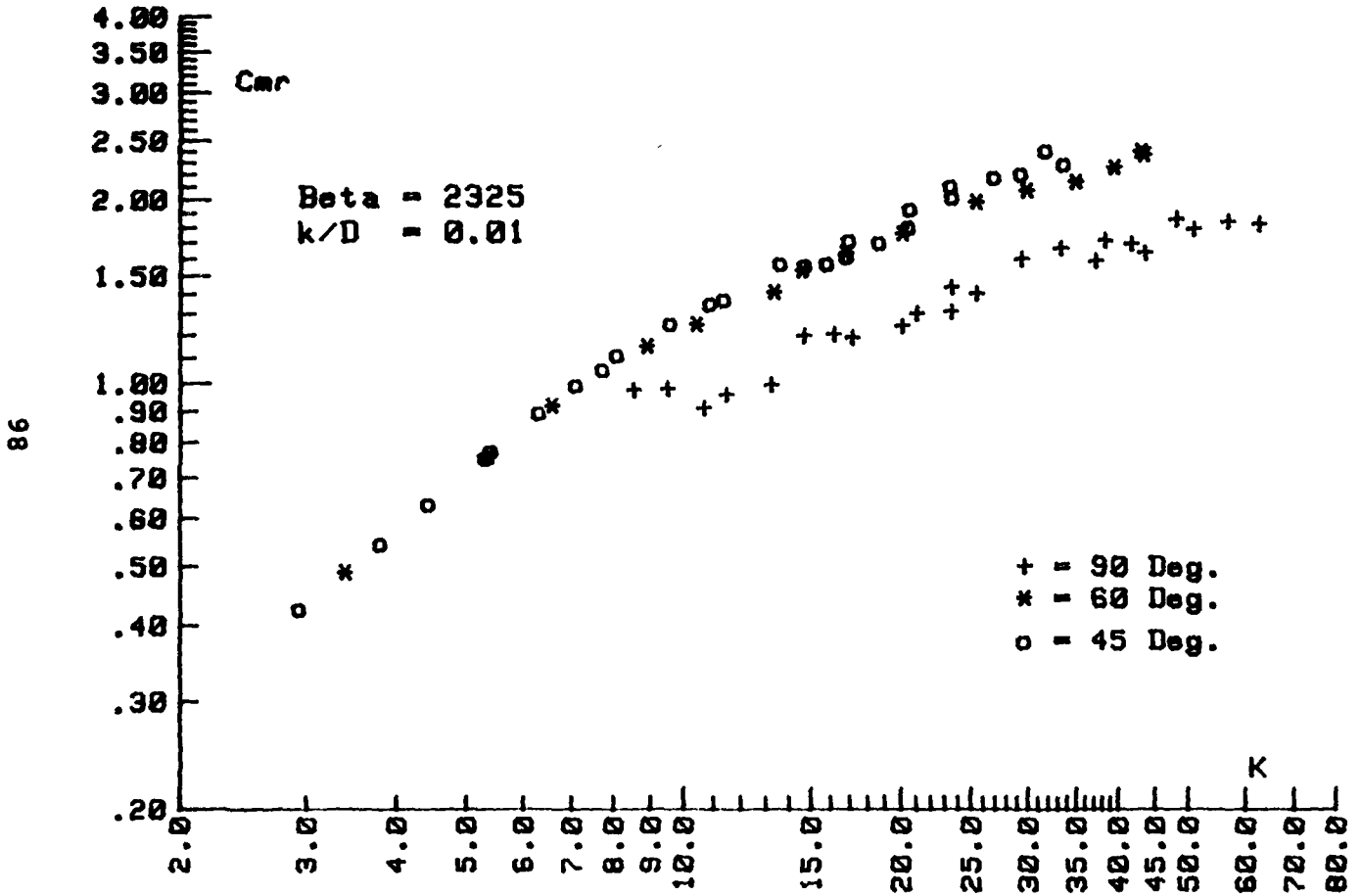

Figure 11e. Comparison of C_{mr} Versus K for β = 2325, k/D = 0.01, α = 90, 60, and 45 Deg.

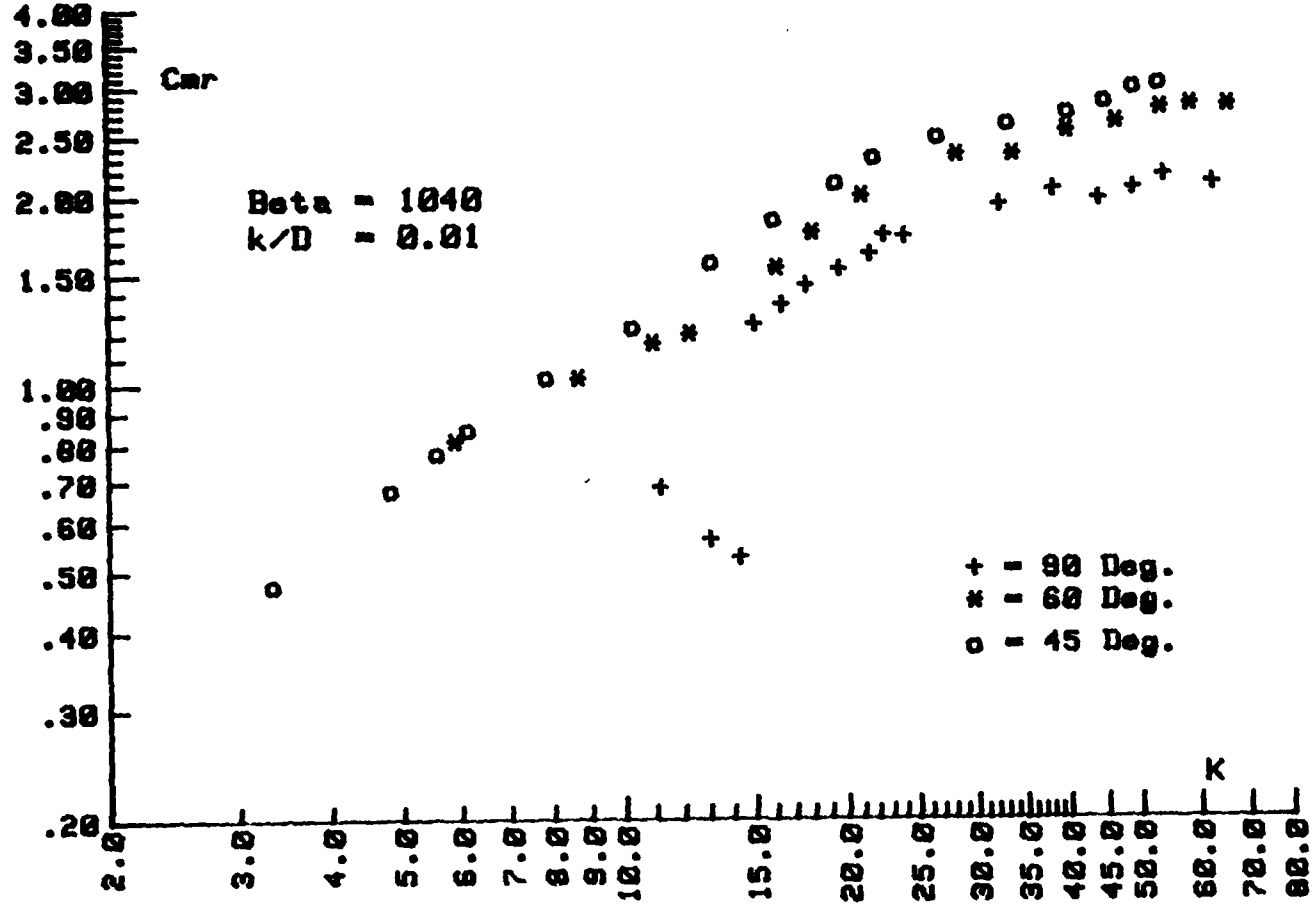

Figure 11f. Comparison of C_{mr} Versus K for β = 1040, k/D = 0.01, α = 90, 60, and 45 Deg.

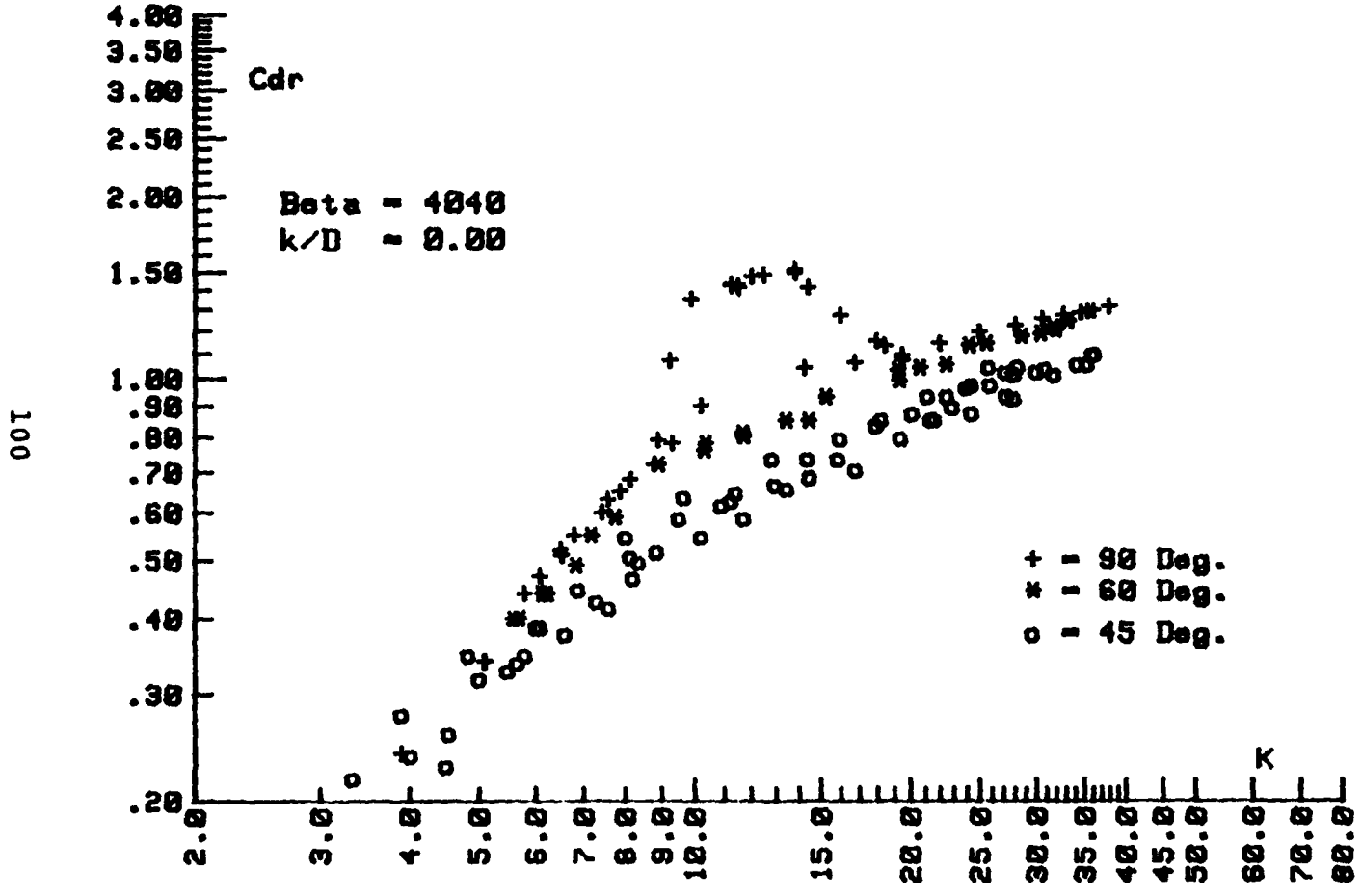

100

Figure 12a. Comparison of C_{dr} Versus K for β = 4040, k/D = 0.00, α = 90, 60, and 45 Deg.

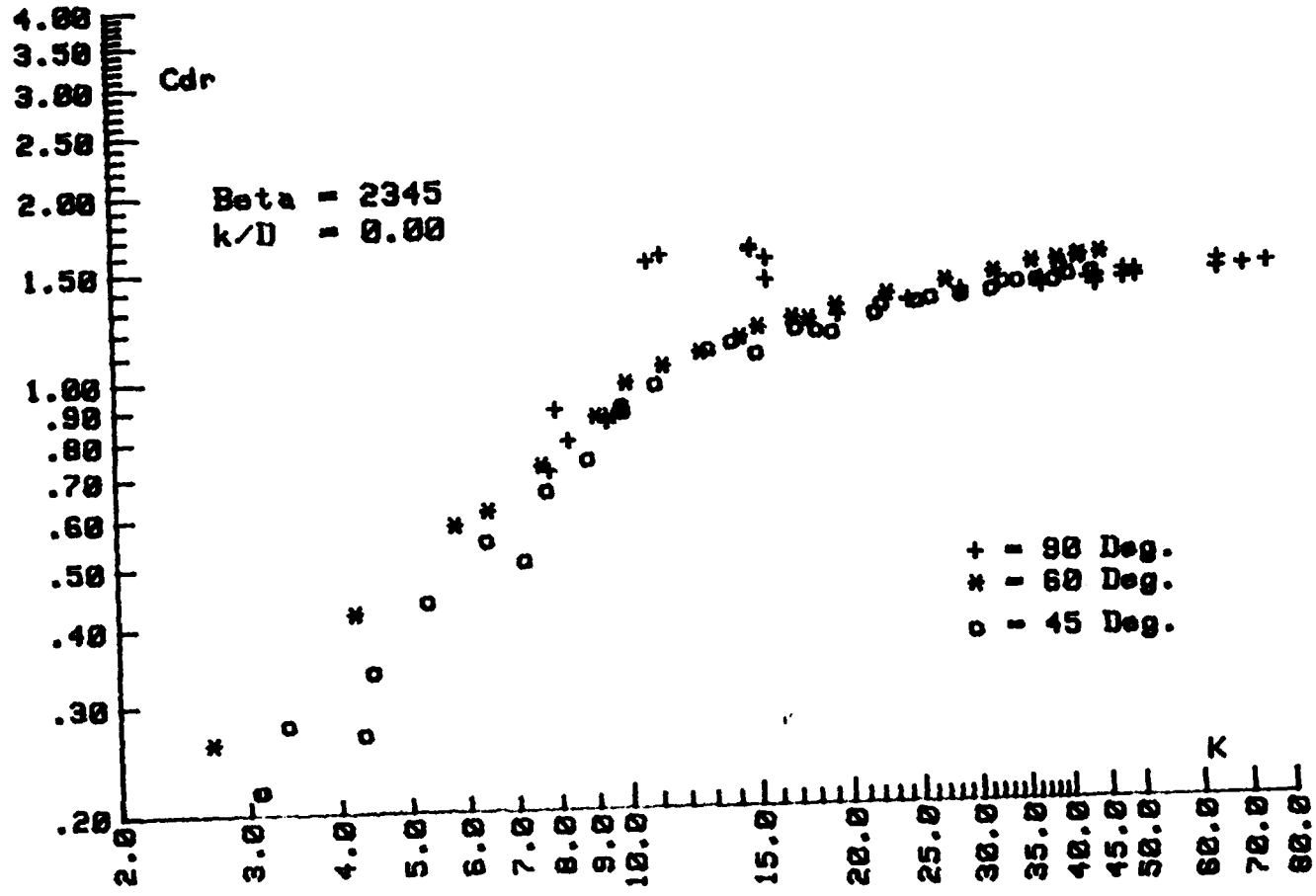

Figure 12b. Comparison of C_{dr} Versus K for β = 2345, k/D = 0.00, α = 90, 60, and 45 Deg.

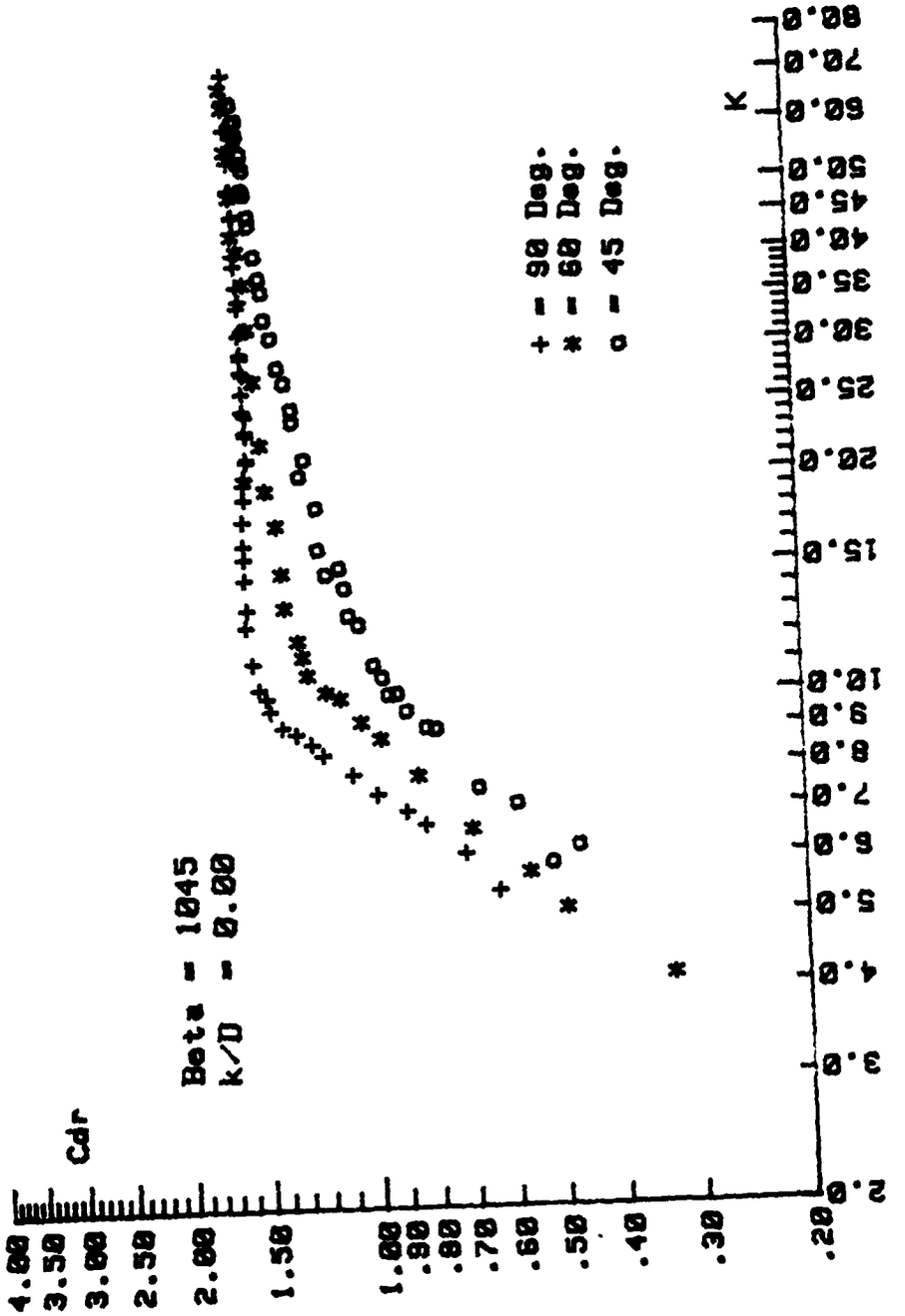

Figure 12c. Comparison of C_{dr} Versus K for β = 1045, k/D = 0.00, α = 90, 60, and 45 Deg.

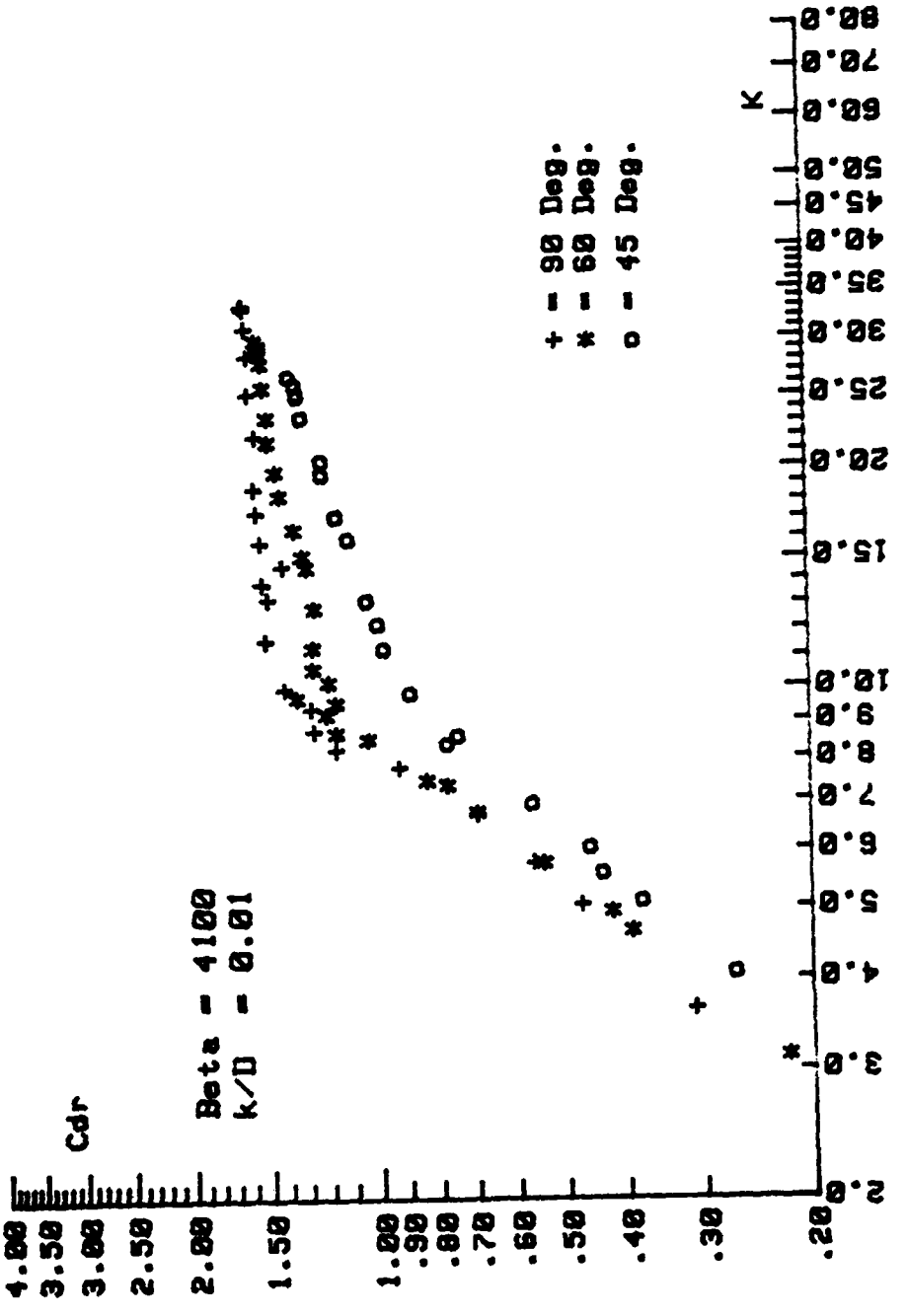

Figure 12d. Comparison of C_{dr} Versus K for β = 4100, k/D = 0.01, α = 90, 60, and 45 Deg.

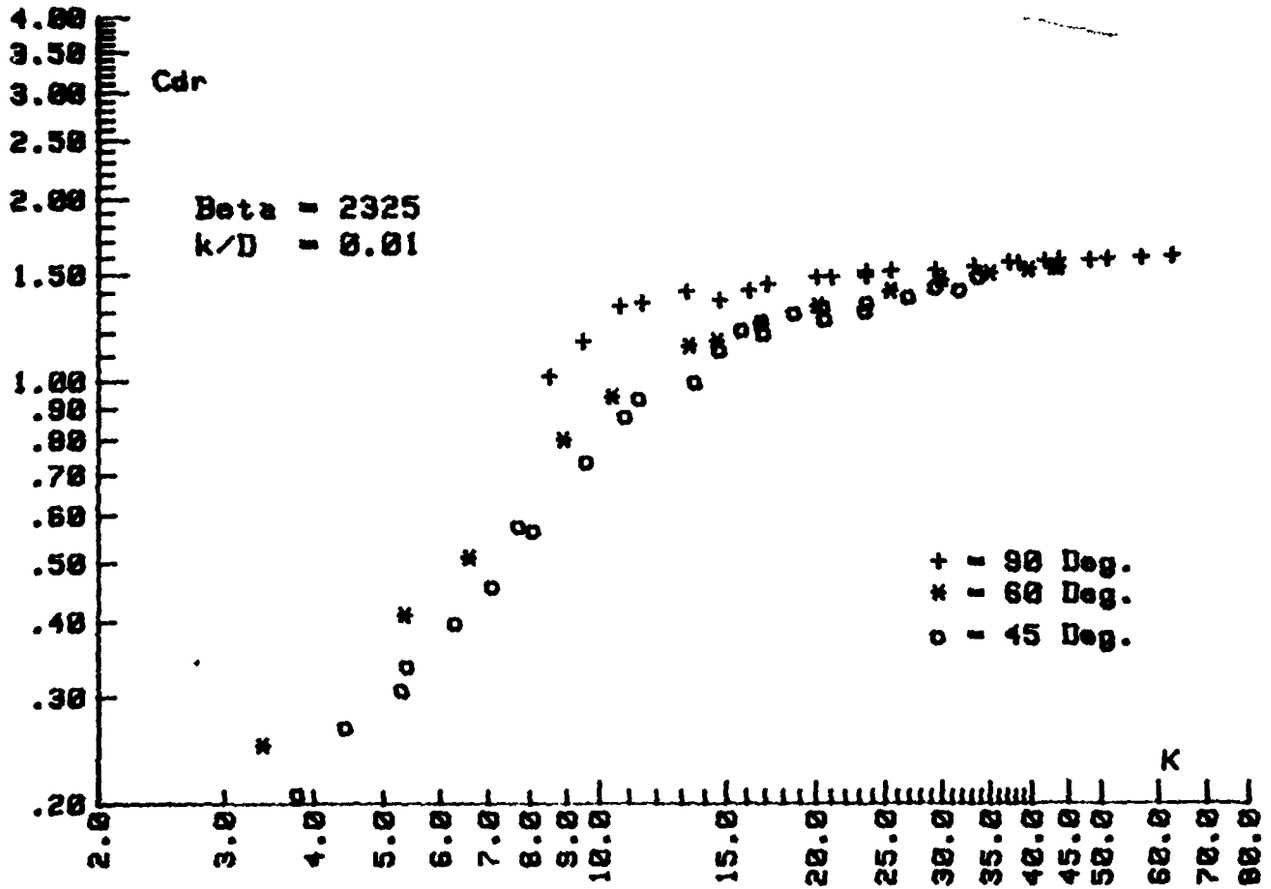

Figure 12e. Comparison of C_{dr} Versus K for β = 2325, k/D = 0.01, α = 90, 60, and 45 Deg.

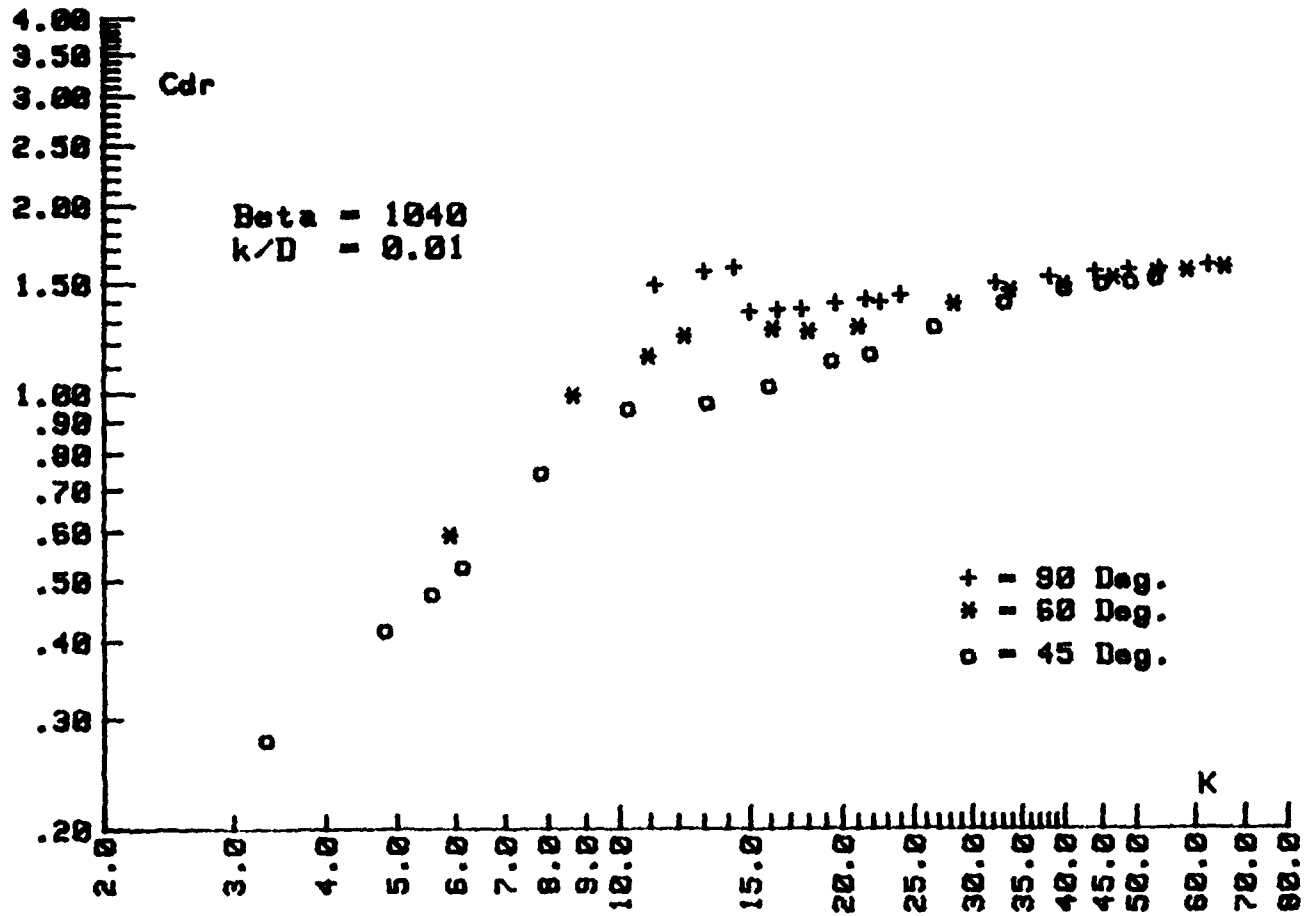

Figure 12f. Comparison of C_{dr} Versus K for β = 1040, k/D = 0.01, α = 90, 60, and 45 Deg.

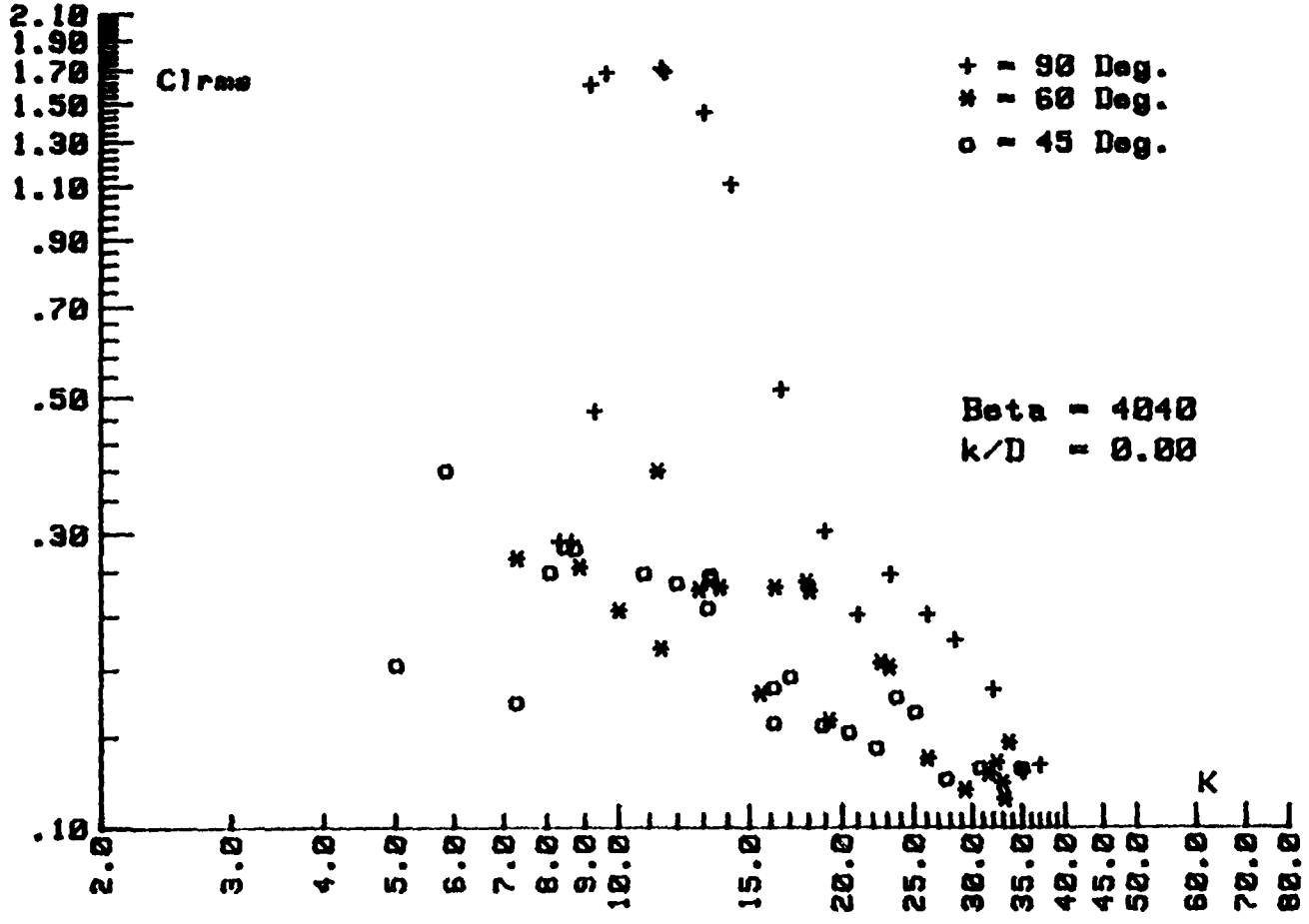

Figure 13a. Comparison of C_{lrms} Versus K for β = 4040, k/D = 0.00, α = 90, 60, and 45 Deg.

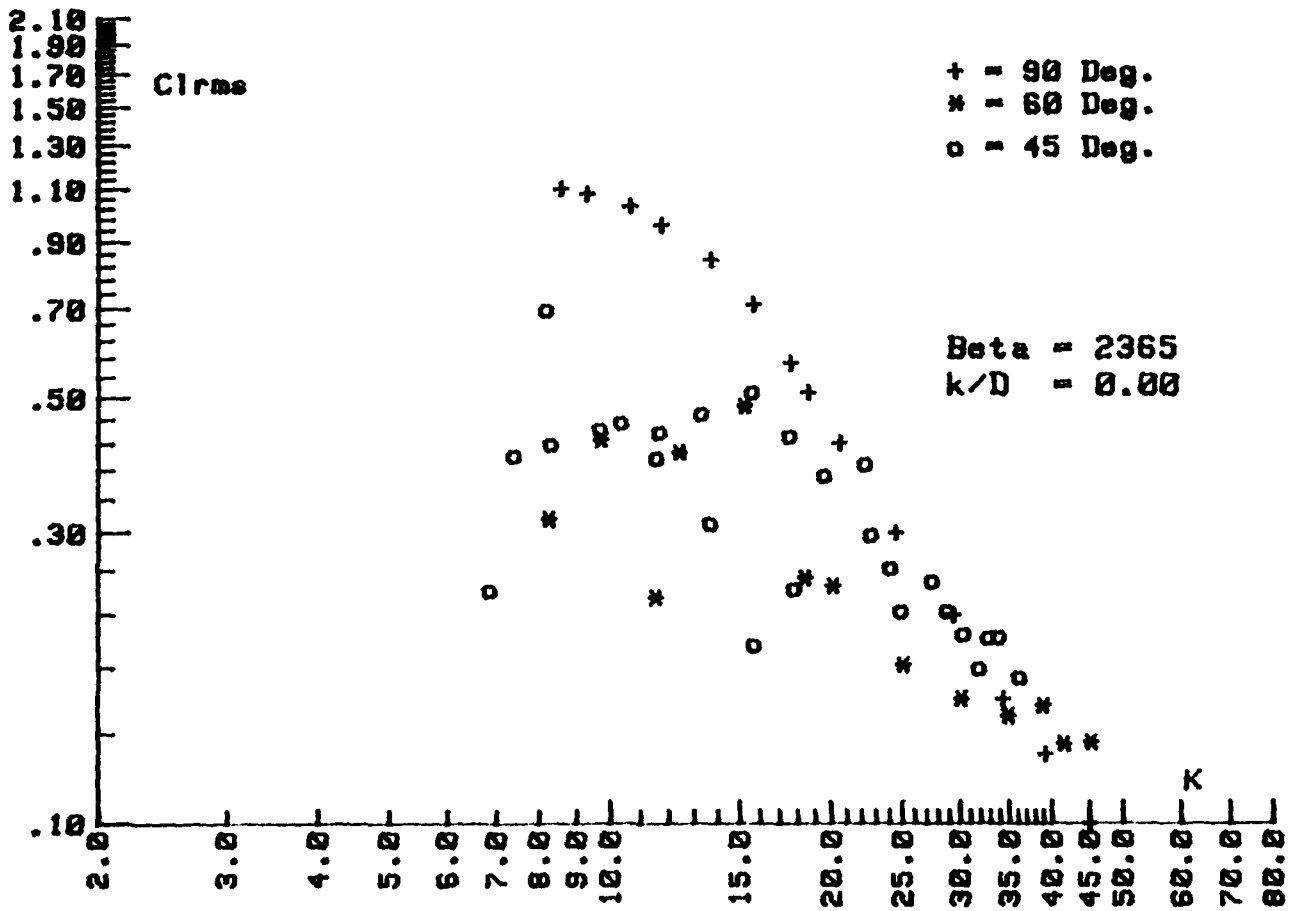

Figure 13b. Comparison of C_{lrms} Versus K for β = 2365, k/D = 0.00, α = 90, 60, and 45 Deg.

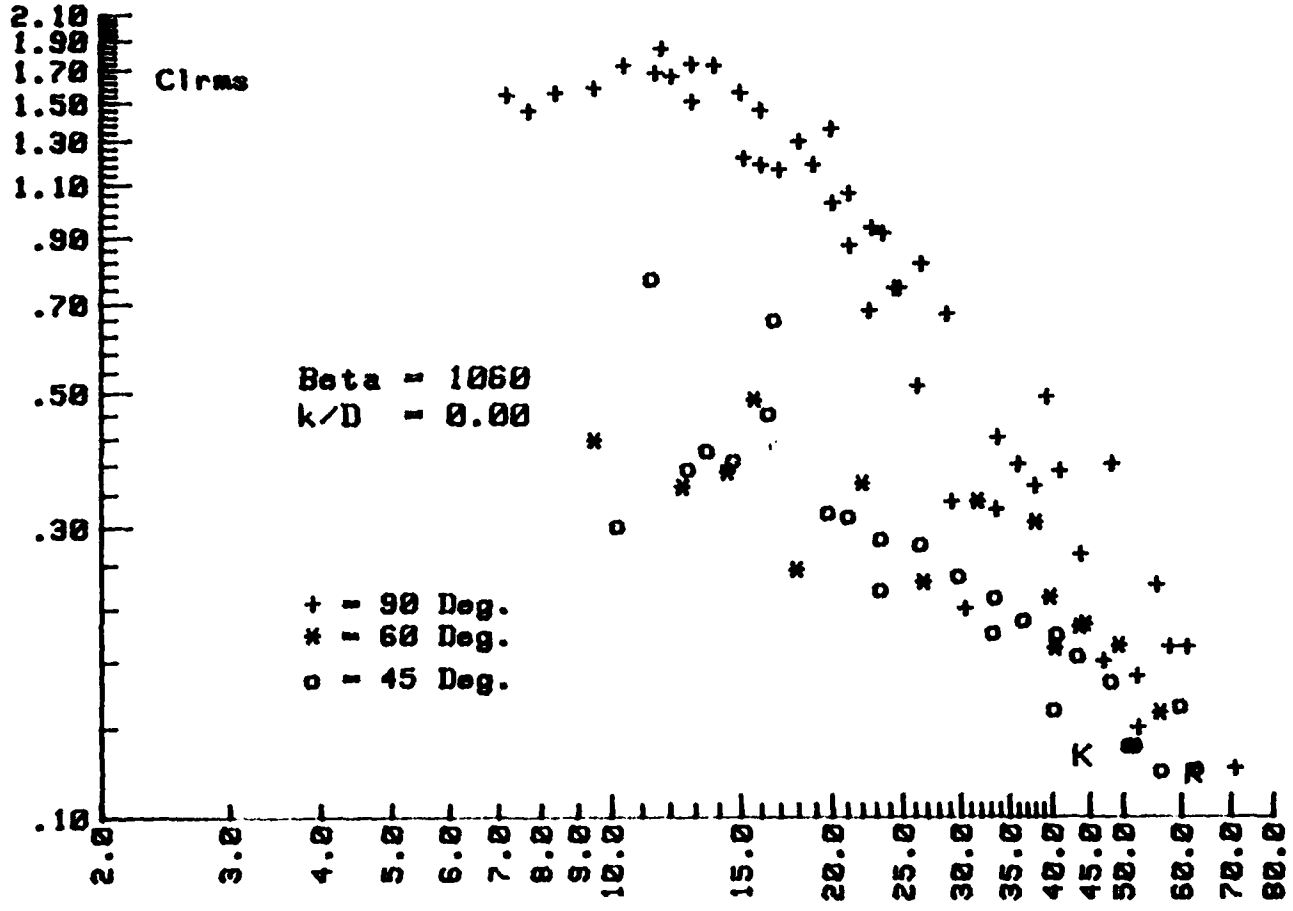

Figure 13c. Comparison of C_{lrms} Versus K for β = 1060, k/D = 0.00, α = 90, 60, and 45 Deg.

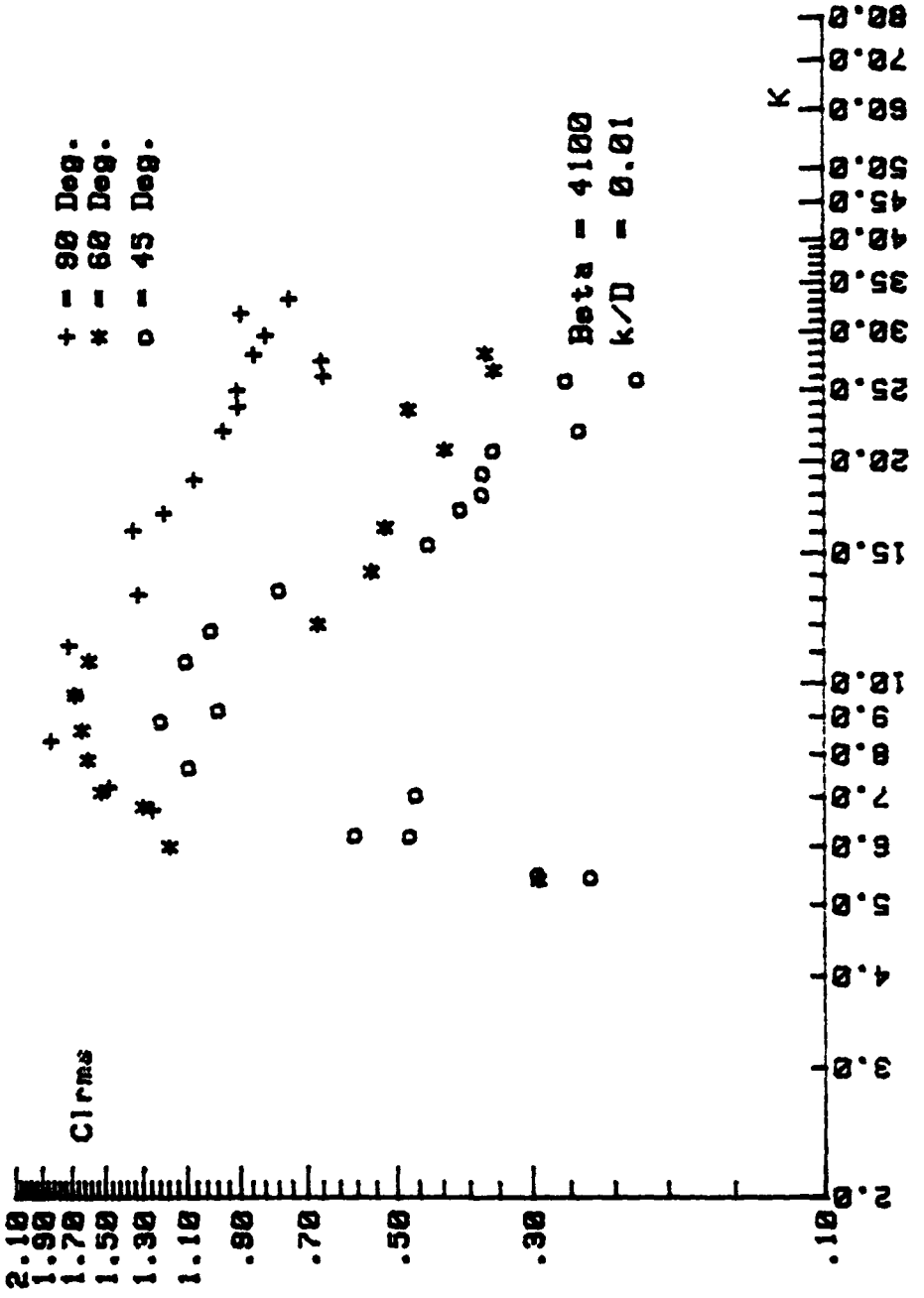

Figure 13d. Comparison of C_{lrms} Versus K for β = 4100, k/D = 0.01, α = 90, 60, and 45 Deg.

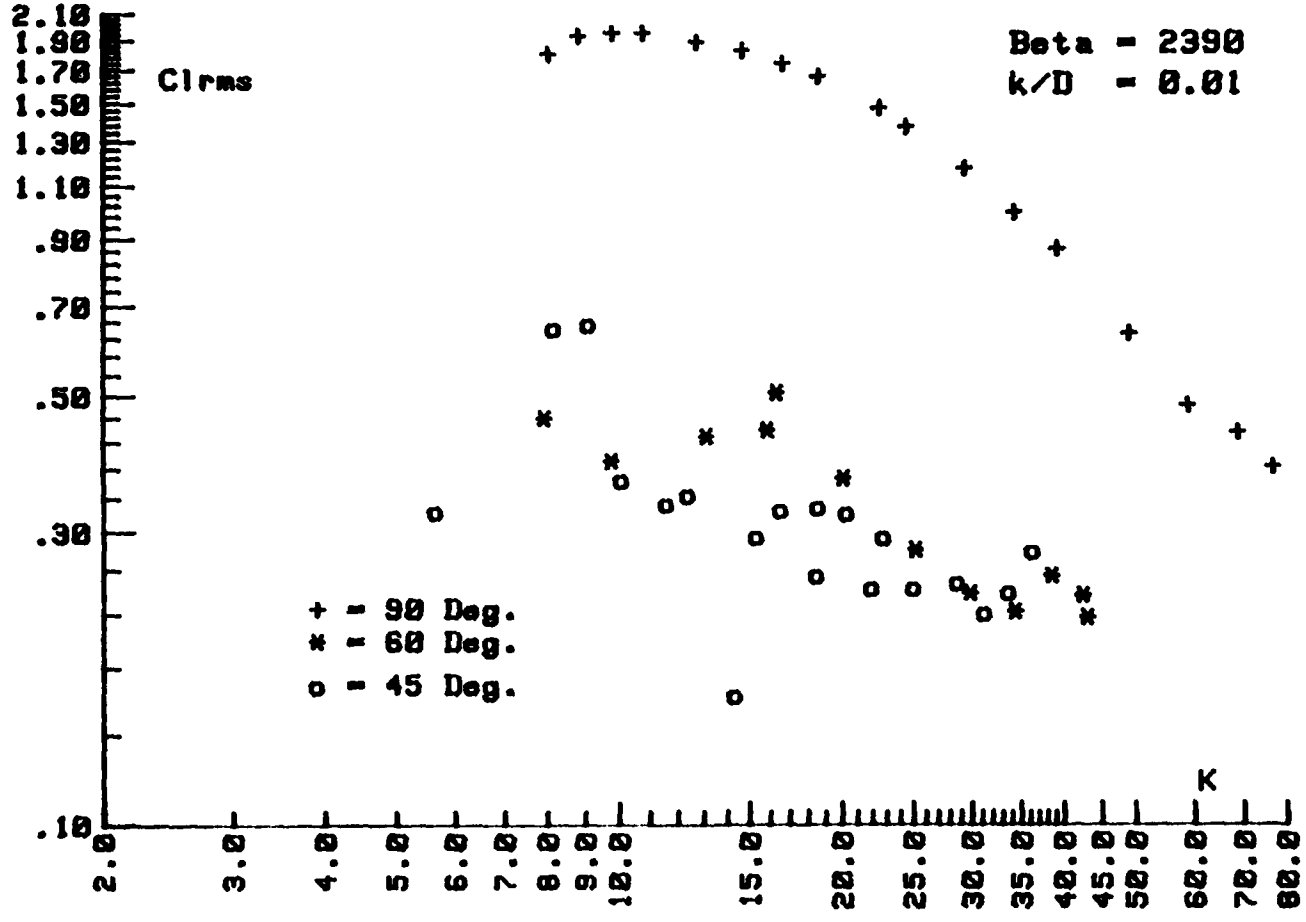

Figure 13e. Comparison of C_{lrms} Versus K for β = 2390, k/D = 0.01, α = 90, 60, and 45 Deg.

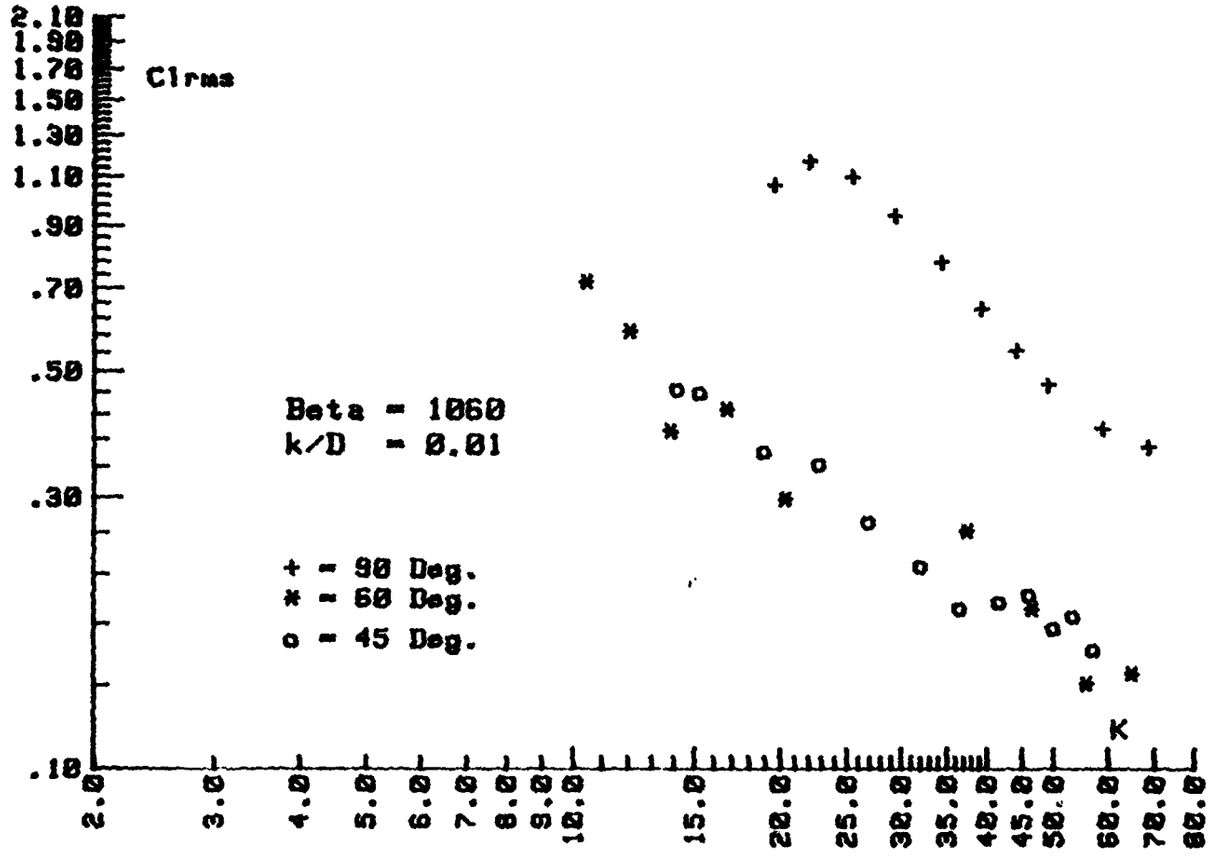

Figure 13f. Comparison of C_{lrms} Versus K for β = 1060, k/D = 0.01, α = 90, 60, and 45 Deg.

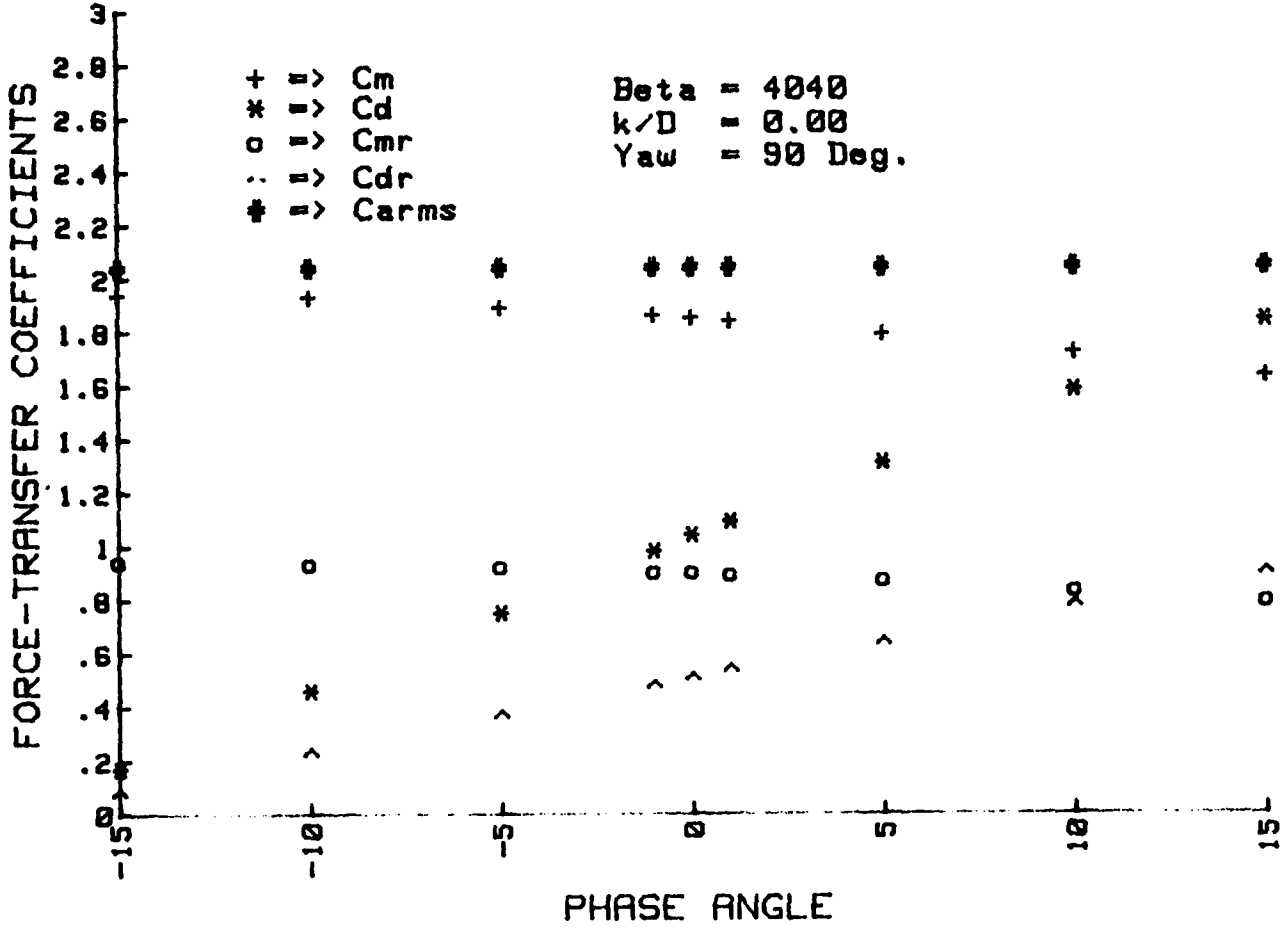

Figure 14a. Force-Transfer Coefficients Versus Phase Angle for K = 6.66.

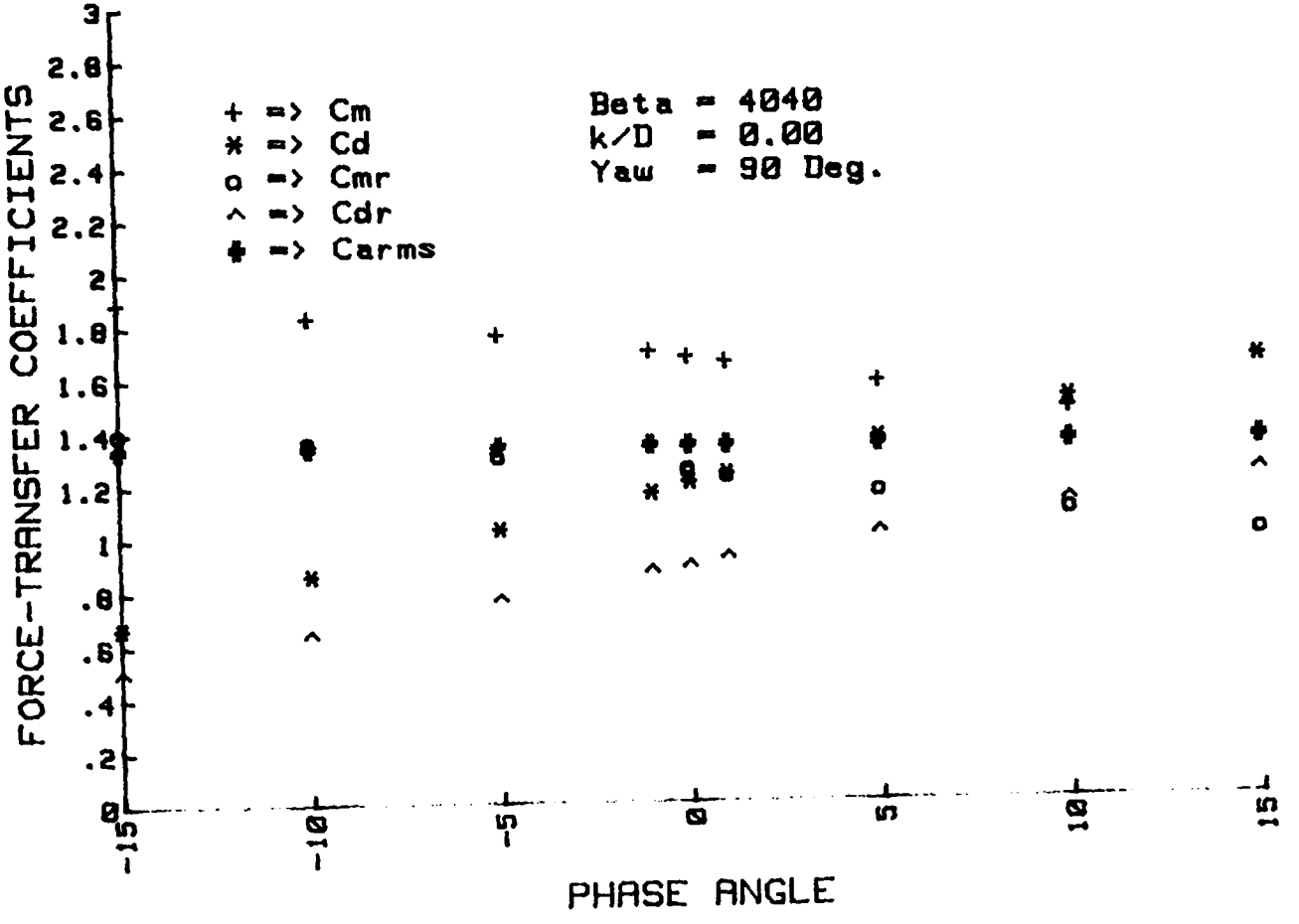

Figure 14b. Force-Transfer Coefficients Versus Phase Angle for K = 10.41.

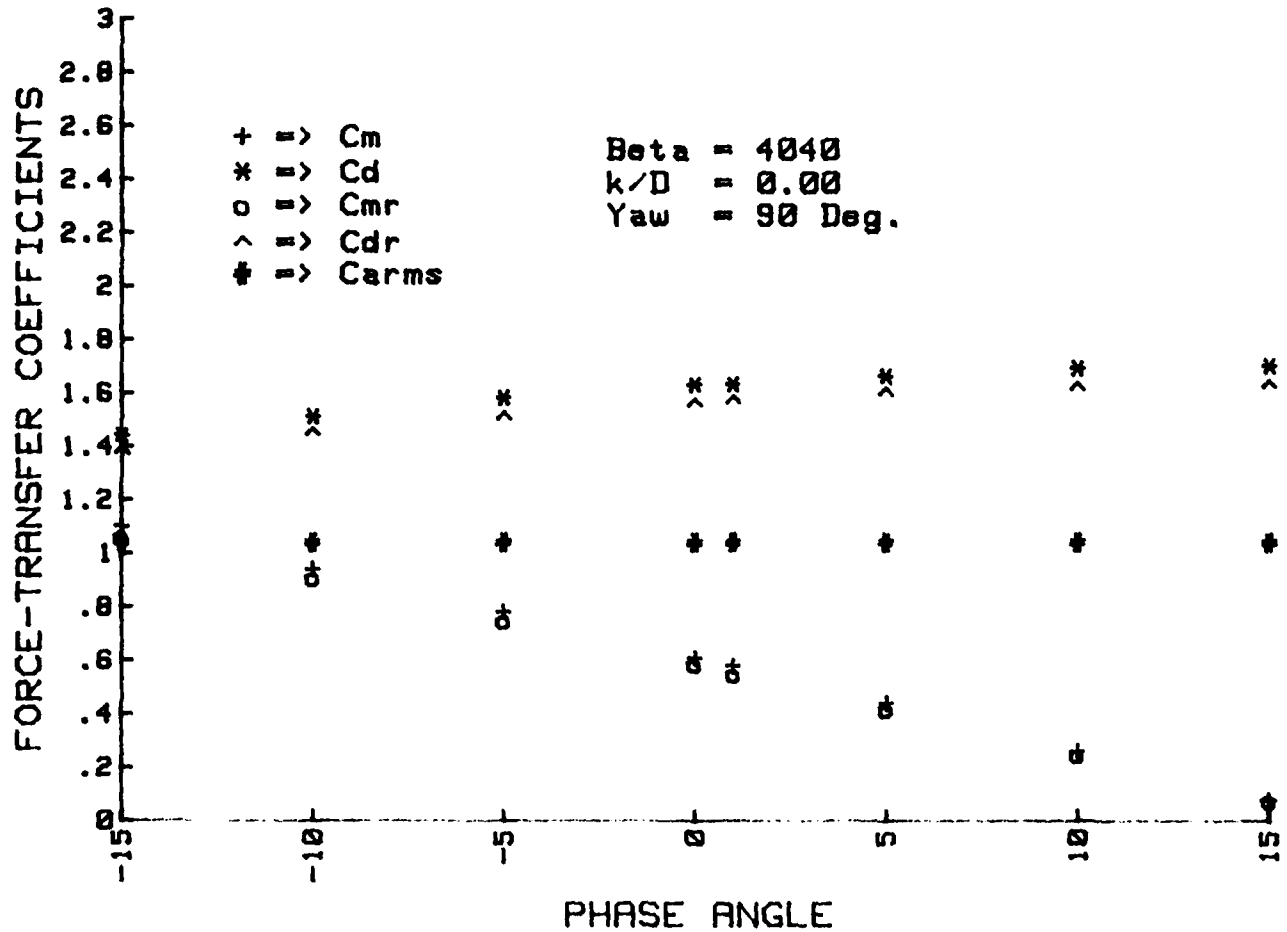

Figure 14c. Force-Transfer Coefficients Versus Phase Angle for K = 14.08.

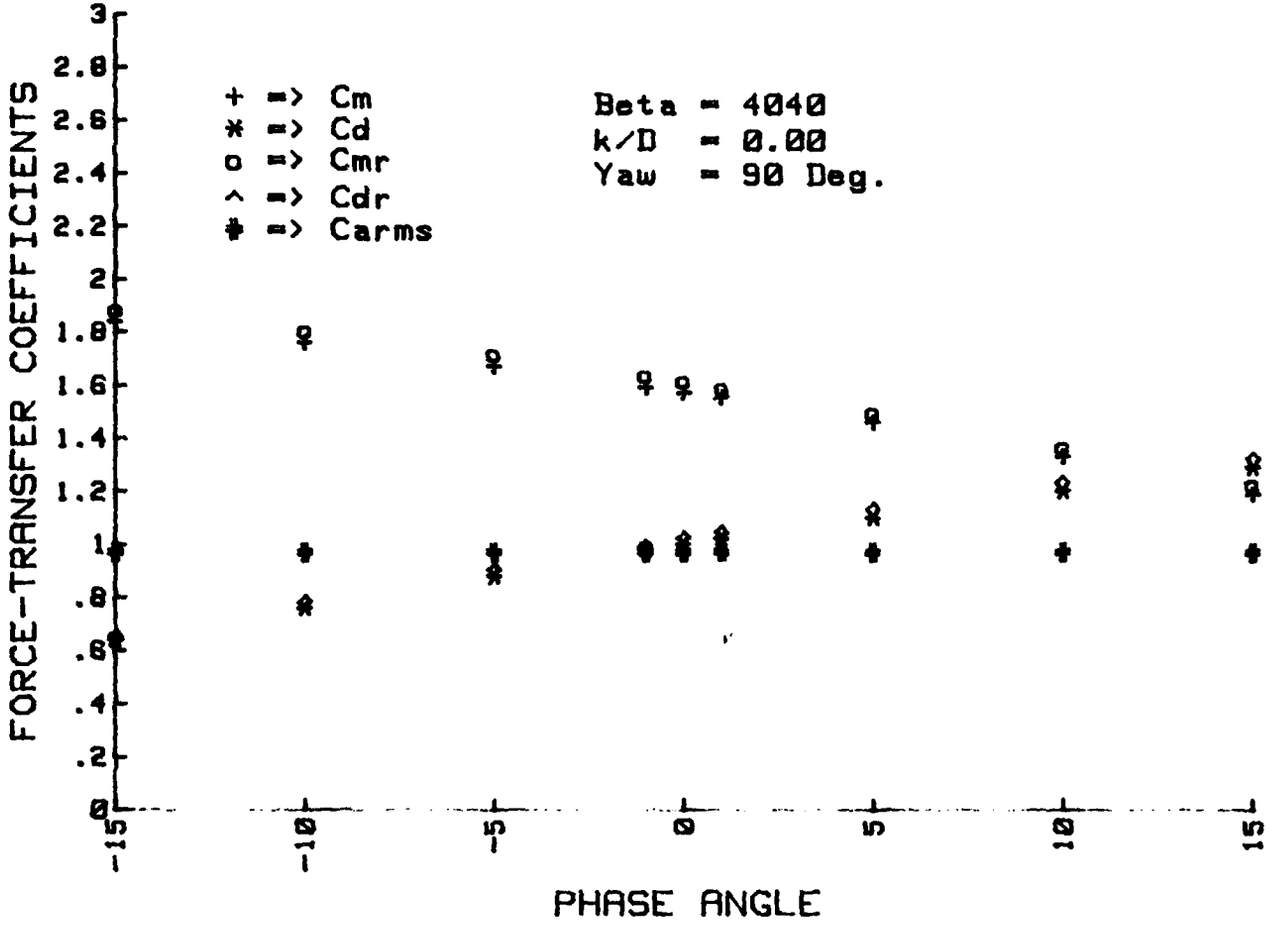

Figure 14d. Force-Transfer Coefficients Versus Phase Angle for K = 14.51.

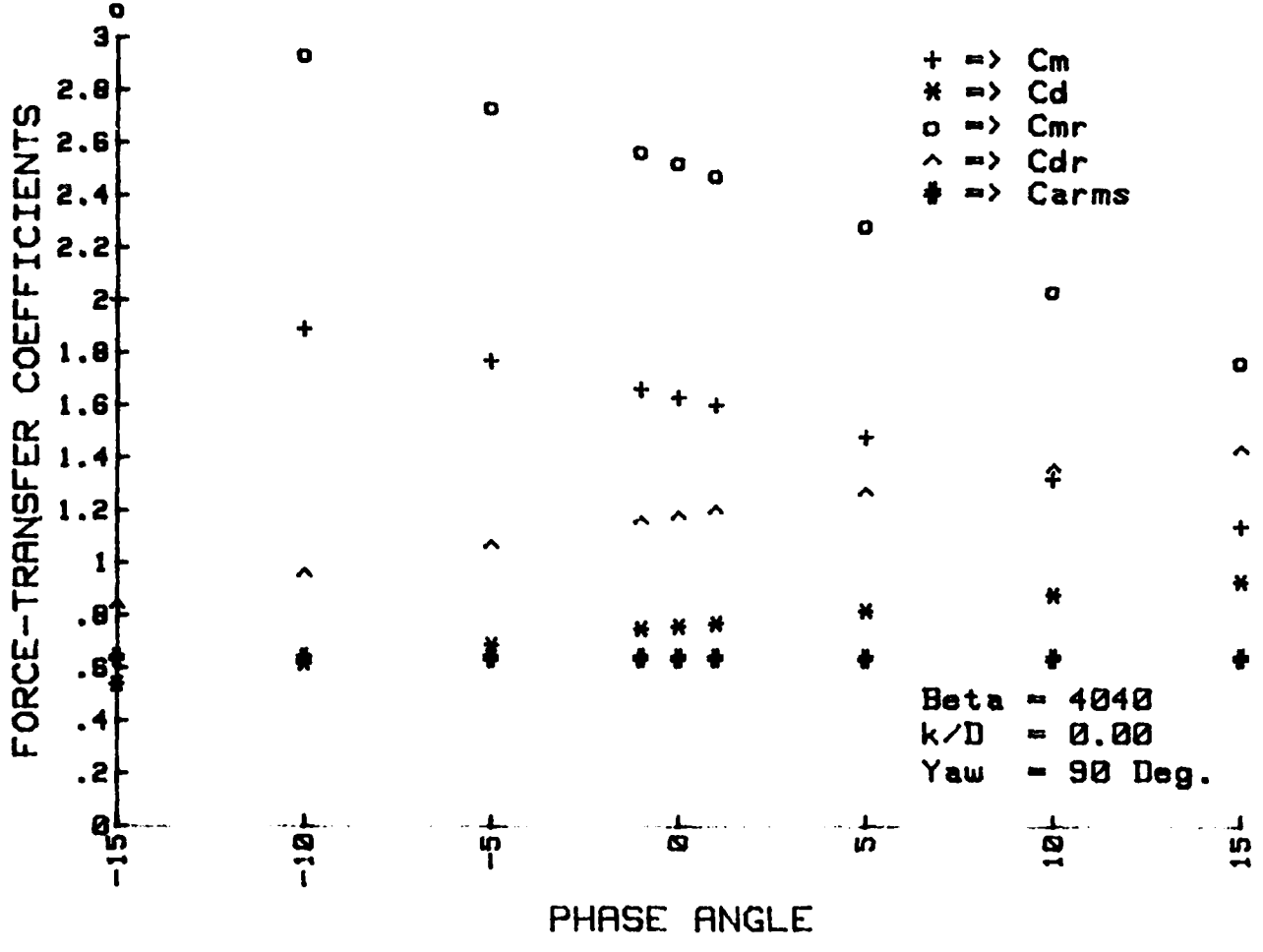

Figure 14e. Force-Transfer Coefficients Versus Phase Angle for K = 25.44.

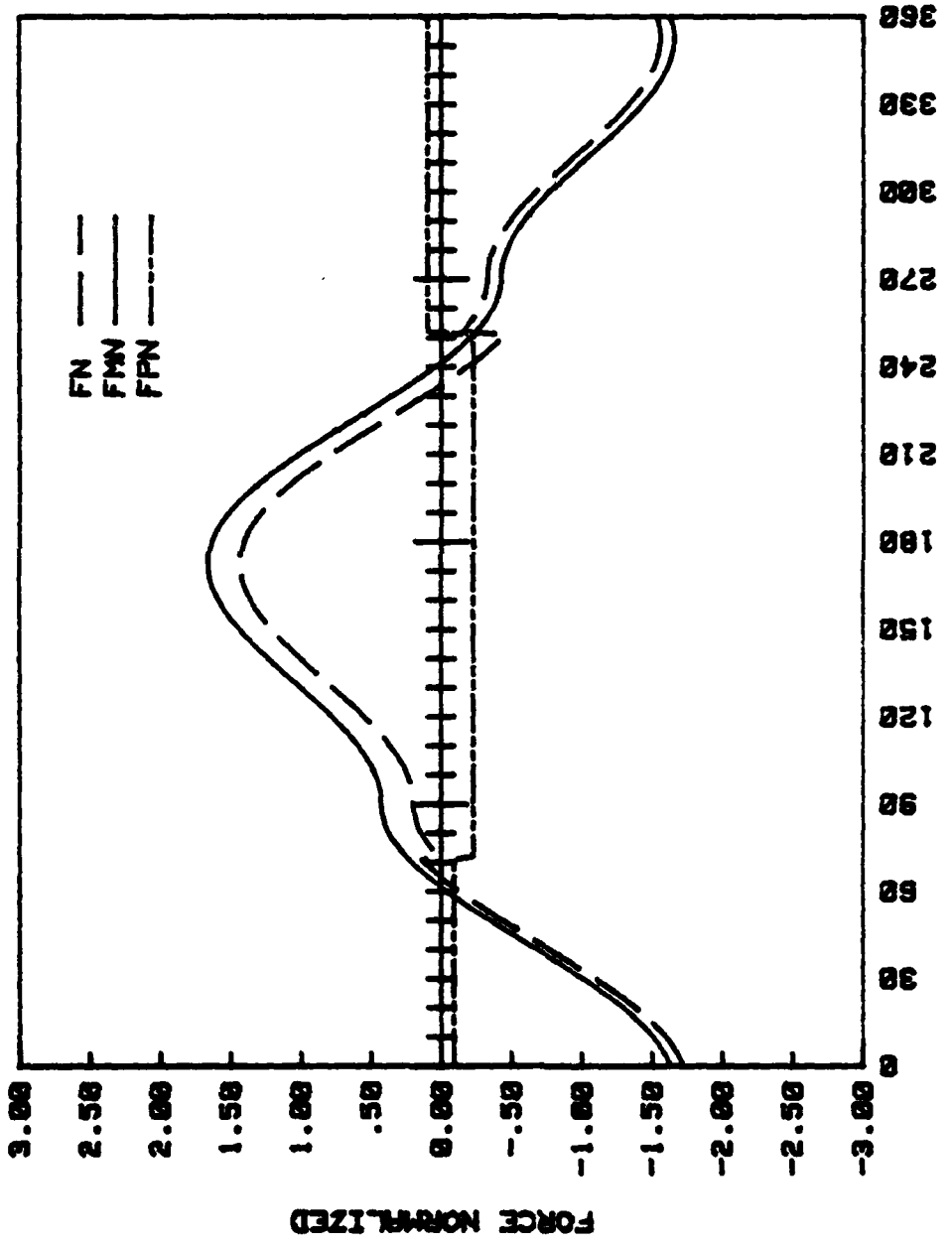

Figure 15a. Normalized Force Plus a Random Disturbance of Frequency Ratio 1.

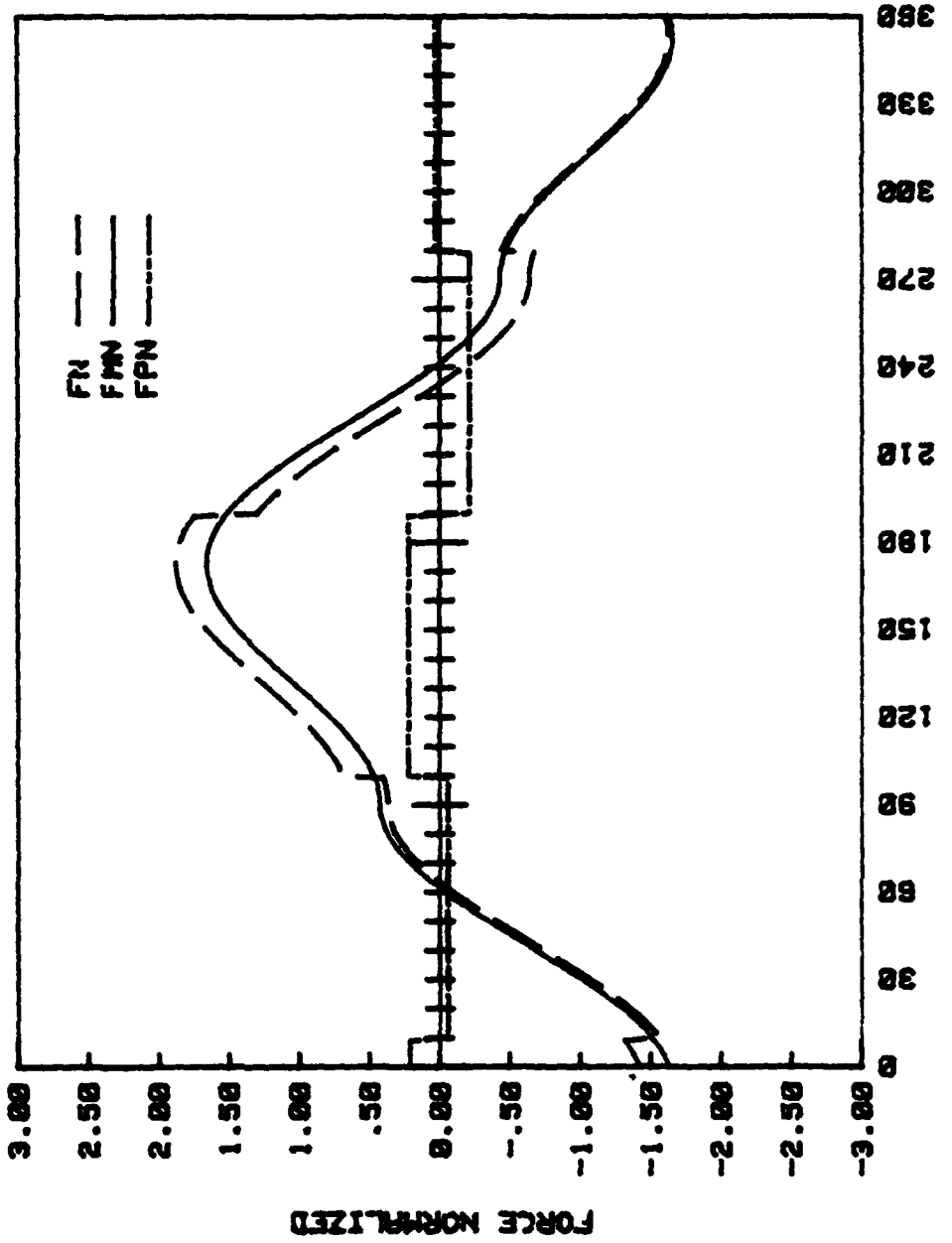

Figure 15b. Normalized Force Plus a Random Disturbance of Frequency Ratio 2.

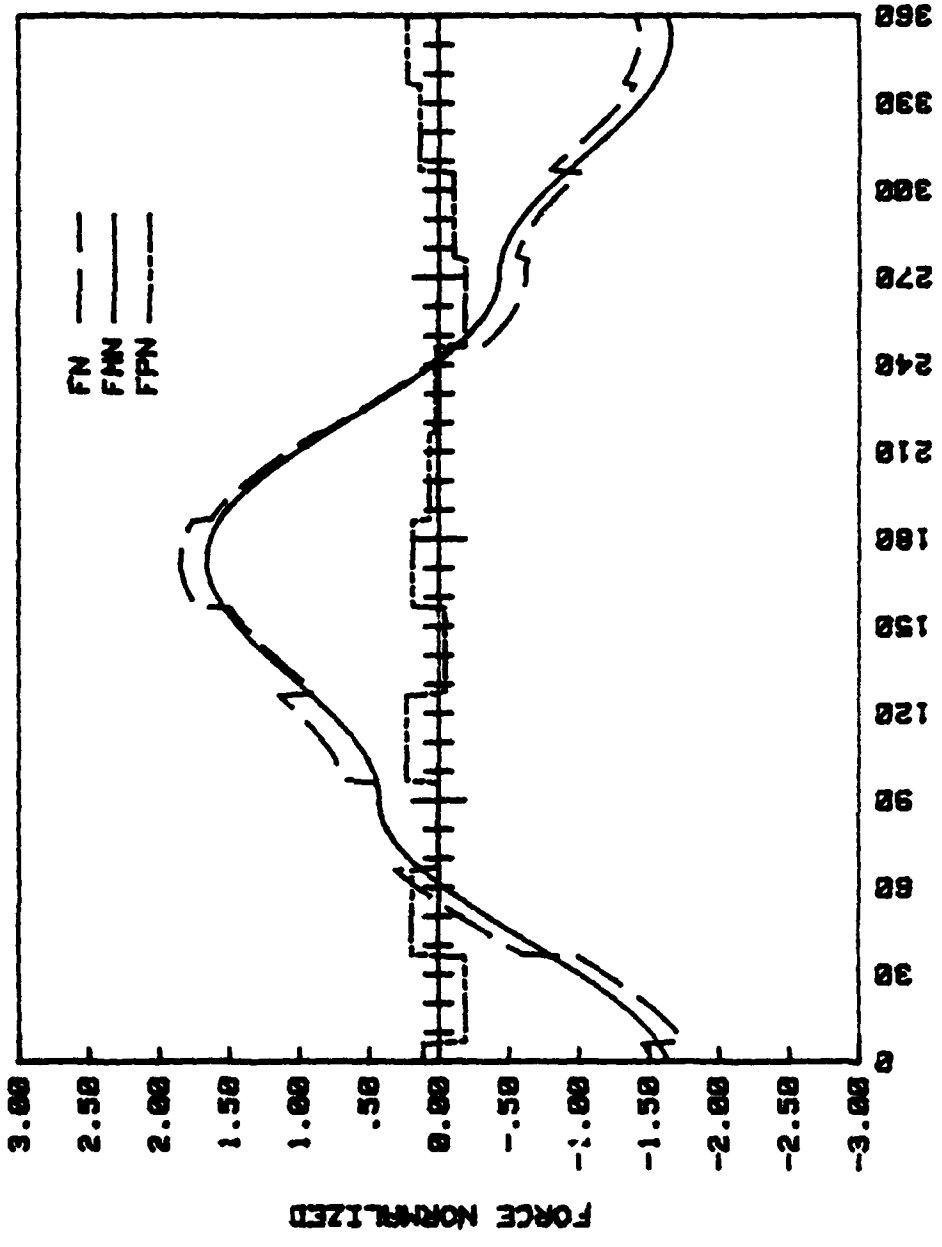

Figure 15c. Normalized Force Plus a Random Disturbance of Frequency Ratio 6.

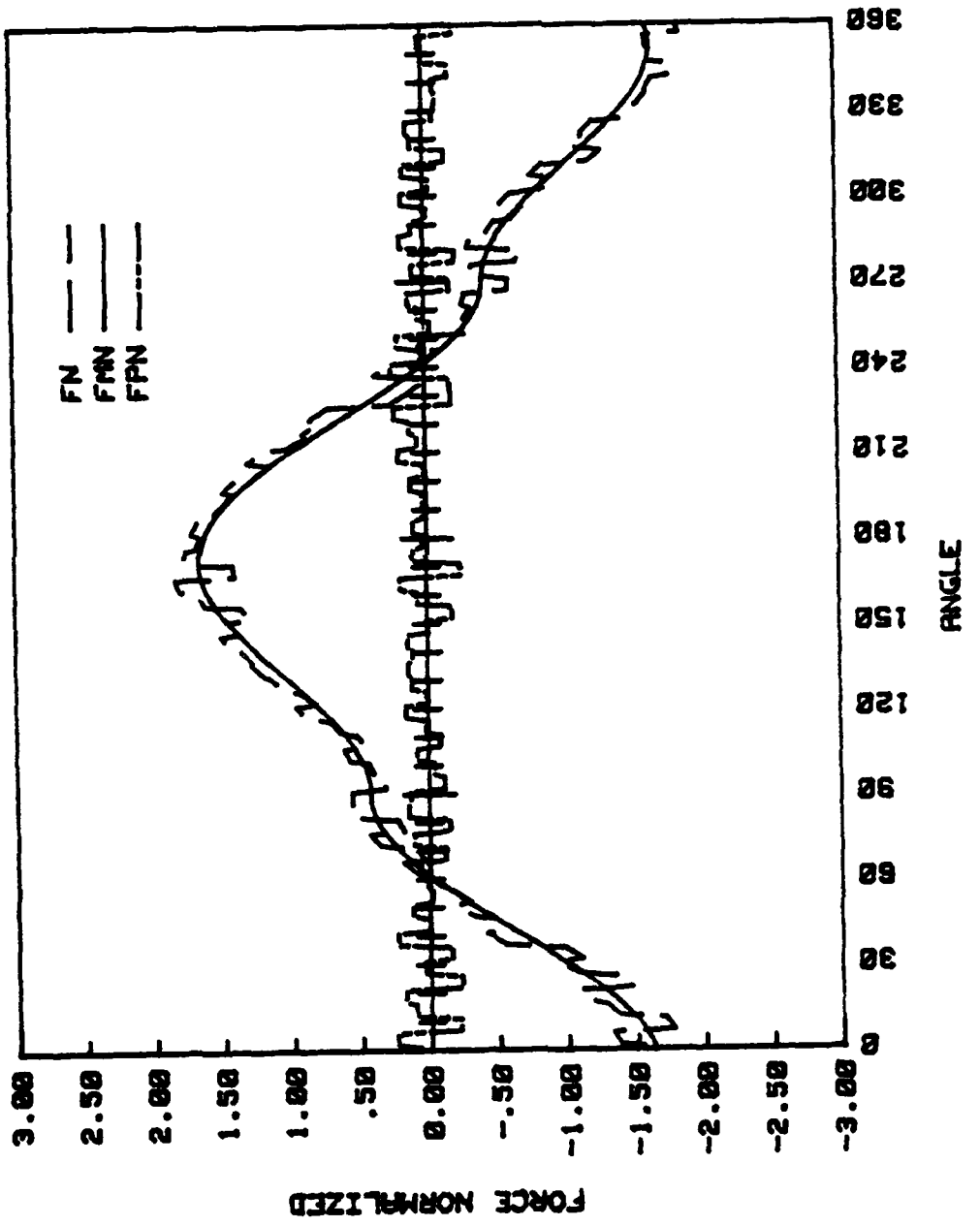

Figure 15d. Normalized Force Plus a Random Disturbance of Frequency Ratio 36.

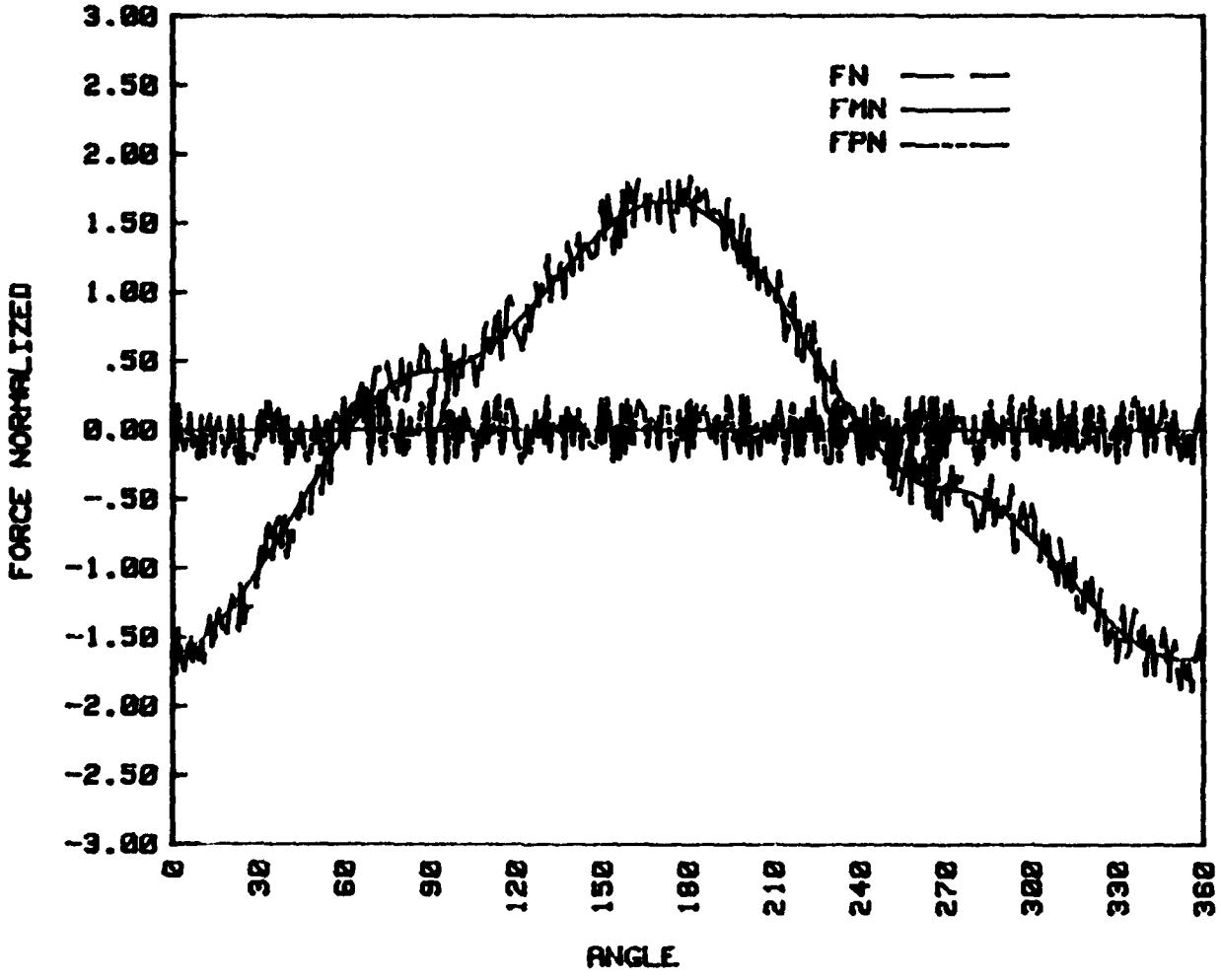

Figure 15e. Normalized Force Plus a Random Disturbance of Frequency Ratio 180.

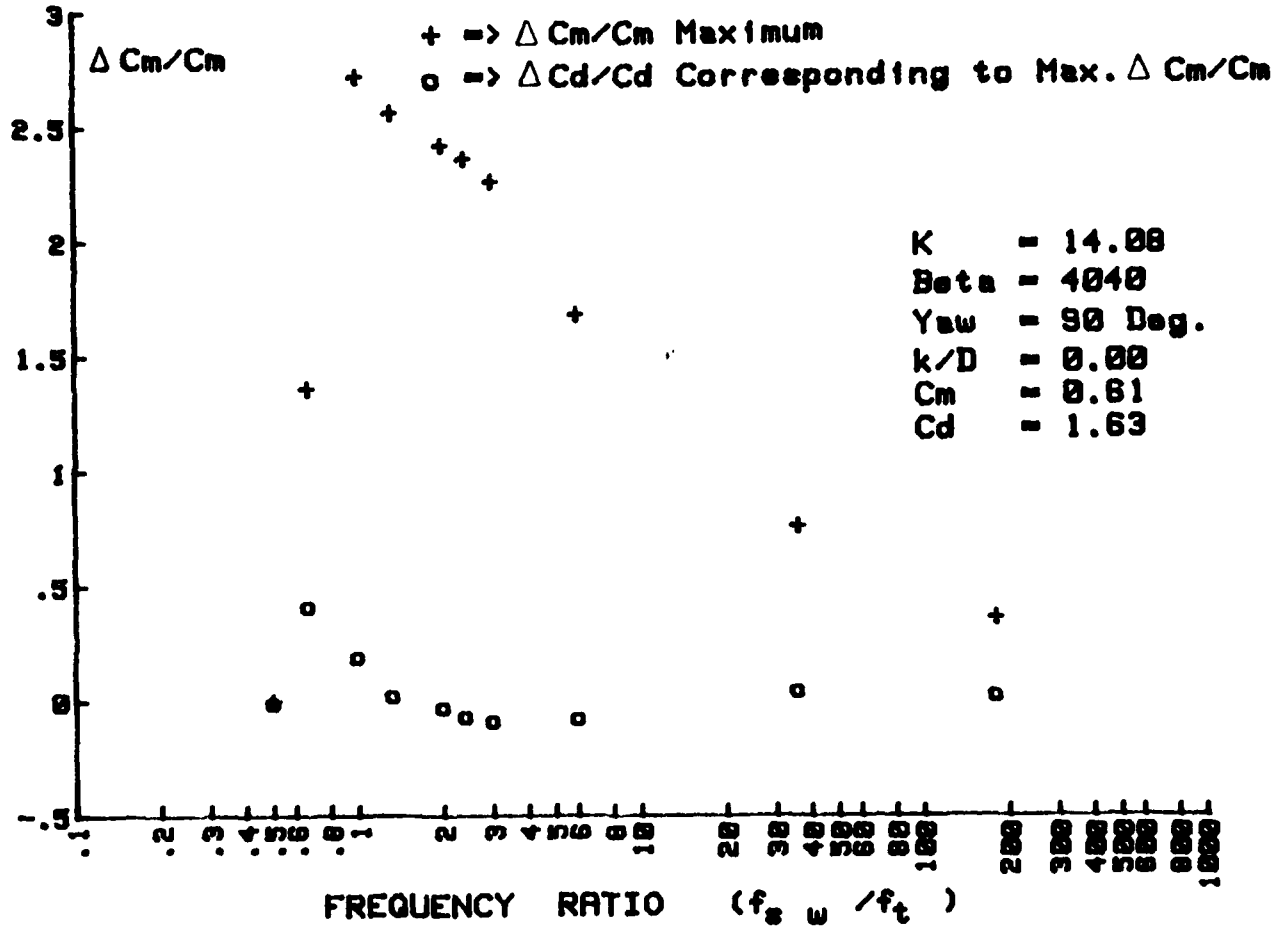

Figure 16a. Response of C_m and the Corresponding C_d to Random Disturbances of Various Frequency Ratios, K = 14.08.

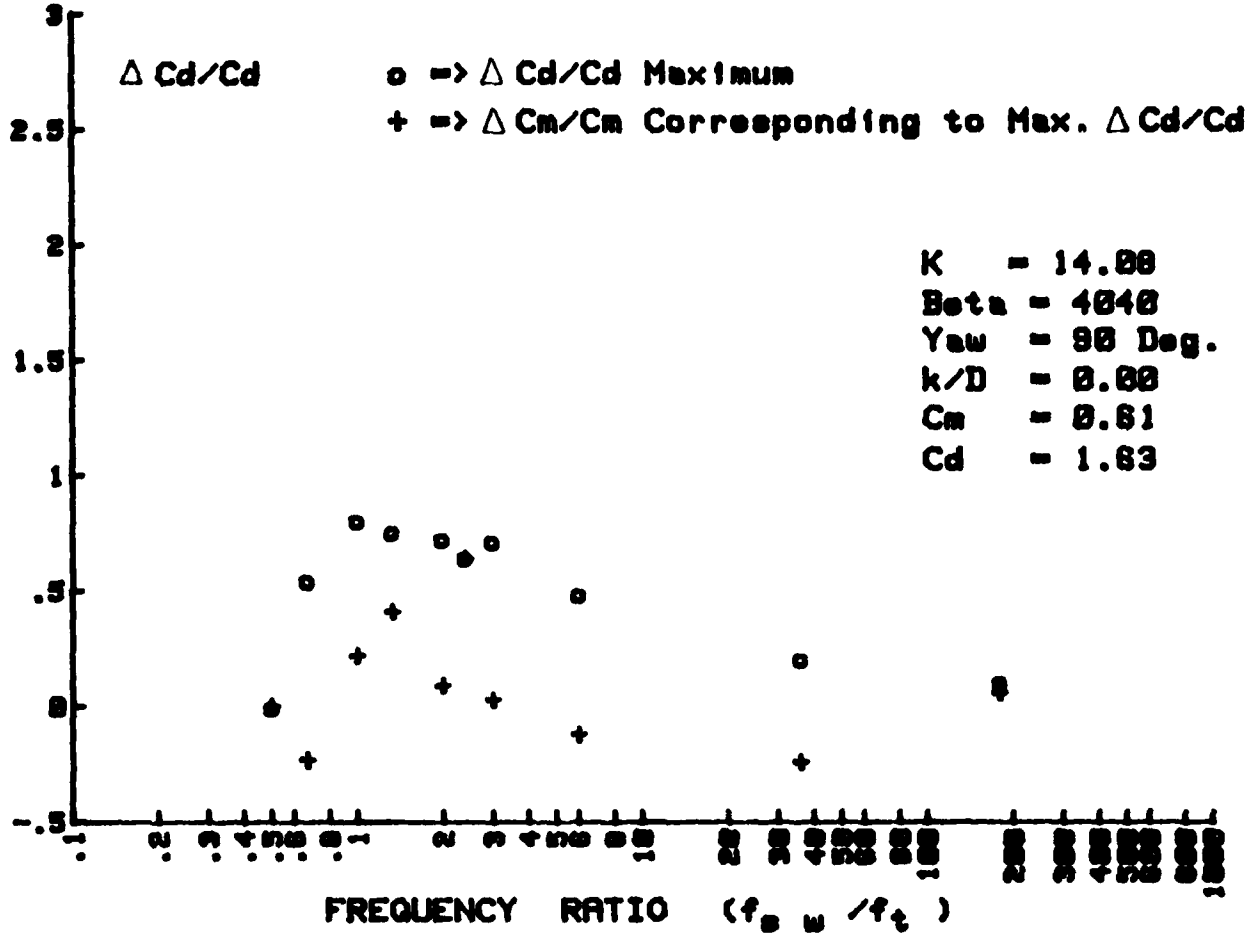

Figure 16b. Response of C_d and the Corresponding C_m to Random Disturbances of Various Frequency Ratios, K = 14.08.

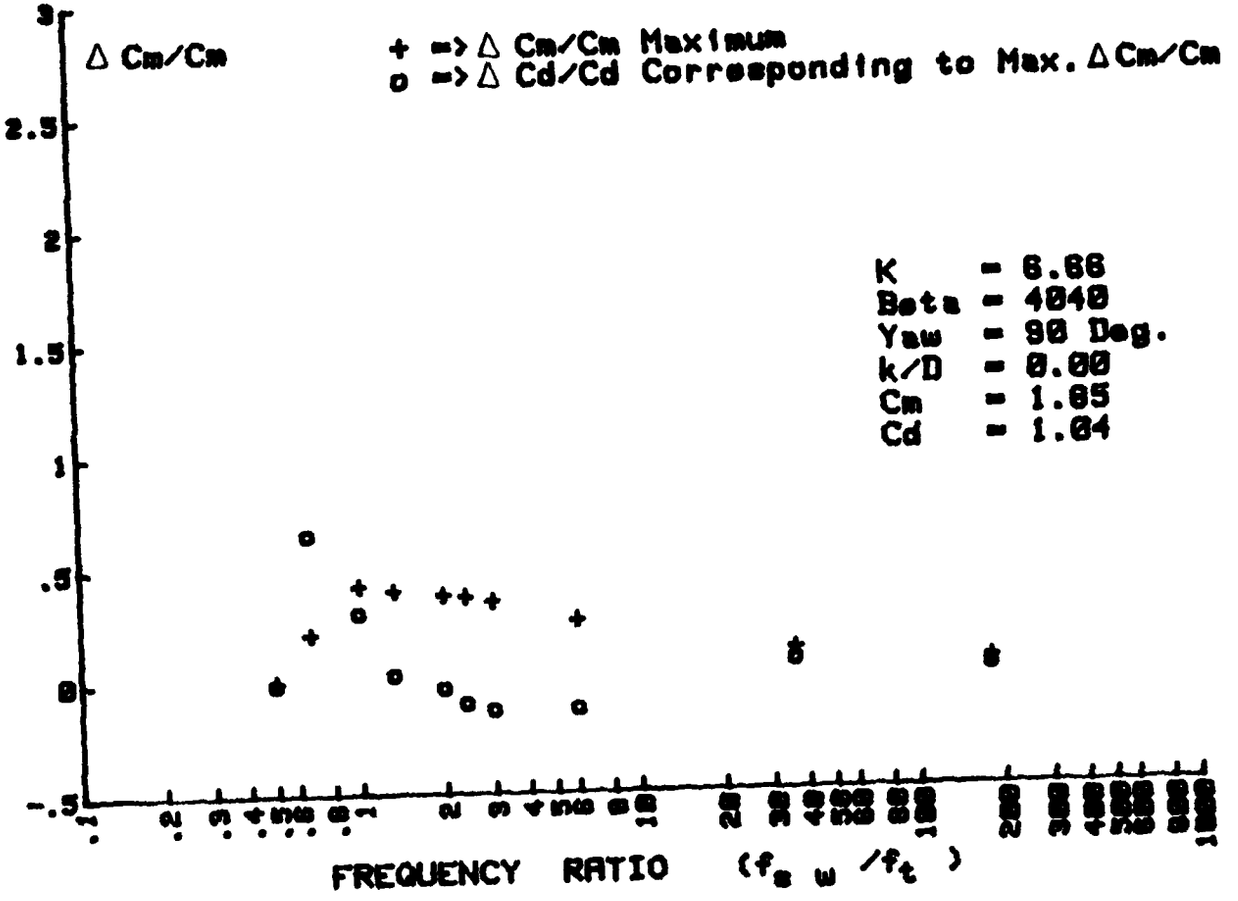

Figure 17a. Response of C_m and the Corresponding C_d to Random Disturbances of Various Frequency Ratios, $K = 6.66$.

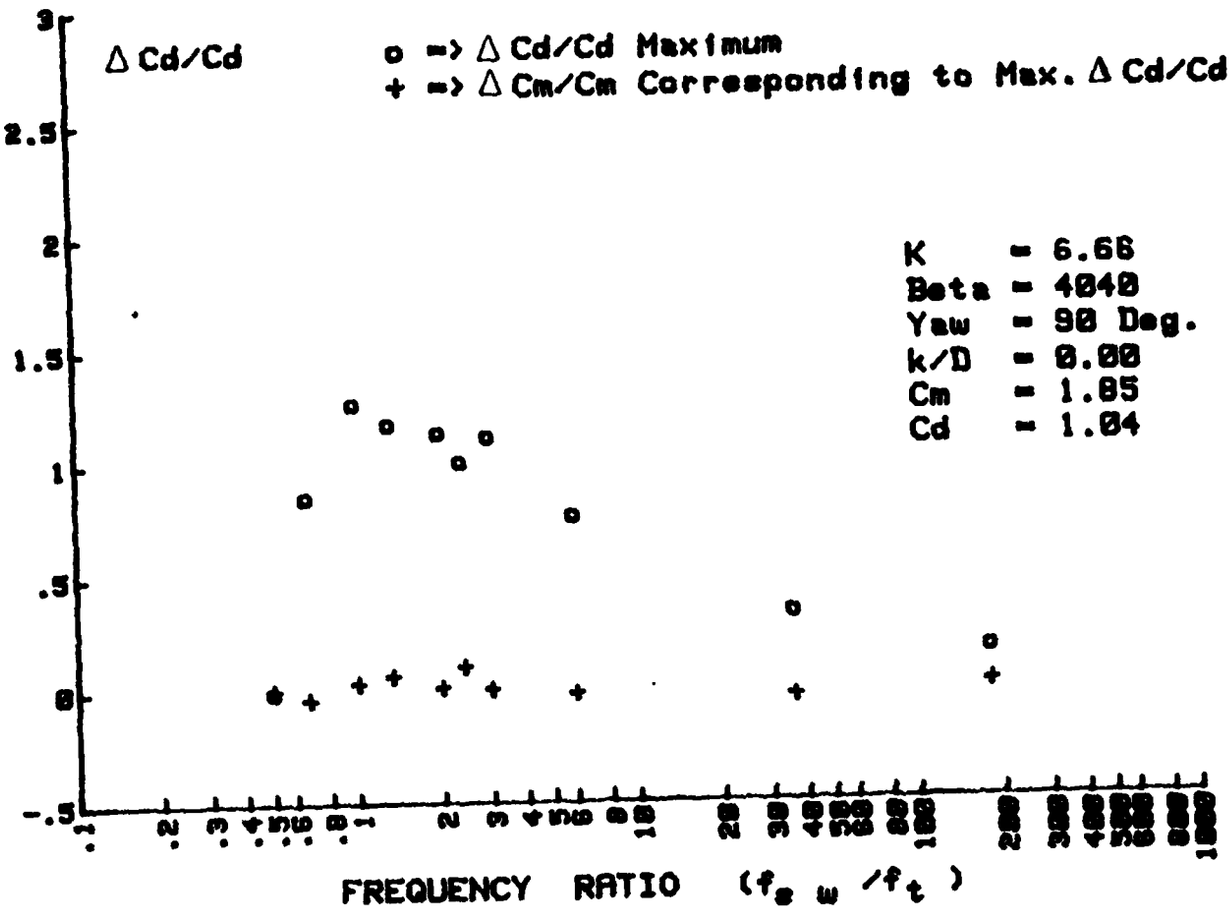

Figure 17b. Response of C_d and the Corresponding C_m to Random Disturbances of Various Frequency Ratios, K = 6.66.

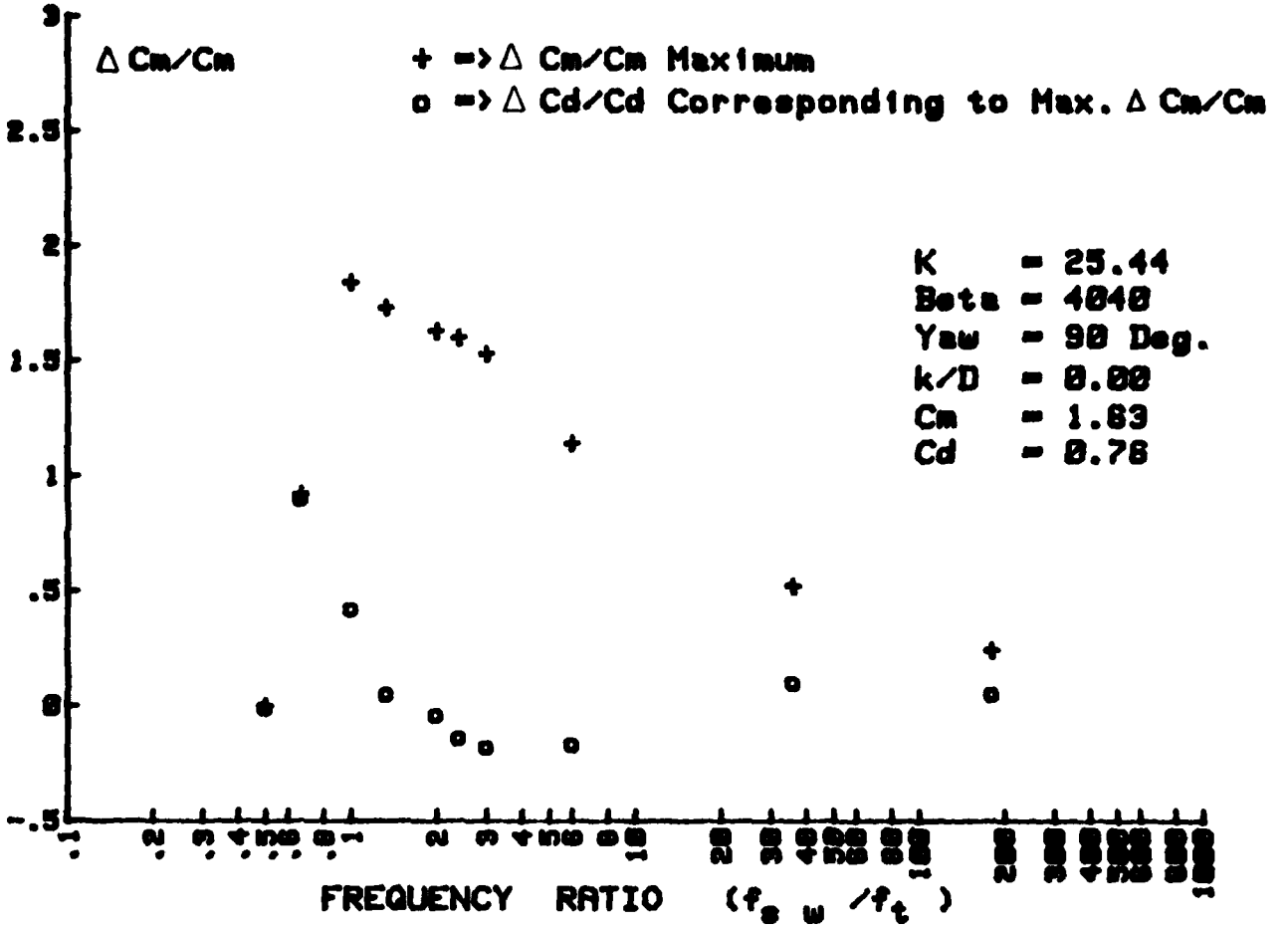

Figure 18a. Response of C_m and the Corresponding C_d to Random Disturbances of Various Frequency Ratios, K = 25.44.

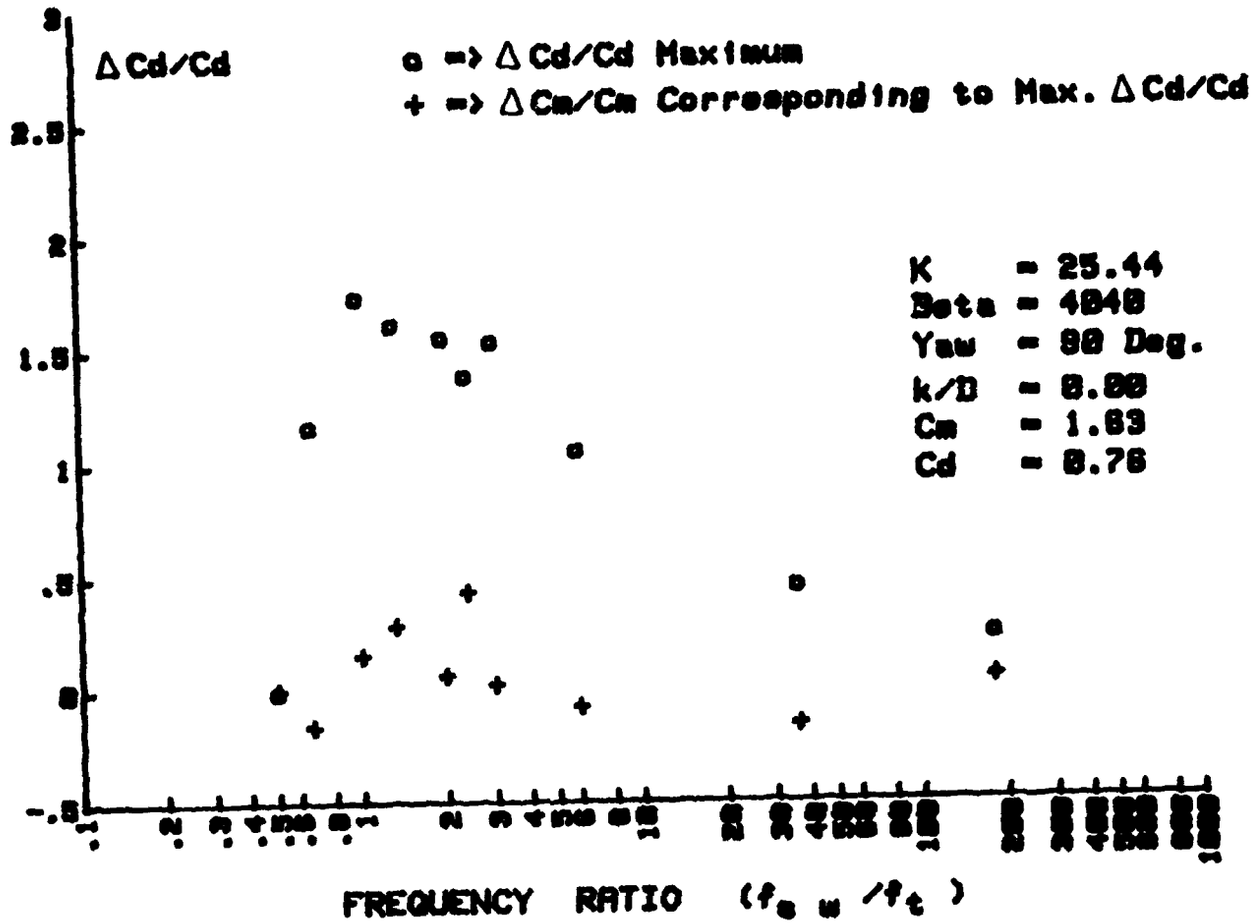

Figure 18b. Response of C_d and the Corresponding C_m to Random Disturbances of Various Frequency Ratios, K = 25.44.

LIST OF REFERENCES

1. Morison, J. R., O'Brien, M. D., Johnson, J. W., and Schaat, S.A., "The Force Exerted by Surface Waves on Piles", Petroleum Transactions AIME, Vol. 189, 1950.

2. Heideman, J. C., Olsen, O. A., and Johnansson, P. I., "Local Wave Force Coefficients", Civil Engineering in the Oceans IV, ASCE, Vol 1, pp. 684-699, 1979.

3. Sarpkaya, T., and Isaacson, M., Mechanics of Wave Forces on Offshore Structures, Van Nostrand Reinhold, New York, 1981.

4. Hoerner, S. F., Fluid Dynamic Drag, 3rd Ed., Book Published by the Author, New Jersey, 1965.

5. Bursnall, W. J. and Loftin, L. K., "Experimental Investigation of the Pressure Distribution About a Yawed Circular Cylinder in the Critical Reynolds Number Range", NACA Technical Note 2463, 1951.

6. Norton, D. J., Heideman, J. C., and Mallard, W. W., "Wind Tunnel Tests of Inclined Cylinders", 1981. Offshore Technology Conference Proceedings, Vol. IV, pp. 67-75, 1981.

7. Raines, T., "Harmonic Flow about Yawed Cylinders", M.E. Thesis, Naval Postgraduate School, Monterey, California, 1981.

8. Rajabi, F., "Hydroelastic Oscillations of Smooth and Rough Cylinders in Harmonic Flow", Ph.D. Thesis, Naval Postgraduate School, Monterey, California, 1980.

9. Bakmis, C., "Harmonic Flow about Cylinders", M.E. Thesis, Naval Postgraduate School, Monterey, California, 1980.

10. Sarpkaya, T., "Vortex Shedding and Resistance in Harmonic Flow about Smooth and Rough Circular Cylinders at High Reynolds Numbers", NPS-59SL76021, Naval Postgraduate School, Monterey, California, June 1976.

11. Keulegan, G. H. and Carpenter, L. H., "Forces on Cylinders and Plates in an Oscillating Fluid", National Bureau of Standards Report No. 4821, 1956.

INITIAL DISTRIBUTION LIST

		No. Copies
1.	Defense Technical Information Center Cameron Station Alexandria, Virginia 22314	2
2.	Library, Code 0142 Naval Postgraduate School Monterey, California 93940	2
3.	Professor T. Sarpkaya, Code 69SL Mechanical Engineering Naval Postgraduate School Monterey, California 93940	5
4.	Chairman, Department of Mechanical Engineering, Code 69 Naval Postgraduate School Monterey, California 93940	2
5.	LCDR Dean O. Trytten, USN 25 Shubrick Rd. Monterey, California 93940	2


END
DATE
FILMED
09-8
DTIC